

2006

The effect of as-large-as grains on the high-temperature fatigue life of waspaloy

Mandy Lorene Brogdon
University of Dayton

Follow this and additional works at: https://ecommons.udayton.edu/graduate_theses

Recommended Citation

Brogdon, Mandy Lorene, "The effect of as-large-as grains on the high-temperature fatigue life of waspaloy" (2006). *Graduate Theses and Dissertations*. 1752.
https://ecommons.udayton.edu/graduate_theses/1752

This Thesis is brought to you for free and open access by the Theses and Dissertations at eCommons. It has been accepted for inclusion in Graduate Theses and Dissertations by an authorized administrator of eCommons. For more information, please contact mschlangen1@udayton.edu, ecommons@udayton.edu.

THE EFFECT OF AS-LARGE-AS GRAINS ON THE HIGH-TEMPERATURE
FATIGUE LIFE OF WASPALOY

Thesis

Submitted to

The School of Engineering of the
UNIVERSITY OF DAYTON

In Partial Fulfillment of the Requirements for

The Degree

Master of Science in Materials Engineering

By

Mandy Lorene Brogdon

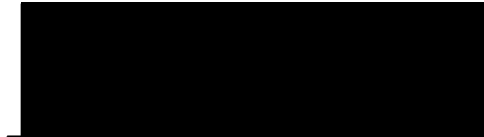
UNIVERSITY OF DAYTON

Dayton, Ohio

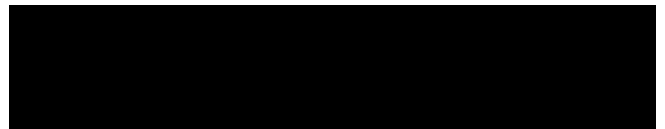
December, 2006

THE EFFECT OF ALA GRAINS ON THE HIGH-TEMPERATURE FATIGUE LIFE OF
WASPALLOY

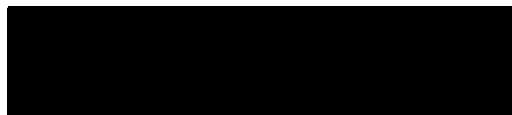
APPROVED BY:



Daniel Eylon, D.Sc.
Advisory Committee Chairman
Director, Materials
Engineering Program



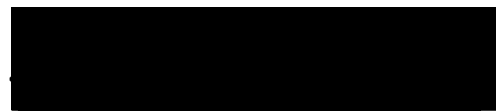
Andrew H. Rosenberger, Ph.D.
Committee Member
Research Engineer,
Wright-Patterson AFB



P. Terrence Murray, Ph.D.
Committee Member
Professor, Materials Engineering



Donald L. Moon, Ph.D.
Associate Dean, Graduate
Engineering Programs &
Research, School of Engineering



Joseph E. Saliba, Ph.D., P.E.
Dean, School of Engineering

ABSTRACT

THE EFFECT OF AS-LARGE-AS GRAINS ON THE HIGH-TEMPERATURE FATIGUE LIFE OF WASPALOY

Name: Brogdon, Mandy Lorene
University of Dayton

Advisor: Dr. Andrew Rosenberger

Waspaloy is a nickel superalloy that, when processed, may contain as-large-as (ALA) grains in the outer surface of the billet. Many components were manufactured containing this ALA region. The common practice now is to remove the ALA-affected region; however, the effect of these ALA grains in Waspaloy has not directly been studied.

To characterize the material and determine the effects of the ALA grains, tensile tests and fatigue tests were performed at 538° C to emulate the operating conditions of Waspaloy aerospace components. Half of the specimens tested were ALA containing specimens and the other half of the specimens were from the mid radius of the billet and did not contain ALA grains. Replicas were taken of several of each group to track crack initiation and growth. The fracture surfaces were also examined in a scanning electron microscope (SEM) where stereo pair

photographs were taken so the surface geography could be viewed in a program called MeX by creating digital elevation maps (DEM).

The tensile tests revealed yield strength variability in the ALA material. The fatigue data showed three types of behavior in the ALA material and two types in the non-ALA material. Based on the average material in both groups, the ALA material had a shorter average life. The short life specimens in each group, however, had almost the same number of cycles to failure, implying that the ALA grains had no specific bearing on the minimum bound of specimen life.

ACKNOWLEDGEMENTS

I would like to thank my advisor, Andrew Rosenberger, for his support and direction on this project, and for his encouragement to pursue this degree. I would also like to thank my other committee members, Danny Eylon and Terry Murray for their help with my project.

I would also like to thank my co-workers at Wright-Patterson AFB, especially those employees of the UDRI Structural Integrity Division who have helped to train me to use the necessary test equipment and aided me in other various ways on this project.

I would also like to thank my mother, father, friends, roommates, and Jeff for their support and love during this time.

TABLE OF CONTENTS

| | |
|---|------|
| ABSTRACT | iii |
| ACKNOWLEDGEMENTS | v |
| LIST OF ILLUSTRATIONS | viii |
| LIST OF TABLES | xii |
| LIST OF ABBREVIATIONS | xiii |
| CHAPTER | |
| I. INTRODUCTION | 1 |
| 1.1 Project Background | 1 |
| 1.2 Waspaloy | 5 |
| 1.3 Problem Statement | 9 |
| 1.4 Objective | 11 |
| II. EXPERIMENTAL EQUIPMENT AND APPROACH | 12 |
| 2.1 Sample Fabrication and Preparation | 12 |
| 2.2 Test Equipment Used | 14 |
| 2.3 Test Types and Procedures | 17 |
| III. RESULTS AND DISCUSSION | 21 |
| 3.1 Tensile | 21 |
| 3.2 Fatigue | 25 |
| 3.3 Discussion | 41 |
| IV. SUMMARY AND CONCLUSIONS | 44 |
| V. RECOMMENDATIONS FOR FUTURE WORK | 46 |
| 5.1 Future Tensile and Fatigue Tests | 46 |

| | |
|--|-----|
| 5.2 Detailed Microstructural Analysis | 47 |
| 5.3 Model Approaches to Link Material Processing to Behavior (Vextec) | 47 |
| 5.4 Fracture Surface Analysis | 48 |
| APPENDICES | |
| A. SEM Images of Specimens | 49 |
| B. MeX Images of Specimens | 76 |
| C. Pertinent Test Information | 103 |
| D. Specimen Life Vs. Billet Location | 106 |
| BIBLIOGRAPHY | 107 |

LIST OF ILLUSTRATIONS

| | |
|--|----|
| 1. Previous Waspaloy fatigue data, 650°C, R=0.05, 10 Hz, [1] | 2 |
| 2. Room temperature tensile data, [1]..... | 3 |
| 3. 649°C tensile data, [1] | 3 |
| 4. 700 °C tensile data, [1] | 4 |
| 5. Location of cylindrical blanks in billet (not to scale) | 6 |
| 6. Non-ALA, mid radius material, at 100X | 9 |
| 7. ALA, edge material, at 100X | 10 |
| 8. A generalized drawing of the specimens | 12 |
| 9. Non-ALA tensile data, 538° C, 0.00785 s ⁻¹ | 23 |
| 10. ALA tensile data, 538° C, 0.00785 s ⁻¹ | 24 |
| 11. All valid tensile data, 538° C, 0.00785 s ⁻¹ | 24 |
| 12. Fatigue data for non-ALA specimens, 538° C, R=0.05, 1 Hz | 26 |
| 13. Fatigue data for ALA specimens, 538° C, R=0.05, 1 Hz | 27 |
| 14. Fatigue data for all specimens, 538° C, R=0.05, 1 Hz | 28 |
| 15. A CDF representation of fatigue data | 29 |
| 16. The shortest life (a) ALA specimen 06-115, N=27,570 cycles, 150X and (b) non-ALA specimen 06-020, N=24,852 cycles, 200X | 30 |
| 17. The shortest life (a) ALA specimen 06-115, N=27,570 cycles, 150X and a long life (b) ALA specimen 06-116, N=437,451 cycles, 200X | 31 |
| 18. Two different long life ALA specimens (a) 06-112, N=531,310 cycles, 200X and (b) 06-114, N=517,296 cycles, 200X | 32 |
| 19. Shortest life non-ALA specimen (a) 06-020, N=24,852 cycles, 200X and longer life non-ALA specimen (b) 06-026, N=207,859 cycles, 200X | 32 |
| 20. Fatigue results with replica specimens segregated | 33 |
| 21. SEM pictures of ALA sample 06-112 at (a) 20X, (b) 200X, and (c) 500X | 37 |
| 22. SEM pictures of non-ALA sample 06-025 at (a) 20X, (b) 200X, and (c) 500X | 38 |
| 23. (a) SEM image and (b) corresponding DEM for ALA specimen 06-132 | 39 |

| | |
|---|----|
| 24. (a) SEM image and (b) corresponding DEM for non-ALA specimen 06-021 | 40 |
| 25. (a) Trace taken on surface of grain and (b) corresponding graphical representation for ALA specimen 06-132 | 41 |
| 26. 06-000 at 200X | 49 |
| 27. 06-002 at 200X | 49 |
| 28. 06-003 at 200X | 50 |
| 29. 06-004 at 200X | 50 |
| 30. 06-005 at 200X | 51 |
| 31. 06-006 at 200X | 51 |
| 32. 06-008 at 200X | 52 |
| 33. 06-009 at 200X | 52 |
| 34. 06-010 at 200X | 53 |
| 35. 06-011 at 200X | 53 |
| 36. 06-012 at 150X | 54 |
| 37. 06-013 at 200X | 54 |
| 38. 06-014 at 200X | 55 |
| 39. 06-015 at 200X | 55 |
| 40. 06-016 at 200X | 56 |
| 41. 06-017 at 200X | 56 |
| 42. 06-018 at 200X | 57 |
| 43. 06-019 at 200X | 57 |
| 44. 06-020 at 200X | 58 |
| 45. 06-021 at 200X | 58 |
| 46. 06-023 at 150X | 59 |
| 47. 06-024 at 200X | 59 |
| 48. 06-025 at 200X | 60 |
| 49. 06-026 at 200X | 60 |
| 50. 06-027 at 200X | 61 |
| 51. 06-029 at 200X | 61 |
| 52. 06-112 at 200X | 62 |
| 53. 06-113 at 150X | 62 |
| 54. 06-114 at 200X | 63 |
| 55. 06-115 at 150X | 63 |
| 56. 06-116 at 200X | 64 |
| 57. 06-117 at 200X | 64 |
| 58. 06-118 at 200X | 65 |
| 59. 06-119 at 150X | 65 |
| 60. 06-120 at 200X | 66 |
| 61. 06-121 at 200X | 66 |
| 62. 06-122 at 200X | 67 |
| 63. 06-123 at 200X | 67 |
| 64. 06-125 at 150X | 68 |
| 65. 06-126 at 150X | 68 |

| | |
|---------------------------|----|
| 66. 06-127 at 200X | 69 |
| 67. 06-128 at 200X | 69 |
| 68. 06-130 at 200X | 70 |
| 69. 06-131 at 150X | 70 |
| 70. 06-132 at 200X | 71 |
| 71. 06-133 at 200X | 71 |
| 72. 06-134 at 200X | 72 |
| 73. 06-135 at 200X | 72 |
| 74. 06-136 at 200X | 73 |
| 75. 06-137 at 200X | 73 |
| 76. 06-139 at 200X | 74 |
| 77. 06-140 at 200X | 74 |
| 78. 06-141 at 150X | 75 |
| 79. 06-000 at 200X | 76 |
| 80. 06-002 at 200X | 76 |
| 81. 06-003 at 200X | 77 |
| 82. 06-004 at 200X | 77 |
| 83. 06-005 at 200X | 78 |
| 84. 06-006 at 200X | 78 |
| 85. 06-008 at 200X | 79 |
| 86. 06-009 at 200X | 79 |
| 87. 06-010 at 200X | 80 |
| 88. 06-011 at 200X | 80 |
| 89. 06-012 at 150X | 81 |
| 90. 06-013 at 200X | 81 |
| 91. 06-014 at 200X | 82 |
| 92. 06-015 at 200X | 82 |
| 93. 06-016 at 200X | 83 |
| 94. 06-017 at 200X | 83 |
| 95. 06-018 at 200X | 84 |
| 96. 06-019 at 200X | 84 |
| 97. 06-020 at 200X | 85 |
| 98. 06-021 at 200X | 85 |
| 99. 06-023 at 150X | 86 |
| 100. 06-024 at 200X | 86 |
| 101. 06-025 at 200X | 87 |
| 102. 06-026 at 200X | 87 |
| 103. 06-027 at 200X | 88 |
| 104. 06-029 at 200X | 88 |
| 105. 06-112 at 200X | 89 |
| 106. 06-113 at 150X | 89 |
| 107. 06-114 at 200X | 90 |
| 108. 06-115 at 150X | 90 |
| 109. 06-116 at 200X | 91 |

| | |
|---|-----|
| 110. 06-117 at 200X | 91 |
| 111. 06-118 at 200X | 92 |
| 112. 06-119 at 150X | 92 |
| 113. 06-120 at 200X | 93 |
| 114. 06-121 at 200X | 93 |
| 115. 06-122 at 200X | 94 |
| 116. 06-123 at 200X | 94 |
| 117. 06-125 at 150X | 95 |
| 118. 06-126 at 150X | 95 |
| 119. 06-127 at 200X | 96 |
| 120. 06-128 at 200X | 96 |
| 121. 06-130 at 200X | 97 |
| 122. 06-131 at 150X | 97 |
| 123. 06-132 at 200X | 98 |
| 124. 06-133 at 200X | 98 |
| 125. 06-134 at 200X | 99 |
| 126. 06-135 at 200X | 99 |
| 127. 06-136 at 200X | 100 |
| 128. 06-137 at 200X | 100 |
| 129. 06-139 at 200X | 101 |
| 130. 06-140 at 200X | 101 |
| 131. 06-141 at 150X | 102 |
| 132. Cumulative distribution function showing life based on location from billet | 106 |
| 133. Representative locations of specimens (color coded with Figure 132) | 106 |

LIST OF TABLES

| | |
|--|-----|
| 1. Previous tensile test results, [1] | 4 |
| 2. Chemical composition of the Waspaloy tested | 7 |
| 3. Tensile data 538 ° C | 23 |
| 4. ALA replica results | 35 |
| 5. Pertinent Test Information | 103 |

LIST OF ABBREVIATIONS

| | |
|--------|---|
| AC- | Air Cool |
| AFRL- | Air Force Research Laboratories |
| ALA- | As Large As Grain |
| CDF- | Cumulative Distribution Function |
| DEM- | Digital Elevation Map |
| EDM- | Electro-discharge Machining |
| MLLMN- | Mechanical Behavior and Life Prediction Section of Materials Directorate |
| MLLMP- | Processing Section of Materials Directorate |
| R- | Stress Ratio ($R = \sigma_{\min} / \sigma_{\max}$) |
| SEM- | Scanning Electron Microscope |
| TMP- | Thermo-mechanical Processing |
| UTS- | Ultimate Tensile Strength |
| VAR- | Vacuum Arc Re-melting |
| VIM- | Vacuum-induction Melting |

CHAPTER 1

Introduction

1.1 Project Background

1.1.1 Original Overall Project

This thesis project began as a part of a larger project meant to investigate the role as-large-as grains (ALAs) play in the functionality of the nickel superalloy Waspaloy. Many parts manufactured from Waspaloy in the past are currently in service and contain these ALAs. In the present day, the area containing ALAs is removed from the forging in a costly and wasteful process. Understanding the effect of the ALAs can lend insight to the ability and projected life of parts currently in service. It could also validate or invalidate the necessity to remove material from the original forging. The objective of the present research is to understand the influence of ALA grains on the crack initiation and total fatigue life of Waspaloy. There is also a connection between this project and another project in AFRL/MLLMP aimed at refining the processing steps of Waspaloy to decrease or eliminate the presence of ALAs.

1.1.2 Previous Work and Results

This project was initiated by another scientist in AFRL [1], who began by running fatigue tests with flat hourglass specimens. This specimen geometry was chosen due to the relative ease of replicating the flat surface and to use an infrared crack detection system to determine when cracks initiate. Unfortunately, specimens with corners can cloud the fatigue behavior of the material, cause cracks to initiate unnaturally at the low constraint corner and give inconclusive results. These specimens were tested at several stresses and at 649°C (Figure 1). At most there were only four tests performed at any stress level. This makes it difficult to truly characterize the life variability of the material.

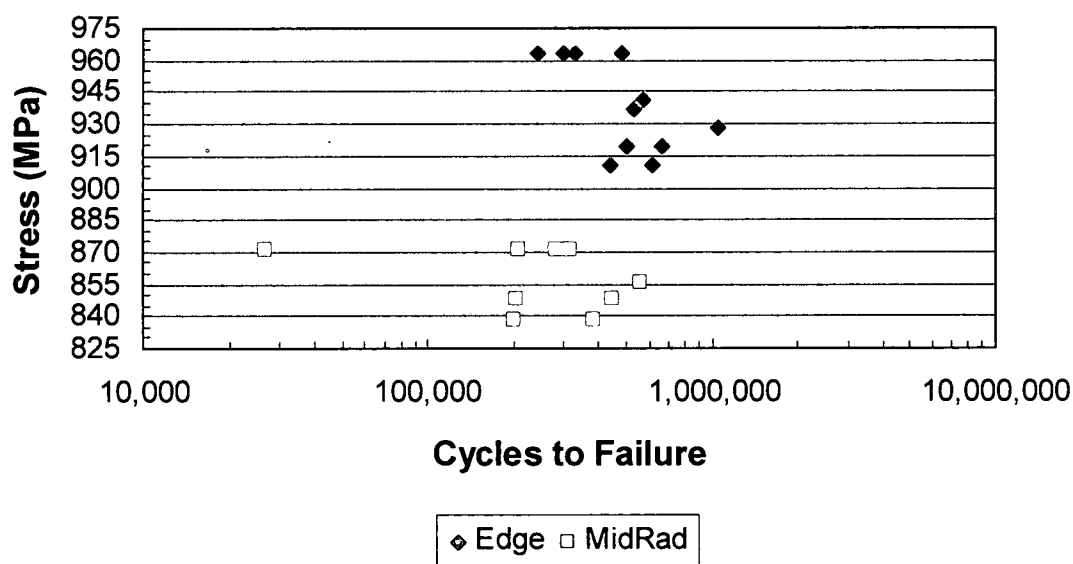


Figure 1. Previous Waspaloy fatigue data, 650°C, R=0.05, 10 Hz, [1]

Baseline tensile tests were run with cylindrical dogbone specimens (Figures 2, 3, and 4). These tests were run at both room temperature

(24°C) and the elevated temperatures of 649°C and 700°C. The yield strengths and ultimate tensile strengths determined by these tests, Table 1, were used to select the stress range in which the fatigue tests were performed.

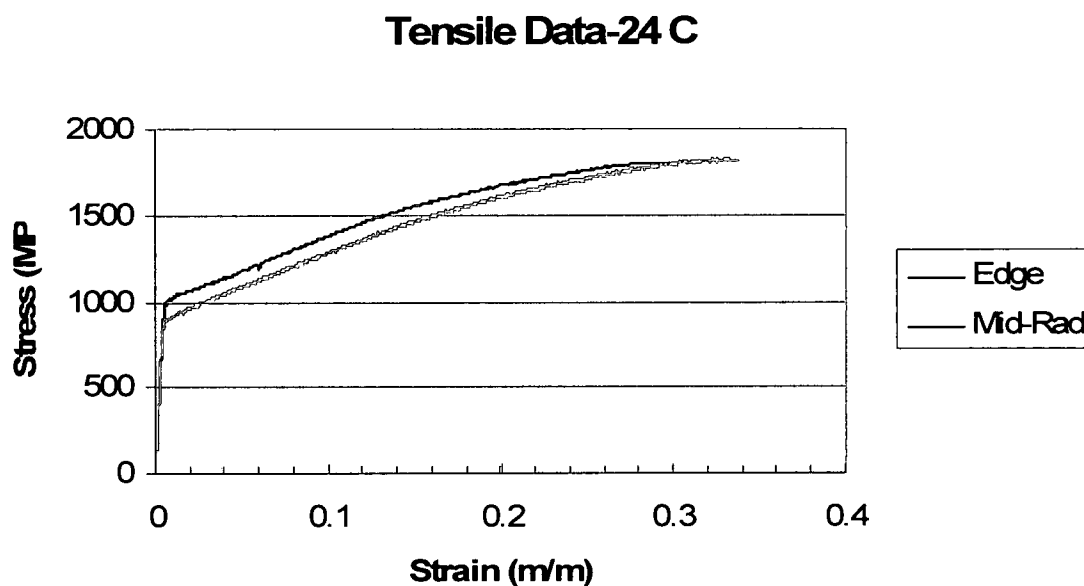


Figure 2. Room temperature tensile data, [1].

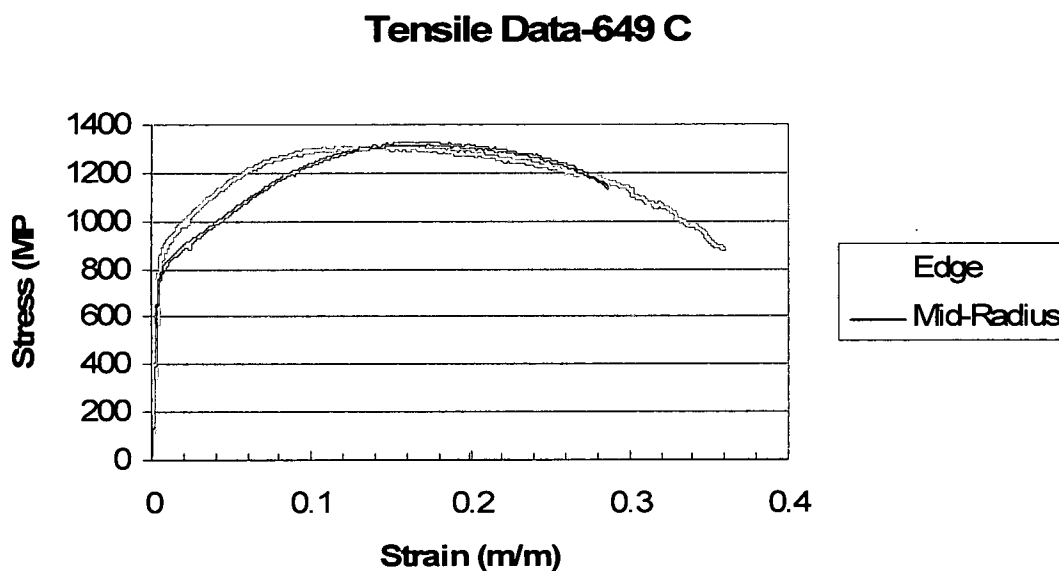


Figure 3. 649°C tensile data, [1].

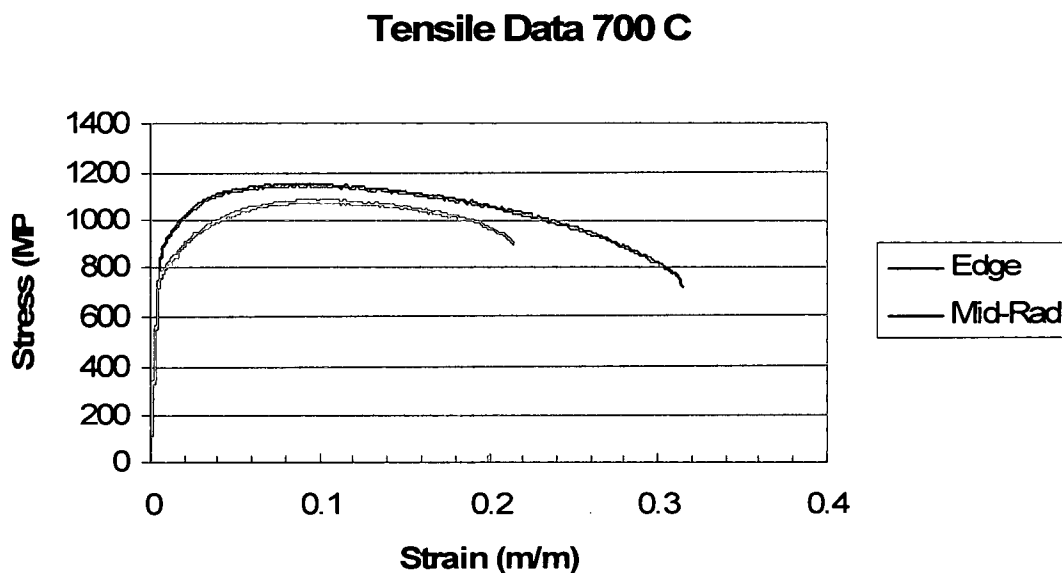


Figure 4. 700 °C tensile data, [1].

Table 1. Previous tensile test results, [1].

| Billet Material | | | | | | |
|-----------------|------------|----------|----------------|------|--------------|-----------------------|
| Location | Grain Size | | Strength (MPa) | | Red. of Area | Test Temperature (°C) |
| | ASTM | dia (μm) | 0.2% YS | UTS | | |
| Mid-Rad | 5 | 63.5 | 887.8 | 1328 | 0.351 | 24 |
| | | | 770.4 | 1098 | 0.352 | 649 |
| | | | 756.8 | 1059 | 0.363 | 700 |
| Edge | 8.5 | 18.9 | 1026 | 1393 | 0.384 | 24 |
| | | | 888 | 1184 | 0.611 | 649 |
| | | | 877.5 | 1081 | 0.599 | 700 |

This test data provided useful starting blocks for the test program, but it left many unanswered questions. This produced a need for a well-repeated fatigue study at constant temperature and stress to more stoutly assess the fatigue life variability of the material.

1.1.3 Connection to Work on Material Processing

Information on the size range and frequency of the ALA grains can help in the modeling of the forging process. It is the desire of the group at AFRL/MLLMP to take this information, along with the fatigue life information, and use them as parameters in modeling the forging process so that changes in the theoretical forging processes can be correlated with new and improved material properties. Ultimately this would result in a modeling capability to bridge the processing to property of a material so that improved material behavior can be a final result of the improved processing.

1.2 Waspaloy

The Waspaloy material for this program was specially produced for the purpose of research on the ALA phenomenon. This product was known to not conform to the high commercial material standards [2] and was known to contain ALA grains near the outer diameter. The regions of ALA grains were determined to be within $\frac{1}{2}$ inch of the outer diameter and cylindrical blanks were cut (by EDM) from the billet in the regions where ALA grains had been identified. It is important to note that the ALA grains do not necessarily occur consistently around the entire billet, which is a result of processing, and which made locating ALA containing areas difficult. Figure 5 illustrates the locations from which the cylindrical blanks

were machined. The blanks near the edge of the billet are the ALA containing specimens, and the blanks in the mid-radius are the control, non-ALA specimens.

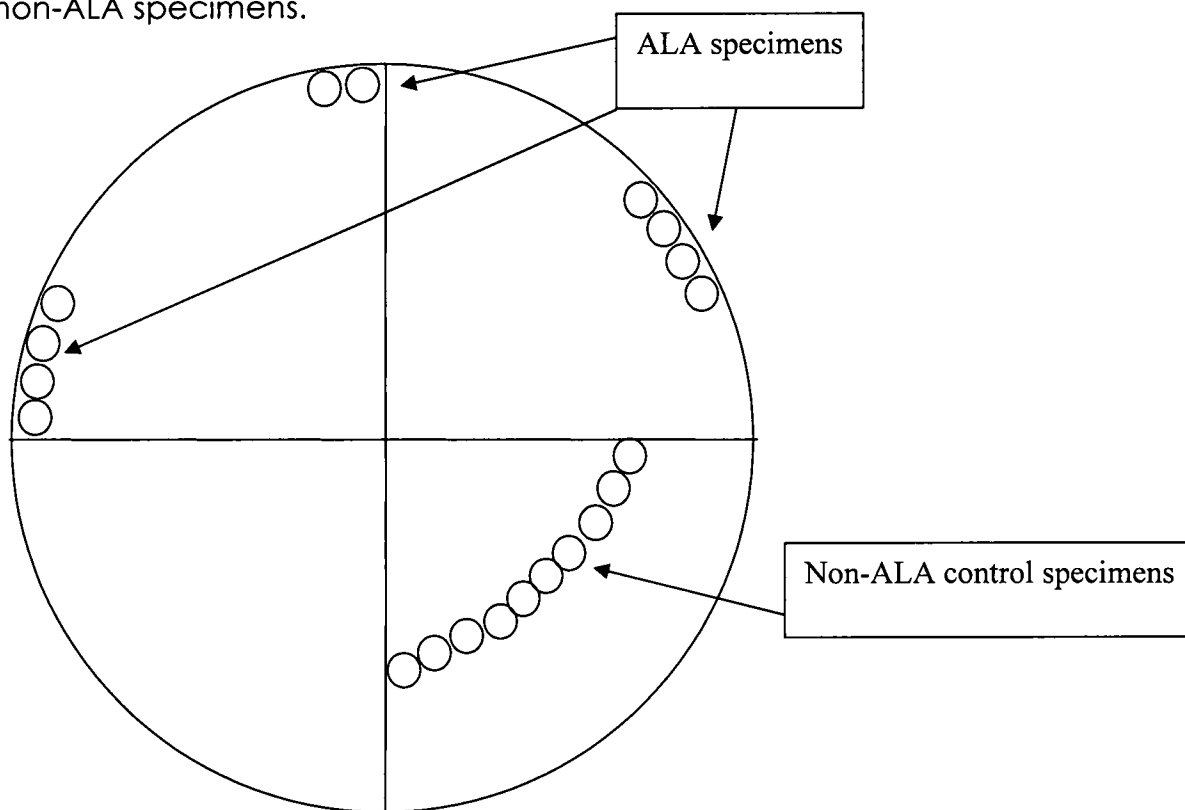


Figure 5. Location of cylindrical blanks in billet (not to scale)

1.2.1 As-Large-As Grains

Large grains dispersed within a finer grain structure are perceived to be linked to abnormal crack initiation and propagation and fatigue behavior. As-large-as grains are defined as outlier grains that make up less than five percent of the specimen area and are at least 3 ASTM grain sizes larger than the rest of the microstructure [3].

1.2.2 Chemical Composition

Waspaloy contains molybdenum, cobalt and chromium to attain its strength in high temperature conditions. It contains aluminum and titanium to improve age hardening properties. It is a slightly stronger alloy with a larger stability range than IN 718 [2].

Table 2. Chemical composition of the Waspaloy tested.

| | | | |
|-----------|--------------|-----------|--------------------|
| Ni | 58.14 | V | 0.03 |
| Cr | 18.42 | C | 0.028 |
| Co | 13.94 | Mn | 0.02 |
| Mo | 3.76 | Nb | 0.02 |
| Ti | 3.17 | Ta | 0.02 |
| Al | 1.53 | Si | 0.015 |
| Fe | 0.81 | B | 0.006 |
| Zr | 0.06 | S | < 0.0003 |
| W | 0.03 | | |

1.2.3 Uses

Waspaloy is a very common turbine engine material, and is used to make turbine and compressor disks and other turbine parts such as cases, fasteners, shafts and spacers [2]. For the purpose of this research, the turbine disk application is of interest. To this end, the material was characterized under temperatures and loading conditions that were applicable to the current use of this material.

1.2.4 Mechanical Behavior

Waspaloy is a high strength, precipitation hardening alloy, with gamma prime and carbide precipitations providing the strength and hardening [2]. It has a yield strength of approximately 735 MPa, an ultimate tensile strength (UTS) of approximately 1175 MPa and a modulus of elasticity of approximately 185 GPa.

1.2.5 Fabrication/Forging Process

To create a Waspaloy ingot, a manufacturer begins with a vacuum-induction melting (VIM) process followed by a vacuum-arc melting (VAR) process. This creates an ingot with very coarse columnar grains, producing undesirable properties for turbine disks [4].

A typical thermo-mechanical processing (TMP) treatment, used for Waspaloy to obtain both good tensile and good creep properties [5], consists of:

- a) Initial forging at 1120°C
- b) Finish forging at approximately 1010°C (produces equiaxed grain size ~ASTM 5)
- c) Solution treating at 1010°C
- d) Aging at 845°C for 4 hours, then Air Cool (AC)
- e) Tempering at 760°C for 16 hours, then AC [6]

Forging and solution treating serve to dissolve the γ' precipitates, anneal the matrix material and promote grain growth to around size ASTM 3. Then the aging step is designed to control γ' and carbide precipitation. The tempering step heats the furnace slightly above the recrystallization temperature to refine the grains to a size ranging between ASTM 5 and 6 (Figure 6).

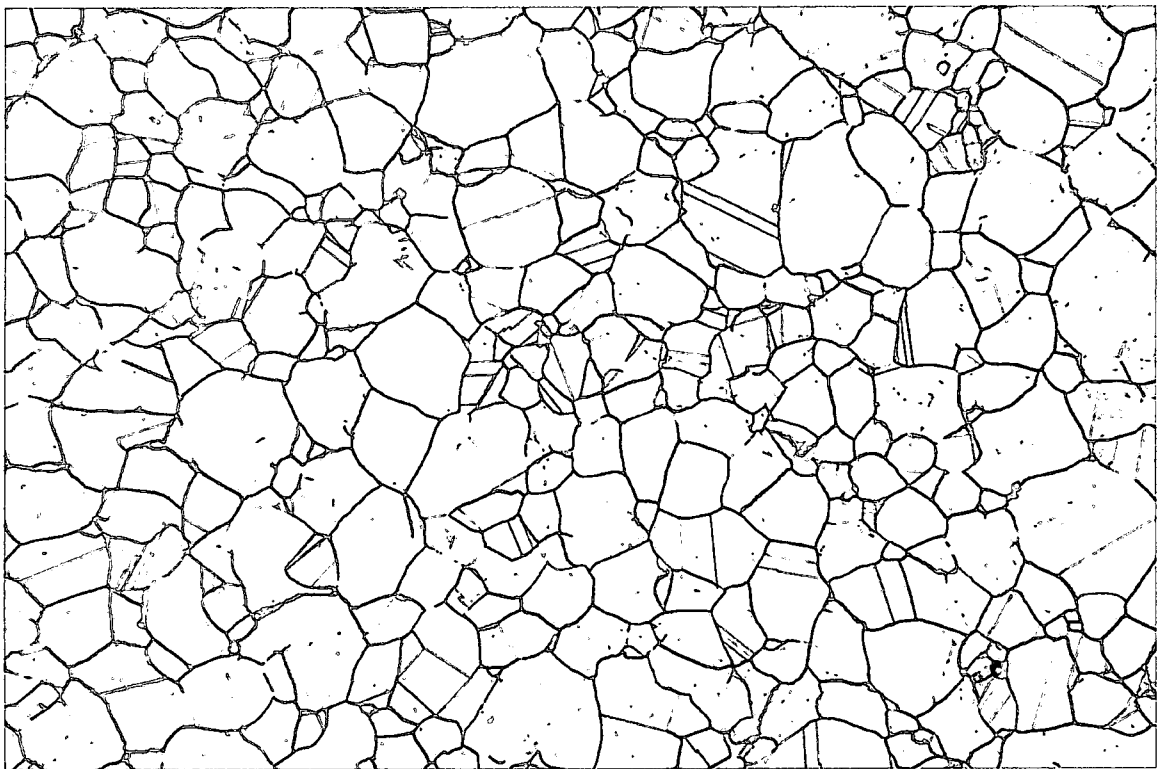


Figure 6. Non-ALA, mid radius material, at 100X

1.3 Problem Statement

The above-stated forging process is an idealized version of the process. It does not account for the formation of the ALA grains. For some reason, perhaps due to regions of insufficient strain density or forging chill, the TMP

CHAPTER 2

Experimental Equipment and Approach

2.1 Sample Fabrication and Preparation

The samples used in this study were a buttonhead, cylindrical dogbone geometry, Figure 8. The nominal length of the samples was 145mm, with a reduced gage section of 5.1 mm in diameter and 15.2 mm in length. This is a common geometry selection for fatigue testing because it removes the corner effects seen in square and rectangular bars. The buttonhead geometry allows for simple and speedy test setup and well controlled alignment.

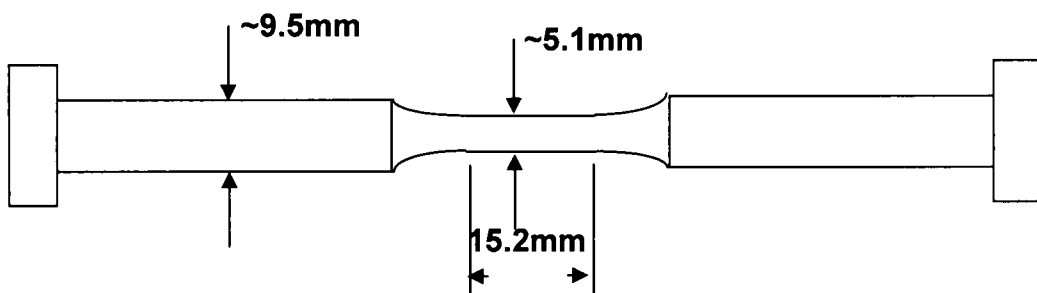


Figure 8. A generalized drawing of the specimens.

2.1.1 Fabrication

In an effort to maximize the amount of test specimens possible for not only this test but future tests in relation to this project, the entire specimen

body is not made of Waspaloy. The EDMed Waspaloy blanks were heat treated as follows:

- 1850° F for one hour, then oil quenched

- 1550° F for four hours, then air cooled

- 1400° F for four hours then air cooled.

Then the heat treated blanks were cut into thirds (each third is 50mm long). This idealized heat treatment was chosen to produce reproducible material behavior (i.e. gamma prime size) that may not be observed in a large component forging. Each of these pieces was used as the gage section of a specimen. The grip sections or ends of the specimens are made of the nickel alloy IN-718. Cylindrical blanks of IN-718 were inertia welded to each end of the gage section material. Once inertia welded, the button heads and 9.5 mm diameter were machined using conventional practice, and then a low stress grinding process was used to create the reduced 5.1mm gage section and fillet.

2.1.2 Preparation

Once received, the specimens were measured and then electro polished in the gage section using a perchloric acid soup with a 19 V DC current at approximately -50 °C. The purpose of electro polishing was to remove the stresses in the surface caused by the low stress machining processes. These surface stresses could make it more difficult for surface

cracks to initiate and cloud the true behavior of the material. The amount of material removed in the electro polishing process was approximately $50\mu\text{m}$, a value chosen based on previous studies performed in the Materials Directorate on surface stresses in nickel alloys. After electro polishing, the specimens were measured again to make sure enough material had been removed and so the cross-sectional area in the gage section could be determined.

2.2 Test Equipment Used

The varying test types and procedures (to be discussed later in this chapter) involved the use of many different pieces of equipment. The physical description, function, and any other pertinent information are listed in this section.

2.2.1 MTS Servo-Hydraulic Test System

The load frames used for both the tensile and fatigue testing in this project were MTS load frames with MTS 458 analogue controllers. They were servo-hydraulic systems with hydraulic collet grips controlled by a computer program called MATE for the tensile tests and either an MTS Microprofiler or a computer program called WinMATE for the fatigue tests. Both MATE and WinMATE were developed in-house by UDRI employee George Hartman [8]. The Microprofiler was used with the test system that

did not have the WinMATE program on its computer, and could not be used in tests where cycle limits were set, such as the replica tests. It is completely controlled by what is programmed and no load feedback was possible. Therefore calculations had to be made to determine how the Microprofiler should be programmed and then the calculations had to be tested and manually fine tuned with the Microprofiler to achieve the desired test parameters within the first few tens of cycles. Each test system had a maximum load capacity of 100kN. Tabulated results in Appendix C document which specimens were tested in which test machine.

2.2.2 Test System Accessories

The heating system used for this project's tests is the Applied Test Systems, Inc. Series 3210 Furnace/Oven. It has a maximum temperature capacity of 900° C. This heating element was used to bring the test to its operating temperature of 538° C.

The K-type thermocouples used to regulate the specimen temperature were made of 36 gage wire and spot welded onto the surface of the specimen at the larger side of the fillet. There was one thermocouple welded at both the top and bottom fillet of the specimen. It was determined using a dummy specimen that the temperature in the gage section could be controlled using measurements on the shoulders to

within 5° C. The welder was a Unitek Equipment Dual Pulse 125 Stored Energy Power Supply. The thermocouples were connected to Barber-Colman model 560 temperature controllers. The controllers worked by regulating the percentage of voltage supplied to the furnace from the power source using a phase angle fired SCR. The percentage of voltage changed based on the reading supplied to the controller by the thermocouples.

An extensometer was also used for several of the tests. It was meant to track strain on the specimens in both tensile and fatigue tests. It was a high temperature extensometer (MTS model 632.51) with ceramic rods. It was held to the surface of the specimen with spring pressure.

2.2.3 Scanning Electron Microscope (SEM)

The SEM was used post test to take magnified pictures between 150X and 500X of the crack initiation site of each fatigue test specimen. These pictures gave a general idea of the size of the initiating site/grain and were also used in stereo pairs to create digital elevation maps (DEM) in a computer program called MeX [9] to better understand the texture of the surface and orientation of the initiating grain.

2.3 Test Types and Procedures

Two types of tests were performed in order to characterize the behavior of the material. Tensile tests were run to determine properties in Waspaloy such as yield strength and ultimate tensile strength. Fatigue tests were run to determine the life of each specimen and in an attempt to track crack initiation and propagation. Both the tensile and fatigue tests were run at a temperature of 538° C.

2.3.1 Tensile

For each tensile test, a specimen was loaded into the MTS load frame and thermocouple wires were spot welded to the surface as specified in section 2.2.2. Then the extensometer was positioned on the surface at a negative percentage (-90 to -95%) to utilize the full range of the extensometer during the test of the specimen. The specimens were heated and once at temperature, the test parameters were entered into the MATE system and a test was performed in crosshead control with an initial strain rate of approximately 0.008 s^{-1} .

2.3.2 Fatigue

For each fatigue test, specimen setup was very similar to that of the tensile test. The main difference was the positioning of the extensometer prior to heating. For the fatigue test it was positioned between -15 to -10

percent because there is much less specimen elongation compared to a tensile test. The extensometer was also not used in all of the fatigue tests due to two reasons. On tests where replicas were taken, the extensometer would prevent the replication of the entire surface of the gage section. The second reason for not using the extensometers was that after several fatigue tests were run, it was found that the extensometer slipped out of position in each test, and consistent data could not be gathered throughout the entire test. The slippage caused some of the tests to be put on hold by engaging the interlock system, delaying the completion of tests. Once this pattern surfaced, a decision was made to continue without the extensometer.

The tests were run at a 1 Hz frequency with a triangular waveform and an R-value of 0.05. Most of the tests were performed at a maximum stress of 955 MPa, but the first tests run on the non-ALA specimens were run at a maximum stress of 910 MPa. The original value was based on an incremental increase in stress from the yield stress calculated during tensile testing of the non-ALA specimens. Once a higher yield stress was determined for the ALA specimens, the maximum stress of 955 MPa was tested.

2.3.2.1 Replica Test Process

Several tests were performed on both the ALA and non-ALA specimens in an attempt to track crack growth and relate it to the life of the

specimen. These tests were also meant to determine when cracks initiated in the specimens. A replica is actually an impression taken of the specimen surface that can detect surface texture caused by any number of things, such as machining marks, scratches, shot peening, grain boundaries and surface cracks.

To take a replica of a specimen surface, a thin acetate film was applied to the surface and wet with acetone, dispensed with a syringe so to control the amount of acetone used. The acetate film was allowed to dry, which could be determined when the film developed a cloudy appearance, and removed from the specimen. It was then adhered to a specimen slide with double-sided tape to be viewed under an optical microscope. This allows mid-test magnified inspection of the specimen surface without removing it from the load frame.

It was only after several uninterrupted tests to failure were performed before any replica tests were performed. By running those tests an expected life range of the specimens could be determined. This knowledge was necessary so tests could be paused at the minimum load in appropriate intervals and cooled to room temperature for the replication. The specimens were manually loaded to 60% of the maximum load for replication.

2.3.2.2 Test to Failure

For the tests purely run to failure, once the specimen was setup as described earlier in this section, the test was started and left to run until final failure. These tests did not have interruptions that could possibly affect the life of the specimen, which is sometimes thought of the replica process, which involves heating and cooling the specimens for each cycle set and applying materials to the surface which might alter the surface chemistry or remove surface oxidation, any of which could have an impact of crack growth and/or initiation. However, other researchers [10] have used this technique on high temperature fatigue tests with no influence of the replication technique on the fatigue lives.

CHAPTER 3

Results and Discussion

3.1 Tensile

For the purpose of this project, seven tensile specimens were tested. Four of the specimens were non-ALA containing and three were ALA containing. Only three of each of the sets provided valid test data; specimen 06-001 was tested after the wrong R-value (0.5) was applied to it during a fatigue test. 06-001 was tested to get a general feel for how the specimens are work hardened by the loads applied during fatigue testing. As shown in Figure 9, the yield value of 06-001 increased by close to 200 MPa compared to the other non-ALA specimens.

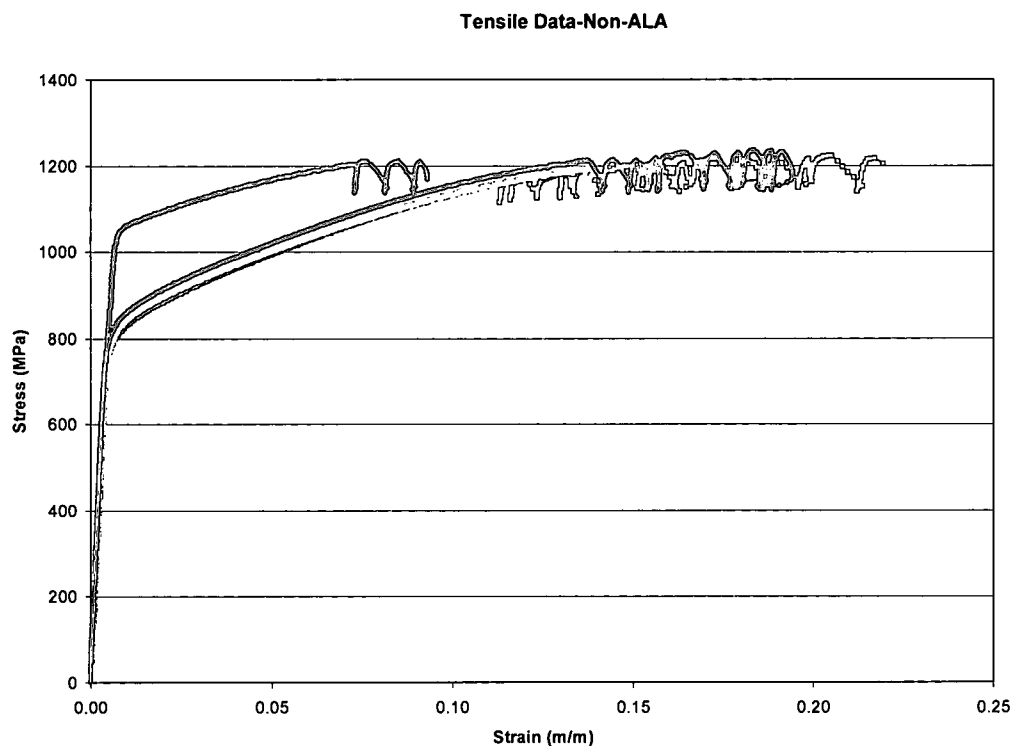
Figures 9 and 10 show the non-ALA and ALA specimens' tensile test data, respectively. Figure 11 is an assemblage of the valid tensile test data from Figures 9 and 10, the ALA specimens being red and the non-ALA specimens being blue. As shown both in Figure 11 and in Table 3, the yield strengths in the non-ALA material were more consistent and higher than the ALA specimens. The reported ultimate tensile strength values as determined for any of the specimens are not valid due to problems with the extensometry accuracy. It can be noted that in all of the tests there is

not reliable strain data throughout final fracture. It can also be noted that there was a phenomenon occurring that caused some type of stress relief, which can be seen in all of the tensile graphs. The serrated motion seen in the graphs was associated with a "popping" noise; each time the noise was heard the stress decreased. At some point during each test, the extensometer would be knocked loose and it was always associated with the noise.

Due to the manner of the test configuration, the possibility of the specimen slipping in the grips was not considered possible. This left the possibility of some type of serrated yielding, dynamic strain aging or grain boundary sliding, but none of these were confirmed. Dynamic strain aging has been confirmed in other nickel base superalloys under certain temperature and strain rates [11] – notice that the phenomena was not present in the earlier tensile tests conducted at room temperature, 649° C and 700° C, (Figures 2, 3, and 4 [1]).

Table 3. Tensile data 538 °C

| Specimen ID | Yield Strength (MPa) | UTS (MPa) | Modulus of Elasticity (GPa) |
|-------------------------|----------------------|----------------|-----------------------------|
| Non-ALA Material | | | |
| 06-007 | 800.157 | 1221.615 | 179.687 |
| 06-022 | 802.064 | 1195.137 | 176.704 |
| 06-028 | 821.139 | 1236.031 | 181.819 |
| Average= | 807.79 | 1217.59 | 179.40 |
| ALA Material | | | |
| 06-124 | 711.398 | 1184.005 | 177.912 |
| 06-129 | 731.913 | 1190.431 | 167.862 |
| 06-138 | 751.496 | 1171.45 | 169.263 |
| Average= | 731.60 | 1181.96 | 171.68 |

Figure 9. Non-ALA tensile data, 538° C, 0.00785 s⁻¹

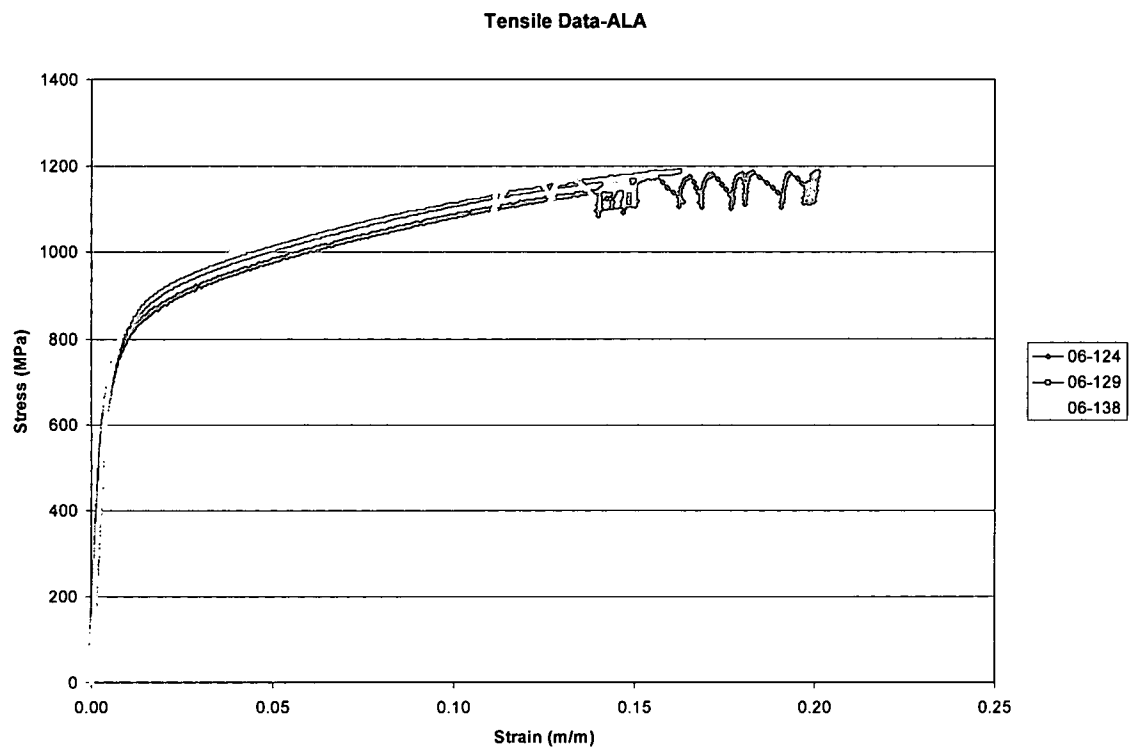


Figure 10. ALA tensile data, 538° C, 0.00785 s⁻¹

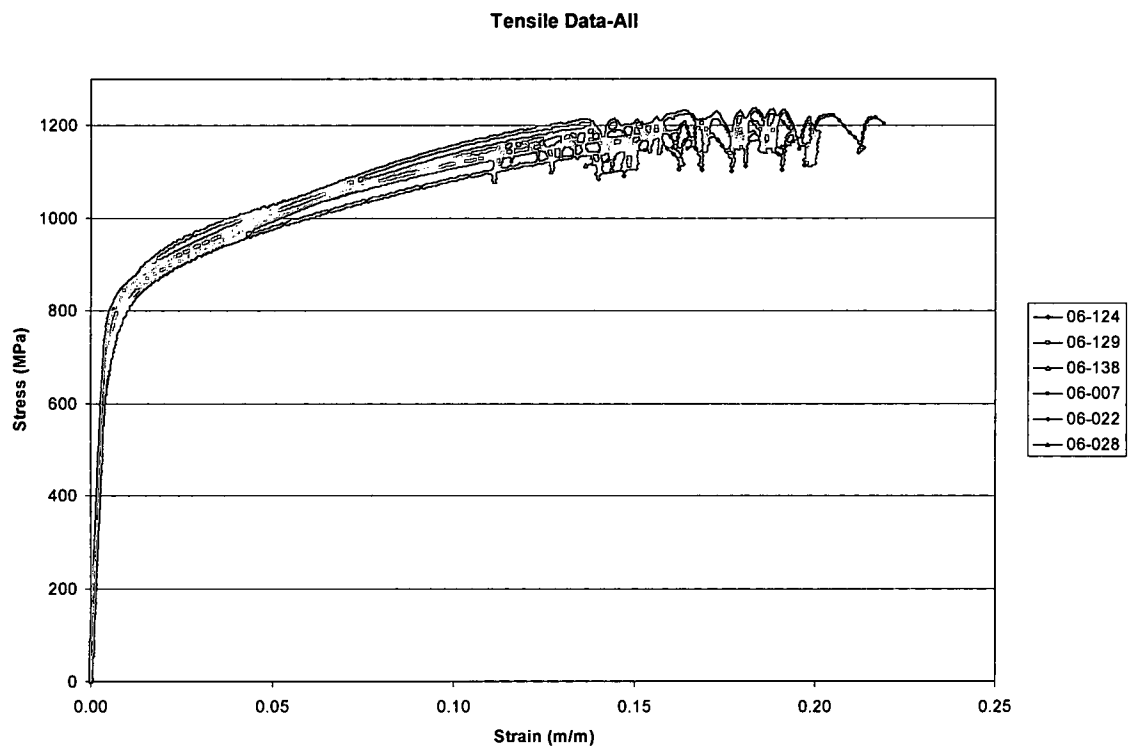


Figure 11. All valid tensile data, 538° C, 0.00785 s⁻¹

3.2 Fatigue

For the fatigue study, fifty-three bars were tested. Twenty-seven of the bars were ALA containing and were tested at 955 MPa. Twenty-six of the bars were non-ALA containing. Twelve of those were tested at 910 MPa and fourteen were tested at 955 MPa. The fatigue life of these specimens in relation to their test stress levels are reported in Figures 12, 13, and 14.

Figure 12 reports the cycles to failure of the 26 non-ALA specimens. They appear as two groupings of specimens-one at 910 MPa and one at 955 MPa, with two outliers in the 955 MPa data. The lives of the specimens tested at 910 MPa range from 202,821 cycles to 453,310 cycles. The lives of the specimens tested at 955 MPa range from 102,377 cycles to 213,340 cycles, not including the two outliers with lives 24,852 cycles and 68,699 cycles.

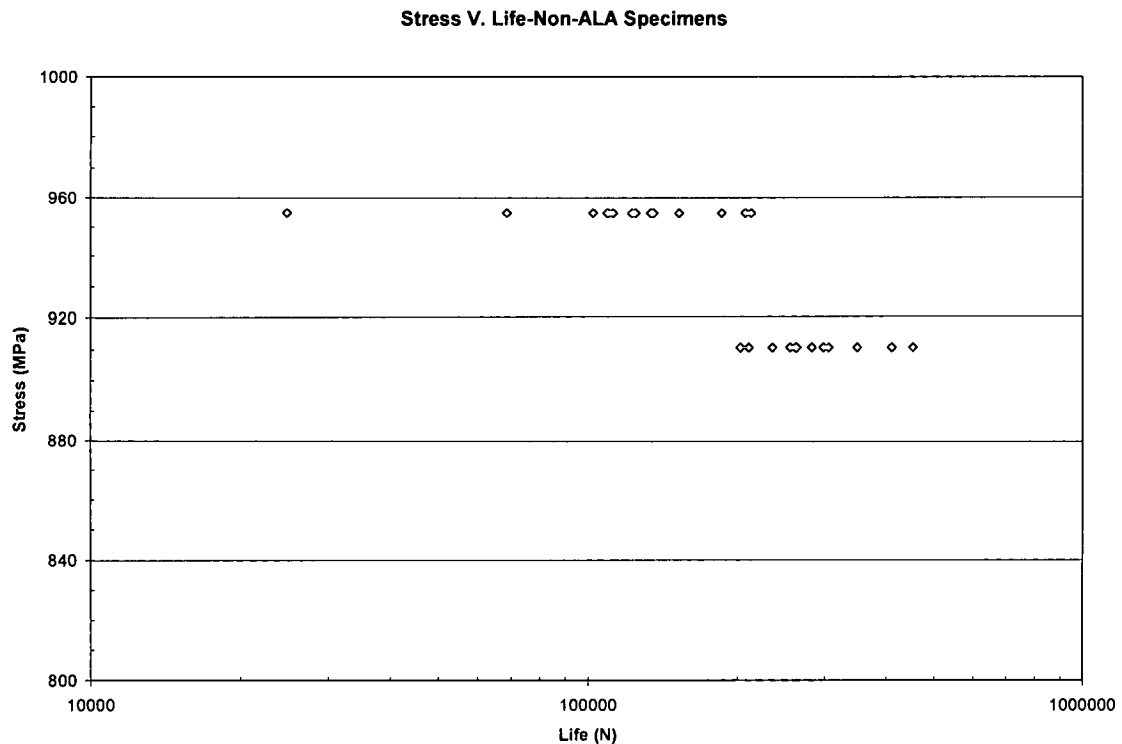


Figure 12. Fatigue data for non-ALA specimens, 538° C, $R=0.05$, 1 Hz

Figure 13 reports the cycles to failure of the 27 ALA specimens. Within the data there appear to be two distinct groupings. There is a group of five specimens with very long lives, ranging from 437,451 cycles to 568,882 cycles. There is another group ranging from 65,491 cycles to 179,404 cycles. There are also two outliers with 27,570 and 44,513 cycles to failure.

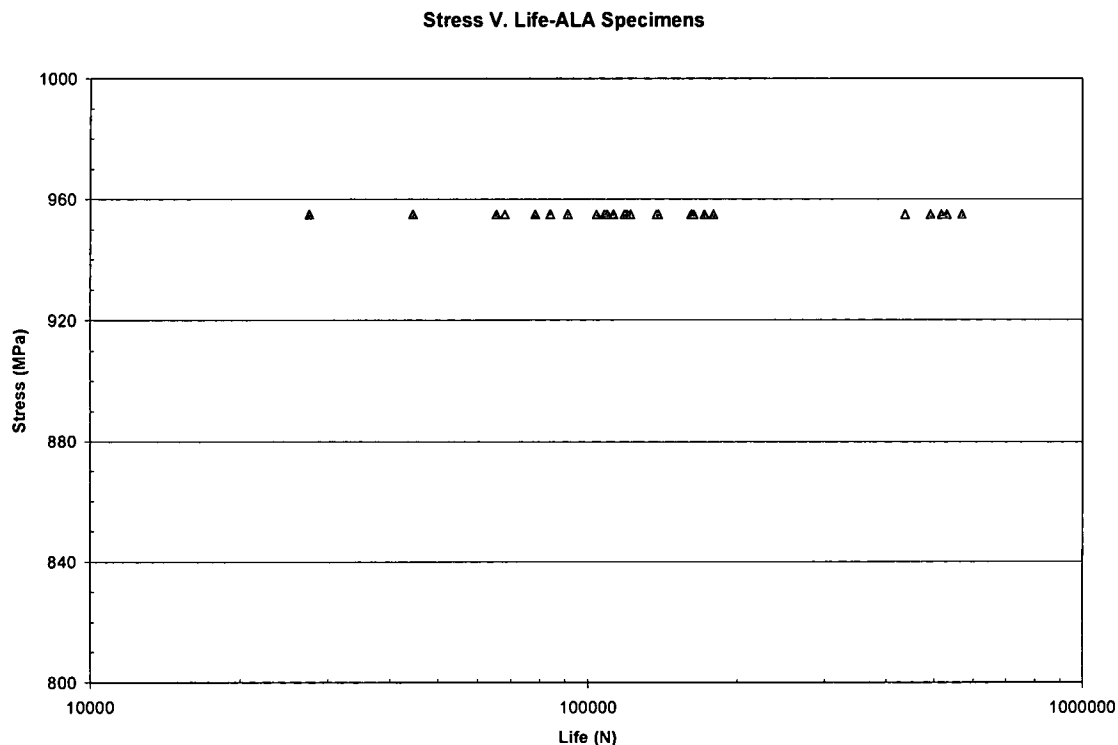


Figure 13. Fatigue data for ALA specimens, 538° C, $R=0.05$, 1 Hz

Figure 14 compares the data from both sets of specimens. Besides the five ALA specimens with lives of over 400,000 cycles, the ALA specimens have on average a shorter life expectancy than the non-ALA specimens. Four of the five long-life specimens came from two blanks that were next to each other as they came from the billet (06-112, 06-113, 06-114, and 06-116) and were blanked away from the rest of the ALA blanks (see Figure 5). Two of those were the only truly internal initiation sites from the ALA material (06-112 and 06-113). All the rest of the initiation sites were surface or very near surface initiations (within 100 microns—data in Appendix C). This peaks curiosity in the differences of the grain structure between those

- blanks and the others tested. Therefore the five long-lived ALA specimens are not a simple population that represents an internal initiation site, as found by Jha [12] in a titanium aluminide, since these are a mix of internal, near surface, and surface.

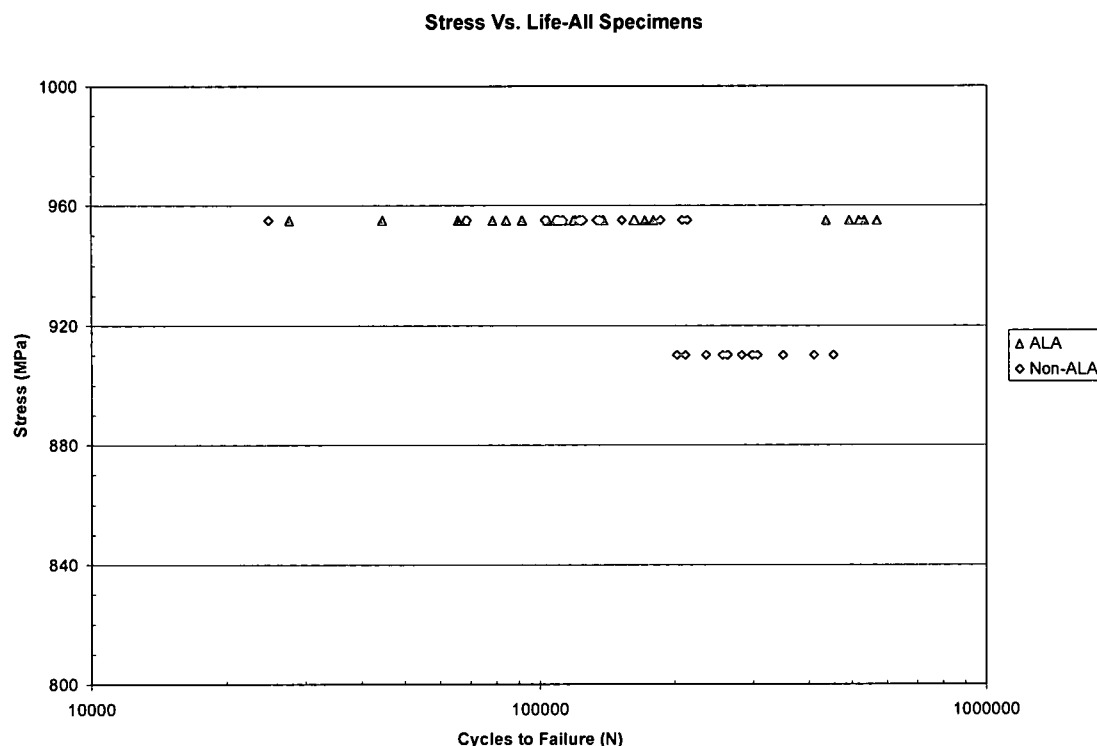


Figure 14. Fatigue data for all specimens, 538° C, $R=0.05$, 1 Hz

Plotting the fatigue results from figure 14 as a cumulative distribution function, figure 15, shows some interesting trends. First, the ALA containing material clearly separates into two distinct populations like earlier work of Jha and Caton [13, 14] with the two outliers forming, maybe, a third population. Clearly the right most population includes the internal initiation specimens where the crack would effectively grow in a vacuum

where the crack growth will be significantly reduced [15]. However, some of these specimens failed at the surface. The CDFs of the non-ALA specimens do not show this right (long life) population, but the samples tested at a maximum stress of 955 MPa did show the short life population. It appears that in both cases, ALA and non-ALA, that the shortest life specimens must have had an earlier initiation than the majority of the specimens. Finally, the slope of the majority of the ALA containing specimens is shallower than that of either of the non-ALA specimens, which have a similar slope at both 910 and 955 MPa maximum stress. This indicates that the inherent fatigue variability of the ALA material is higher than the non-ALA material.

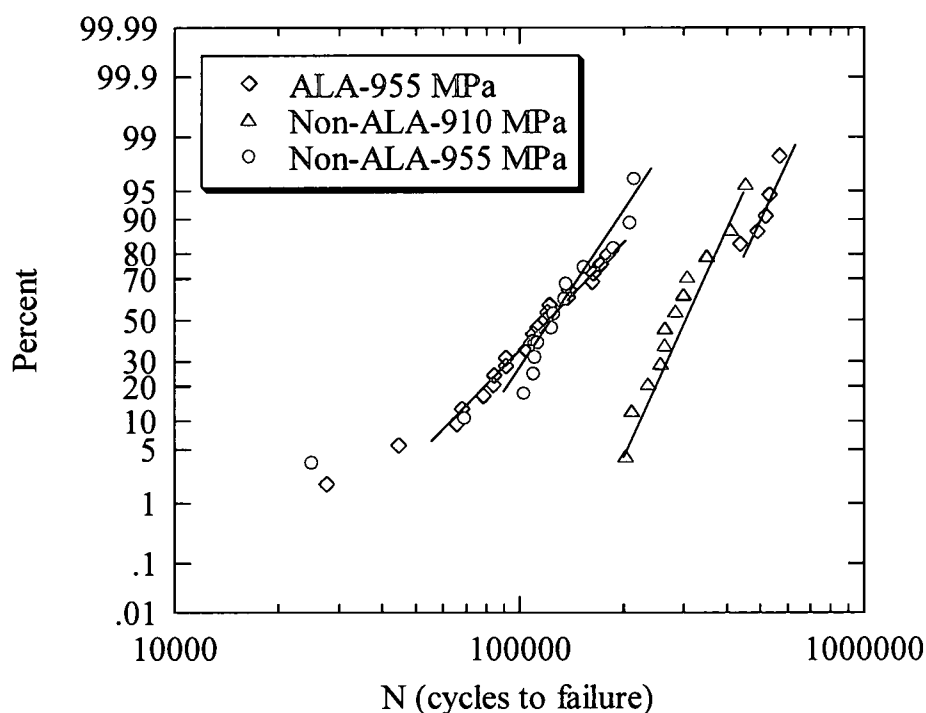


Figure 15. A CDF representation of fatigue data.

Figures 16, 17, 18, and 19 show side-by-side comparisons of specimen fracture surfaces, investigating the similarities and difference between short and long life specimens, different long life behaviors, and ALA and non-ALA specimens. Figure 16 shows the shortest life ALA specimen (06-115) and shortest life non-ALA specimen (06-020). Although they have very similar lives, the initiation sites have different appearances. Each is a surface initiation and has a feature of about 200 μm size, but 06-020 shows a very flat initiation site, which not only differs from 06-115, but also from most of the non-ALA specimens.

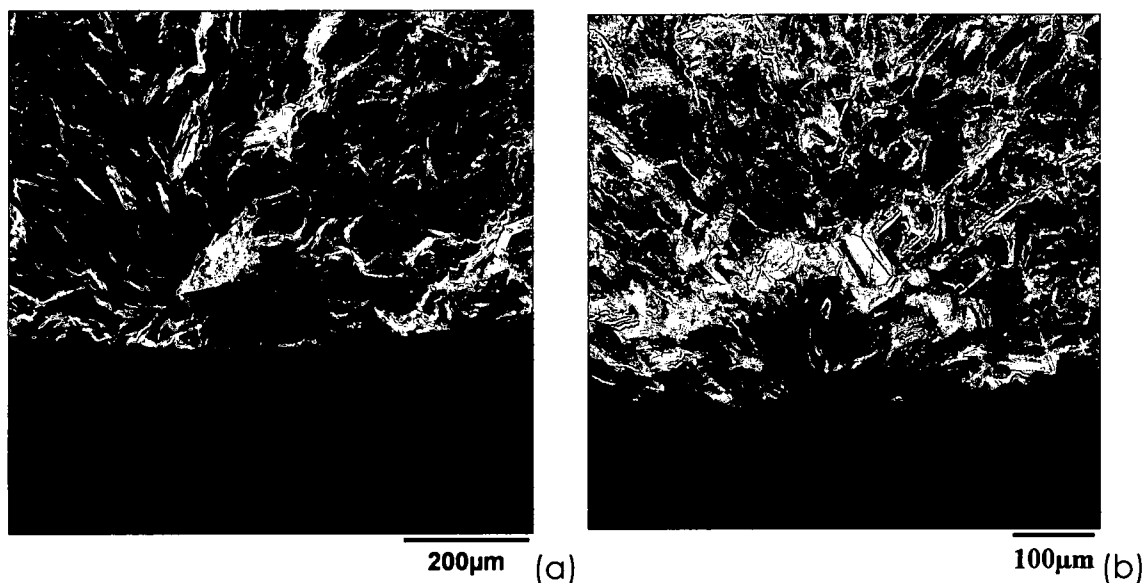


Figure 16. The shortest life (a) ALA specimen 06-115, $N=27,570$ cycles, 150X and (b) non-ALA specimen 06-020, $N=24,852$ cycles, 200X

Figure 17 again shows ALA specimen 06-115, but compares it with a long life specimen, 06-116. Each has a similar initiation site, except the initiating grain for 06-116 is approximately half the diameter of 06-115. This raises interesting questions as to whether reducing the size of the initiating

grain by one half could increase the life of the specimen by nearly 16 times, and whether there was a difference in microstructure that lead to this vast difference in specimen life.

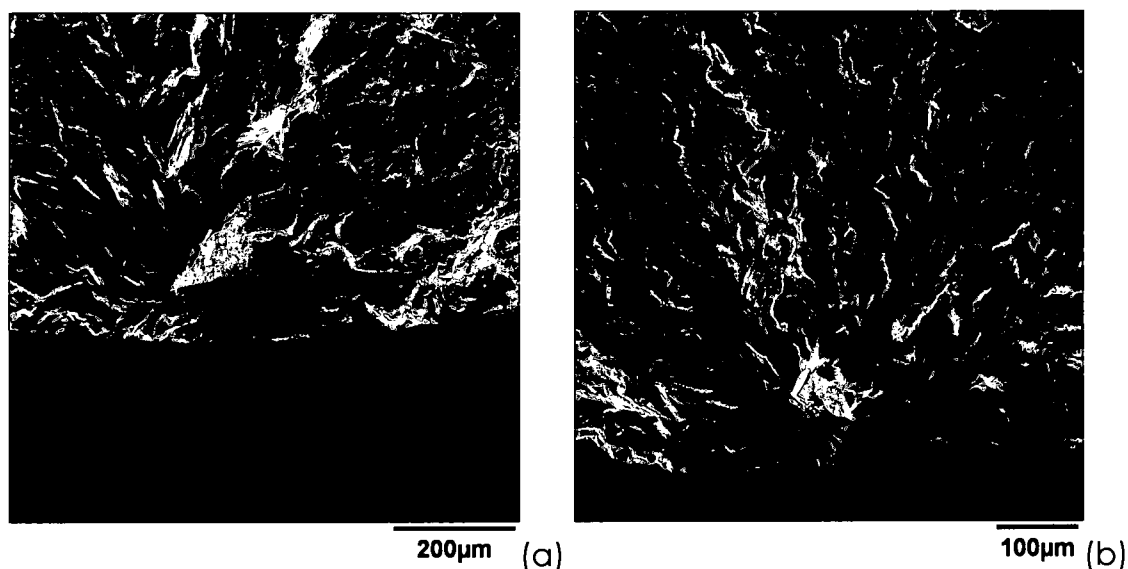


Figure 17. The shortest life (a) ALA specimen 06-115, N=27,570 cycles, 150X and a long life (b) ALA specimen 06-116, N=437,451 cycles, 200X

Figure 18 shows two of the long life ALA specimens, 06-112 and 06-114. These two specimens had very similarly sized initiating grains and very similar life lengths, but 06-114 initiated on the surface and 06-112 initiated approximately 750 μm from the surface, with completely internal crack growth. Convention would lend to an internal initiation specimen having a much longer crack growth life than a surface initiation specimen. Therefore the crack must have initiated much later in 06-114. Once again this raises the question of differences in the microstructure between two specimens that came from the same blank of material from the billet.

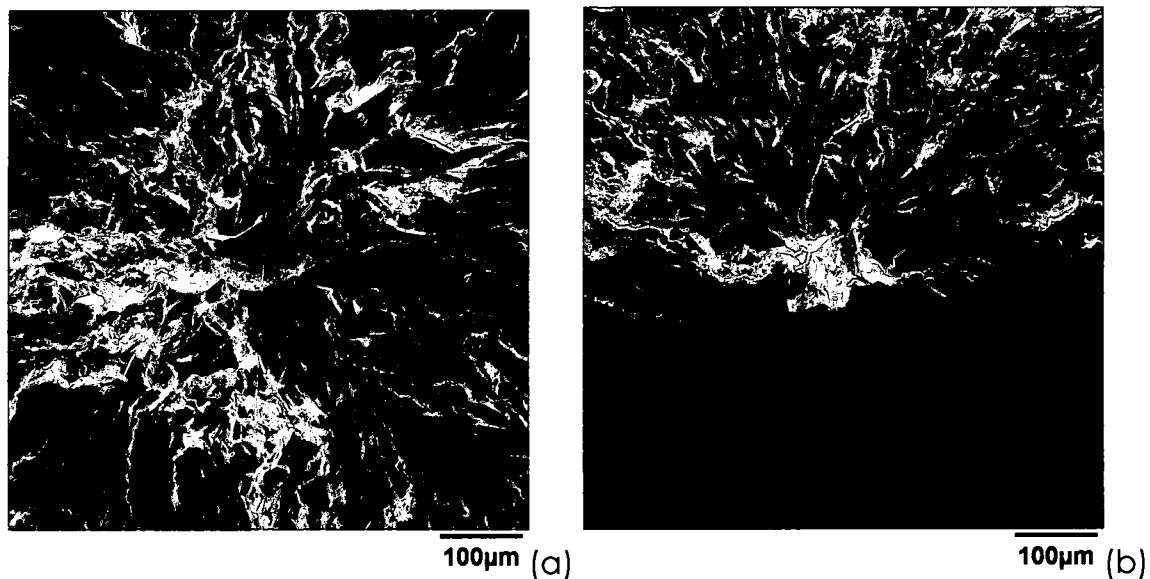


Figure 18. Two different long life ALA specimens (a) 06-112, N=531,310 cycles, 200X and (b) 06-114, N=517,296 cycles, 200X

Figure 19 compares shortest life non-ALA specimen 06-020 and longer life non-ALA specimen 06-026. Each shows similar surface initiation behavior and 06-026 shows a larger, ALA-like grain initiation site. This does not correlate with 06-026 having a life over eight times longer than 06-020.

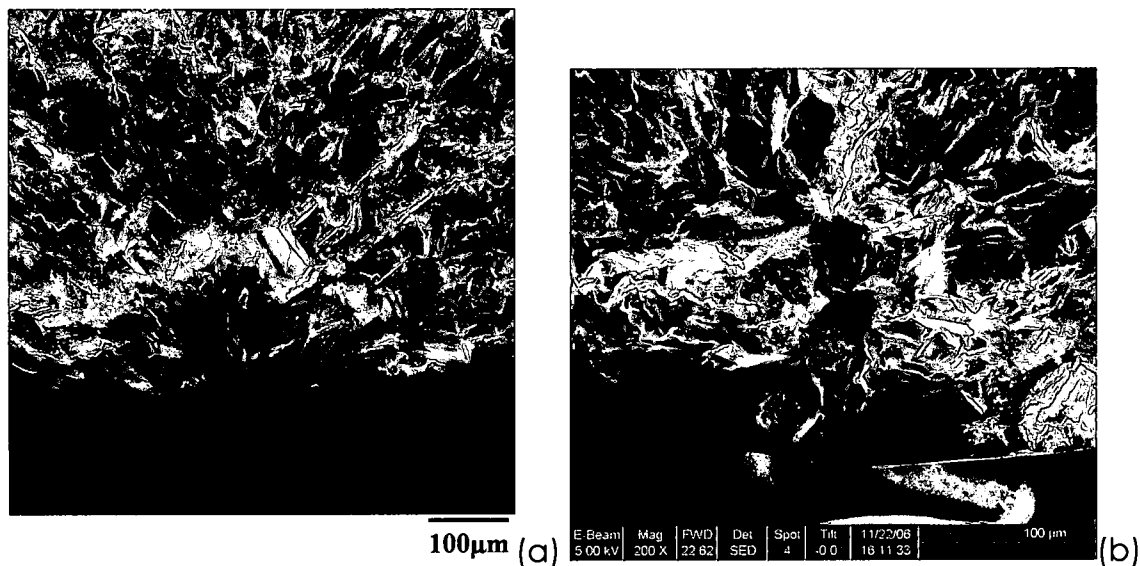


Figure 19. Shortest life non-ALA specimen (a) 06-020, N=24,852 cycles, 200X and longer life non-ALA specimen (b) 06-026, N=207,859 cycles, 200X

3.2.1 Replica Results

Replicas were taken on eight specimens- four ALA and four non-ALA specimens at 955 MPa. One of the ALA specimens was an internal initiation site (06-113), so there was no valid data collected during that replica process. This does indicate that the replication process does not adversely affect the fatigue characterization of the material. As shown in Figure 20, the specimens that were replicated had lives that were within the normal scatter of the representative material.

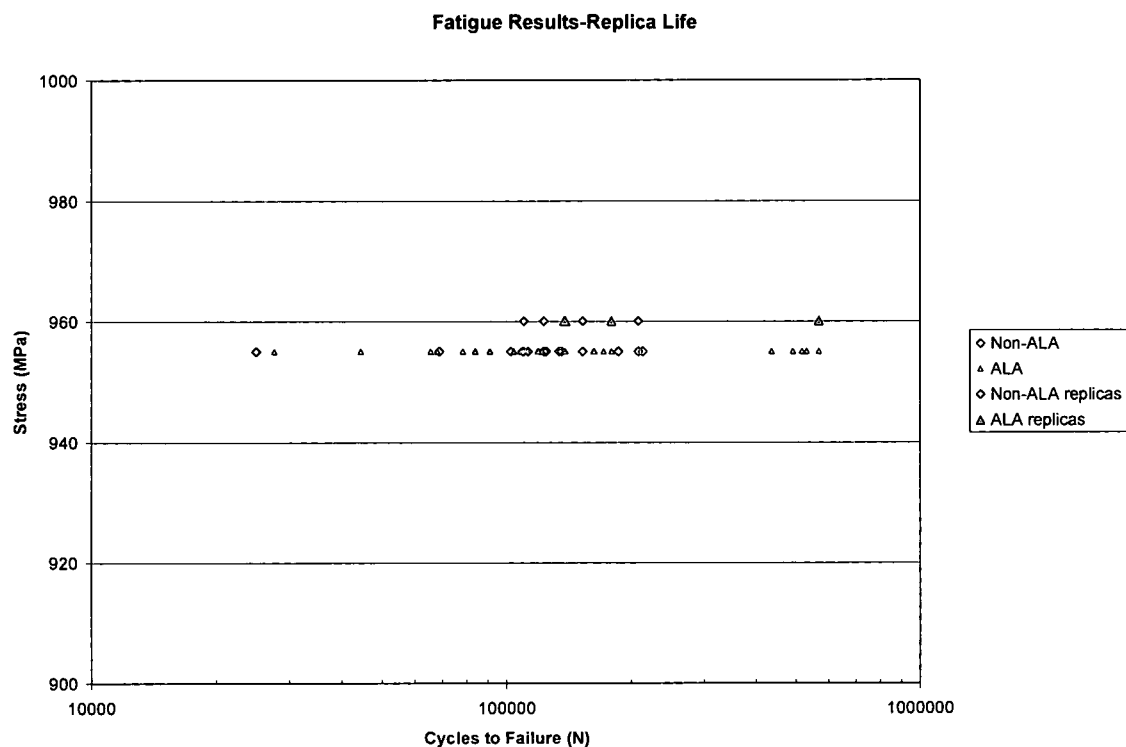


Figure 20. Fatigue results with replica specimens segregated.

For the other ALA specimens (06-121, 06-131, and 06-139) and non-ALA specimens (06-011, 06-014, 06-024, 06-026), the crack data is shown in Table 4.

Specimen 06-014 was six cycles away from final failure when stopped for the last set of replicas and is probably the best example of crack growth. 06-014, like all the other replica samples, did not show signs of crack growth until the second to last set of replicas taken. The second to last set was taken at 100,000 cycles, and final fracture was 100,006 cycles later. During that time the crack grew from less than 200 microns to over two millimeters. The results from the replicas lend to a situation where crack initiation does not start from the first loading of the specimen but rather starts at some point when enough dislocations or cumulative plastic strain have built up to create a crack.

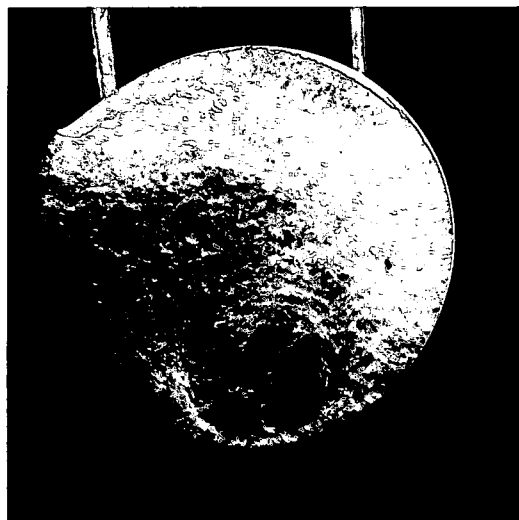
Table 4. ALA replica results.

| Specimen ID | 2nd to Last Replica | Last Replica | Cycles to Failure |
|-------------------------|-------------------------------------|---------------------------------------|-------------------|
| Non-ALA Material | | | |
| 06-011 | 110,000 | 120,000 | 122,719 |
| | no crack | 849 μm | |
| 06-014 | 100,000 | 110,000 | 110,006 |
| | 192 μm | 2,063 μm | |
| 06-024 | 140,000 | 150,000 | 152,658 |
| | no crack | no crack | |
| 06-026 | 190,000 | 200,000 | 207,859 |
| | no crack | no crack | |
| ALA Material | | | |
| 06-121 | 120,000 | 130,000 | 137,819 |
| | no crack | 151 μm | |
| 06-131 | 150,000 | 175,000 | 179,404 |
| | 78 μm | 706 μm | |
| 06-139 | 120,000 | 130,000 | 138755 |
| | no crack | 291 μm | |

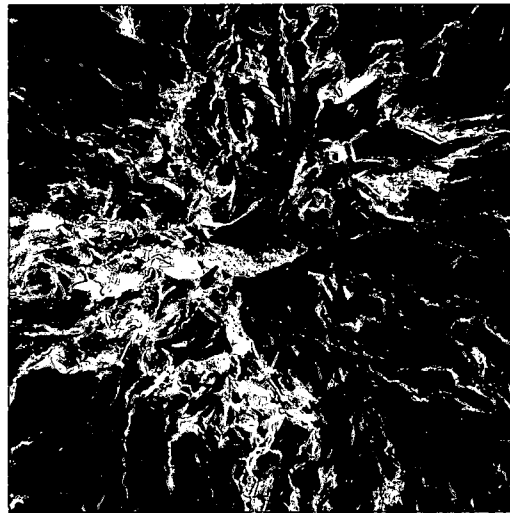
Notice that the maximum number of cycles that a specimen lasted with a measurable crack is 29,404 cycles, ALA specimen 06-131. This is remarkably close to the minimum lives for the ALA and non-ALA specimens, 27,570 and 24,852 cycles respectively. Therefore it appears that the left tail of the fatigue lifetime distribution could be correlated with immediate crack initiation and a life consisting completely of crack growth. This has been found to be the case in several other material systems, [13, 14] and appears to work for Waspaloy as well.

3.2.2 SEM Results

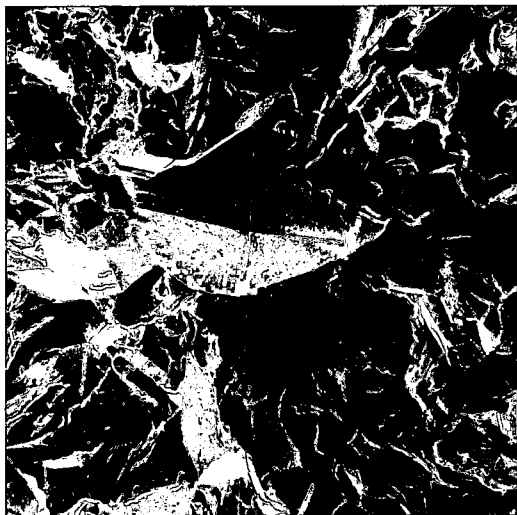
One of the fracture surfaces of all fifty-three of the fatigue specimens was removed with a diamond saw after the test was complete, cleaned and photographed on the scanning electron microscope (SEM). These images were used to determine the size and location of the crack-initiating grain. Photographs were taken at three different magnifications for each specimen: a low magnification (20X or 50X), a medium magnification (150X or 200X) and a high magnification (300X or 500X). The magnifications were based on the size of the crack-initiating grain (medium and high magnifications) and the SEM used to take the images (low magnifications). At the medium and high magnifications, a stereo pair was also taken at a seven degree tilt. Two samples are shown below in Figures 21 and 22. One magnification of each specimen (medium) is catalogued in Appendix A.



1mm (a)



100μm (b)



60μm (c)

Figure 21. SEM pictures of ALA sample 06-112 at (a) 20X, (b) 200X, and (c) 500X.

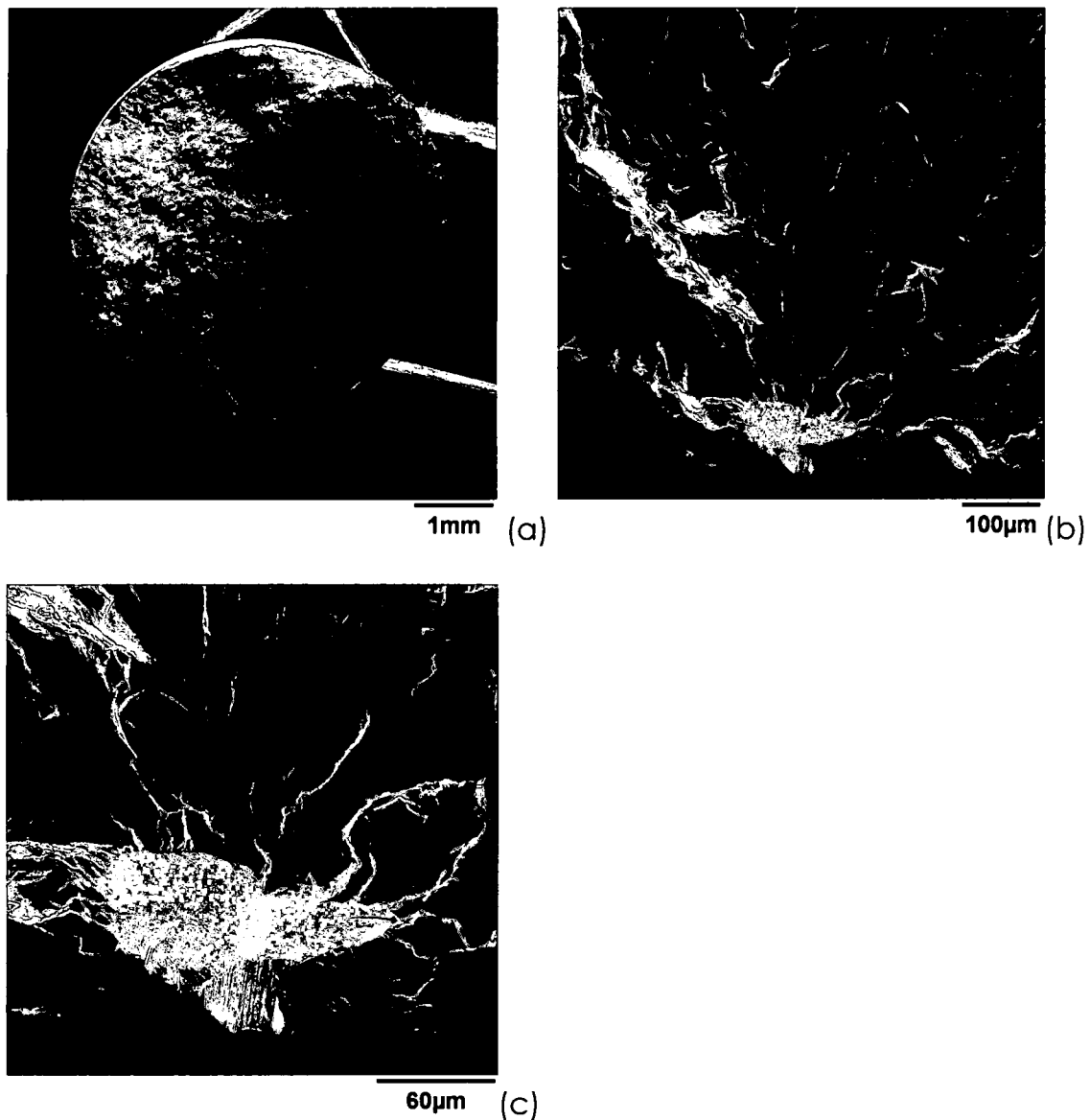


Figure 22. SEM pictures of non-ALA sample 06-025 at (a) 20X, (b) 200X, and (c) 500X.

A summary of the fatigue initiation sites for all the specimens is presented in Appendix C showing the sample number, stress level, cycles to failure, test machine, initiation location, distance of initiation from surface, and location of specimen as it was machined from the billet (billet location information in Appendix D).

3.2.3 MEX Results

Each of the SEM photographs taken as stereo pairs were then loaded into a program called MeX [9] that created a digital elevation map (DEM) of the fracture surface. This was done to better understand the texture of the grains because the two-dimensional pictures can be and were somewhat misleading, as shown in Figures 23 and 24.

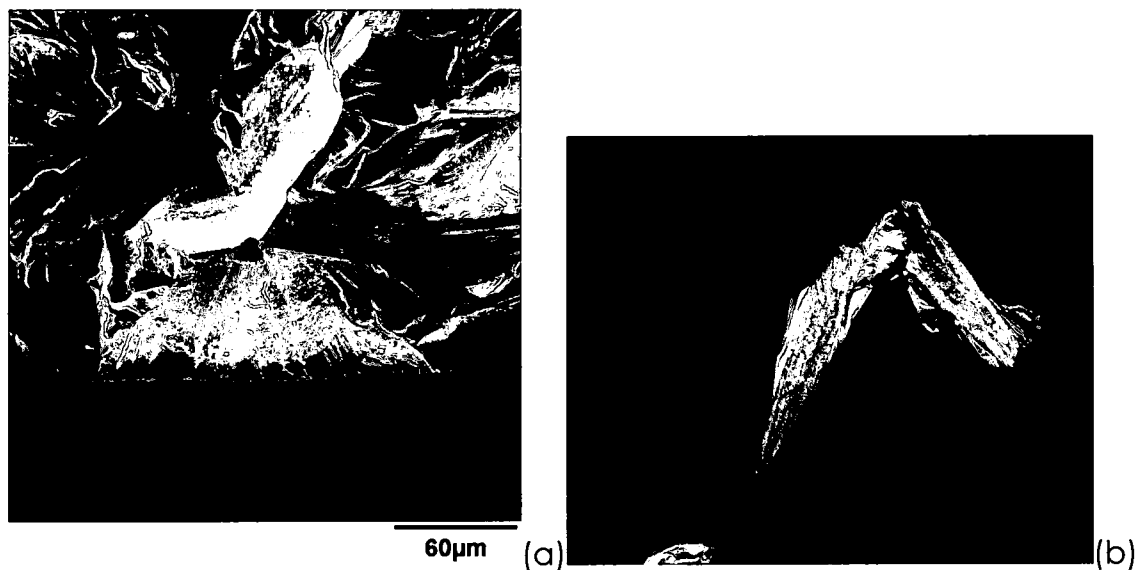


Figure 23. (a) SEM image and (b) corresponding DEM for ALA specimen 06-132.

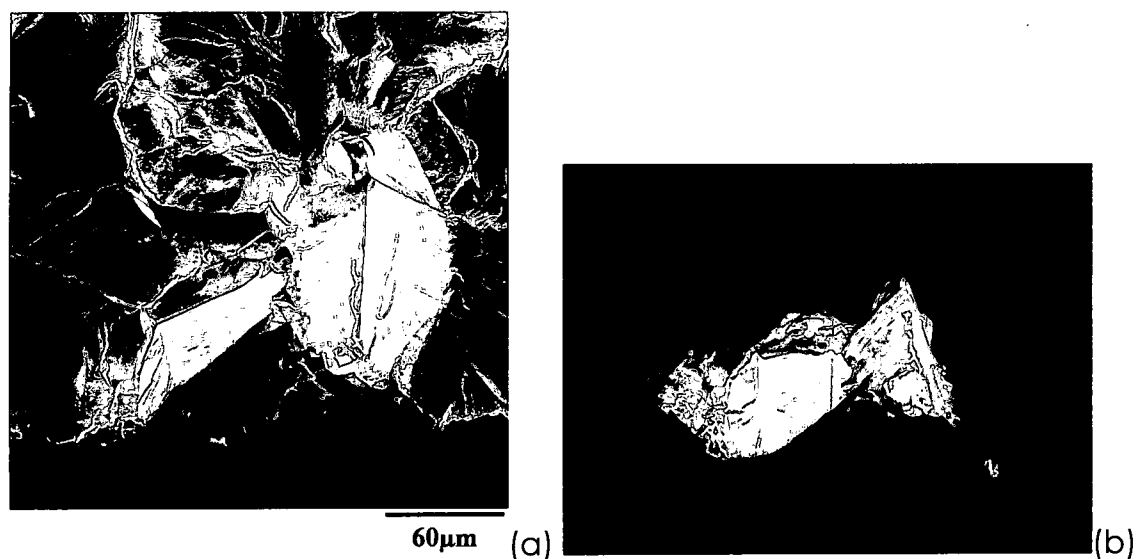
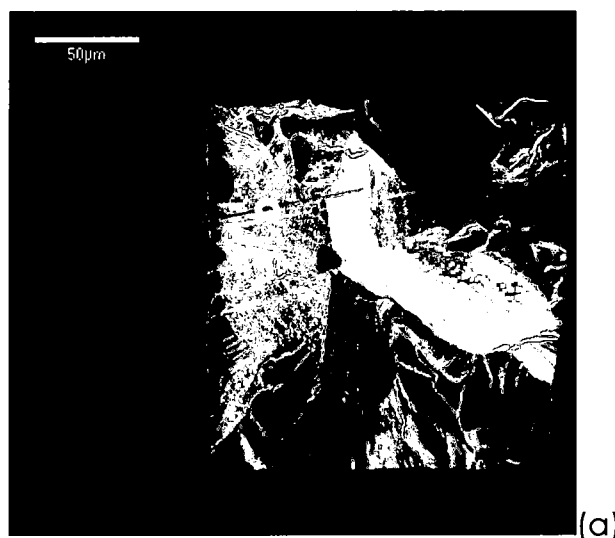
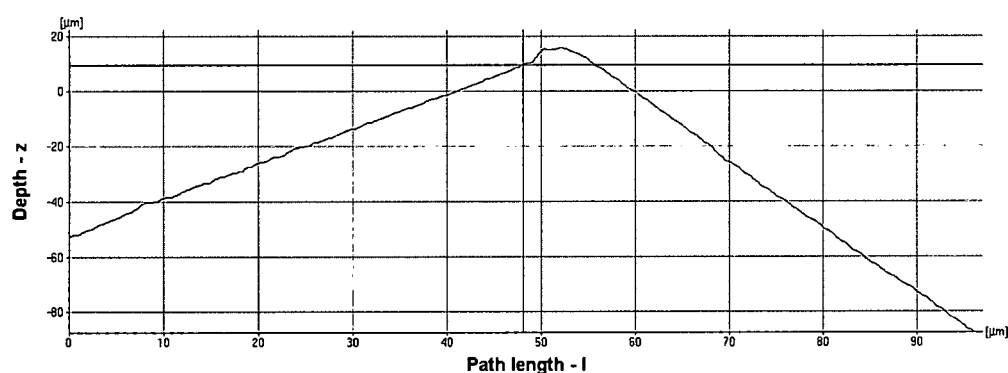


Figure 24. (a) SEM image and (b) corresponding DEM for non-ALA specimen 06-021.

A trace could also be taken across any area of interest and a graphical representation of the length of the trace compared to the elevation of the surface along the trace, as seen in Figure 25. This could provide useful data as to the slip character that causes crack initiation, but was considered beyond the scope of this project and was not conducted on each specimen.



(a)



(b)

Figure 25. (a) Trace taken on surface of grain and (b) corresponding graphical representation for ALA specimen 06-132.

3.3 Discussion

3.3.1 Crack Initiation Behavior

Based on the information collected from the replica tests and corresponding SEM images, in general, cracks required a number of cycles to initiate and did not initiate at the beginning of the tests. Specimen 06-024 had no sign of crack growth on the surface of the specimen up to approximately 2,700 cycles before final fracture, even

though the initiating grain was on the surface of the sample. However sample 06-014 and 06-131 showed cracks 10,006 and 29,404 cycles, respectively, before failure. As noted previously, this indicates conclusively that the shortest life specimens in both ALA-containing and non-ALA specimens could initiate very early in life, or be assumed to initiate immediately.

3.3.2 Small Crack Growth

Once the crack in any given specimen began, it did not take long for the specimen to reach final fracture. The critical crack length for the specimens seemed to be between 1.5 and 2 millimeters (see example in Figure 16(a)). A careful examination of the replication data shows some of the variability in the small crack growth rates. Cracks were found in the ALA material at small sizes ranging from 78 μm to 291 μm . As expected, the sample with the shortest crack, 06-131 had the longest crack growth life, 29,404 cycles. However, specimen 06-121 required 7,819 cycles to grow a 151 μm crack to failure while specimen 06-139 required 8,755 cycles to grow a larger, 291 μm crack, to failure. This gives insight into the variability of the small crack growth rates. Additional (and time consuming) experiments would be required to accurately identify the range of small crack growth rates.

3.3.3 Effect of ALA Grains

The ALA grains had a mild effect on the life of the material. Based on the bounds of the "normal" material results from both the non-ALA and ALA material tested at 955 MPa, the life of the ALA material is about 35,000 cycles less than the non-ALA material. That is between a 15 and 20% decline in life. However, the minimum fatigue lives for the two materials are similar, 24,852 for non-ALA material and 27,570 for ALA material. Therefore the usable life for the two materials is similar and improved processing to completely eliminate ALAs will only have a benefit on average properties, not minimums.

CHAPTER 4

Summary and Conclusions

This thesis investigated the effect of ALA grains on the high temperature fatigue life of the nickel superalloy Waspaloy. This information is important for understanding the fatigue life of aerospace components currently in use. It is also important in determining the necessity of removing the ALA affected area. Currently this area is removed under the assumption that it has an adverse effect on the life. The material was characterized by performing several tensile on both the ALA material and the mid radius, non-ALA control material. Once characterized, a series of fatigue tests were run on both sets of material. Some of the fatigue specimens were monitored with a surface replication process. All of the specimens were photographed in stereo pairs with a SEM and analyzed for crack initiation and surface geometry.

Based on the tensile tests performed, it can be concluded that there is noticeable variability in yield strength of the ALA material and that at 538°C and a strain rate of approximately 0.008 s^{-1} , there was either: serrated yielding, grain boundary sliding, or dynamic strain aging. None

of the three were confirmed but it was most likely dynamic strain aging [11].

Based on the fatigue tests performed, several things can be concluded. There were possibly three (if the outliers are considered as their own group) groups in the ALA material: short life, the average material life, and the long life. The non-ALA material only had the first two groups. In the average material lives, the ALA had a shorter life than the non-ALA. In the short life, the lives of the ALA and non-ALA were very similar, and due to replica results, it is possible that the short-lived specimens have immediate crack initiation and crack growth the entire life of the specimen. Because of the short life data is similar for non-ALA and ALA specimens, the usable life for both materials is similar and it does not seem that improved processing would improve minimum properties. For the average materials and the long life materials, both ALA and non-ALA, cracks are initiating at some point during testing, and have relatively quick crack growth and small critical crack length.

CHAPTER 5

Recommendations for Future Work

5.1 Future Tensile and Fatigue Tests

When the edge specimens were originally blanked from the billet, several of them were considered unusable because they did not contain the ALA grains. This raises questions about processing. How much of the edge of the billet is actually effected by the ALA grains? What is different about the areas that do not contain these grains? Can the processing be altered to produce edge material that is ALA free for the entire circumference?

In the future, specimens taken from the ALA-free edge material may provide a better comparison as to what effect the ALAs have. These specimens would have the same overall fine grain size as the ALA specimens (ASTM 8), but would not have the ALA grains – making them a better control group of specimens. There might be an improved fatigue capability in these specimens which may help to explain the set of ALA specimens with considerably longer lives. It would also be interesting to investigate the differences in temperature and force between the two types of edge material during the actual forging process.

5.2 Detailed Microstructural Analysis

Due to time constraints and limited availability of equipment, no OIM analysis was performed. This leaves many questions about the statistics of the grain structure and orientation in each subset of the material. Since the initiating grains in the non-ALA material very closely resembled the initiating grains in the ALA material, it would be of interest to characterize how often grains with the ALA orientation occur in the non-ALA material. Knowing the differences in grain structure between the "average" ALA material, the shorter-life outliers, and the long-life ALA material may help explain the differences in life among the samples. The same is true for understanding the outliers in the non-ALA material. Also, having a general understanding of the grain orientation would provide information on the processing and consequent grain formation.

5.3 Model Approaches to Link Material Processing to Behavior (Vextec)

A company named VEXTEC Corporation, largely under Department of Defense funding, has produced a prognosis tool, VPS-MICRO™, to predict total life of different aerospace components. It predicts crack nucleation and growth, and was tested on Waspaloy [16]. Taking the material parameters collected during this project and using VEXTEC's model to see if the fatigue data agrees with it would further verify their mechanistic

modeling and possibly provide an alternative to lengthy mechanical test programs.

5.4 Fracture Surface Analysis

The initiation sites in many of the specimens indicated a similar crystallographic nature. More detailed MeX analysis or MeX analysis with true crystallographic orientation information from an OIM technique could help to understand the initiation processes in Waspaloy. For example, using MeX's tracing option, it could be possible to calculate angles between the initiating grain's surfaces and determine orientation and the slip planes where the cracks are propagating.

Appendix A

SEM Images of Specimens

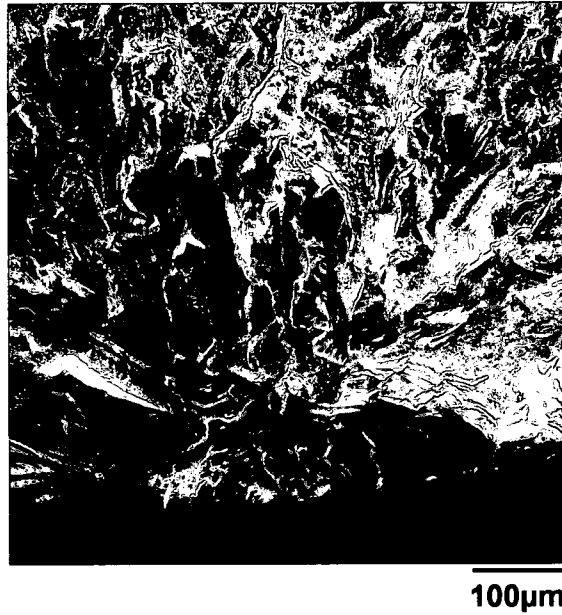


Figure 26. 06-000 at 200X

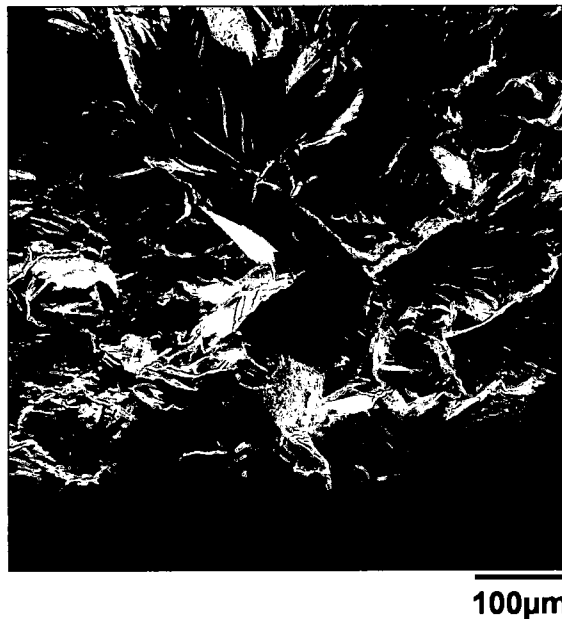


Figure 27. 06-002 at 200X

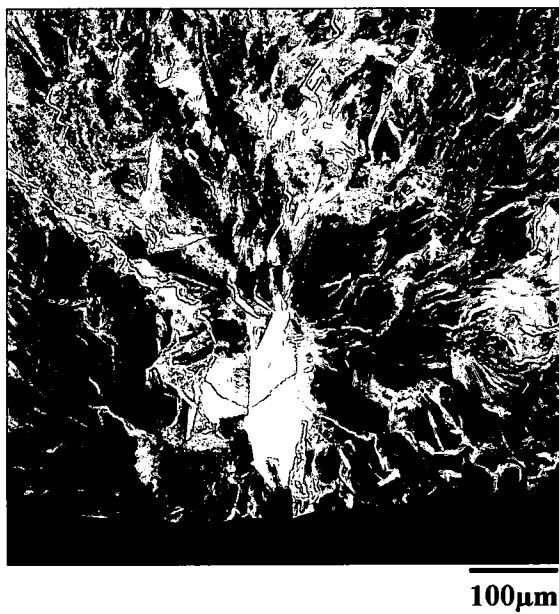


Figure 28. 06-003 at 200X

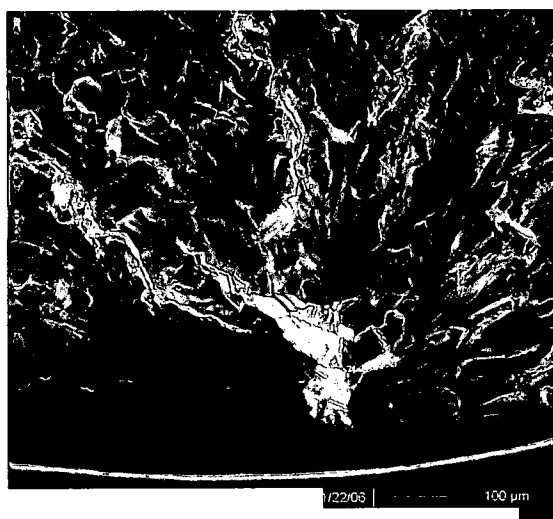


Figure 29. 06-004 at 200X

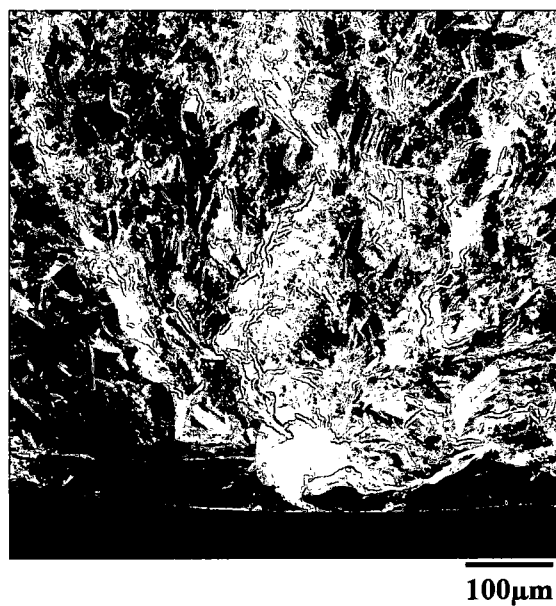
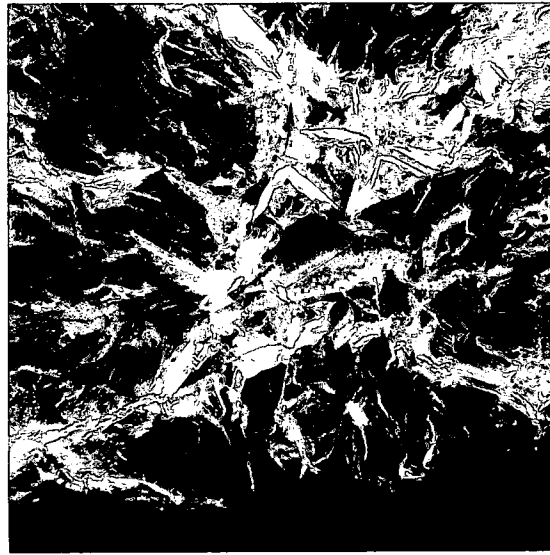


Figure 30. 06-005 at 200X

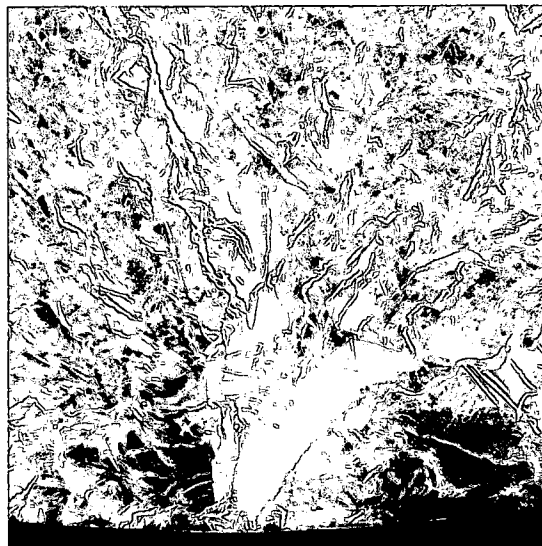


Figure 31. 06-006 at 200X



100μm

Figure 32. 06-008 at 200X



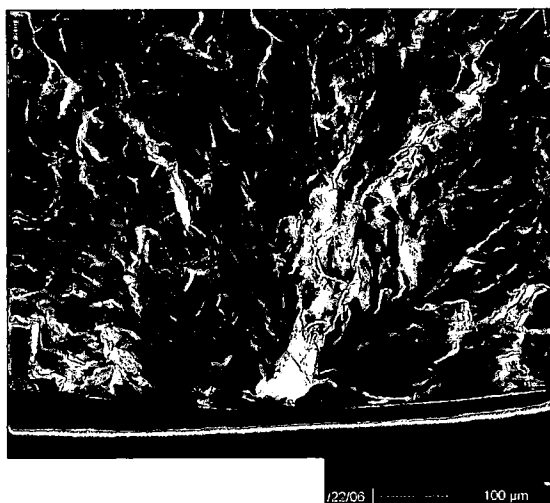
100μm

Figure 33. 06-009 at 200X



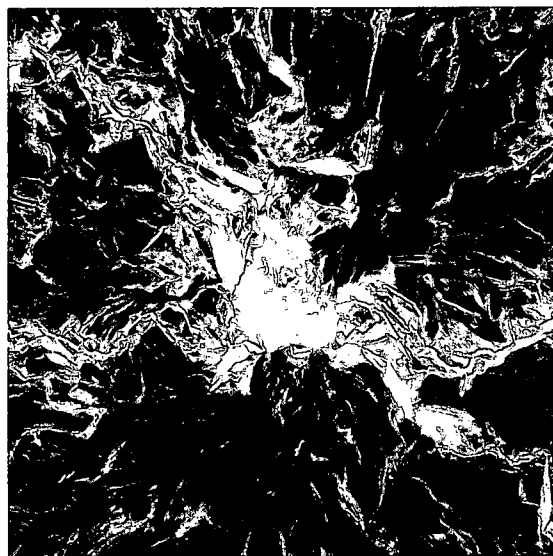
100μm

Figure 34. 06-010 at 200X



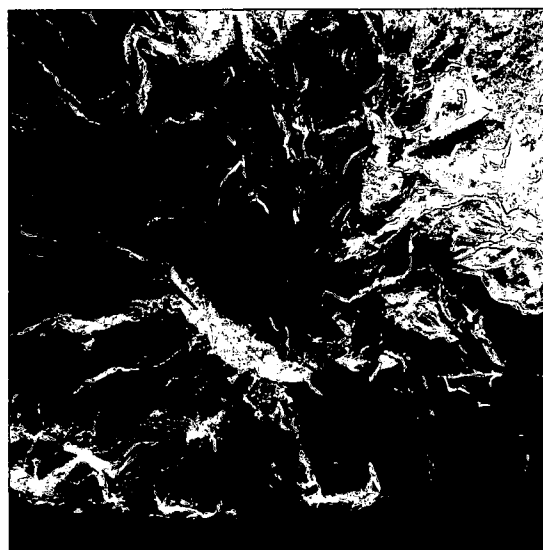
1/23/08 100 μm

Figure 35. 06-011 at 200X



200μm

Figure 36. 06-012 at 150X



100μm

Figure 37. 06-013 at 200X

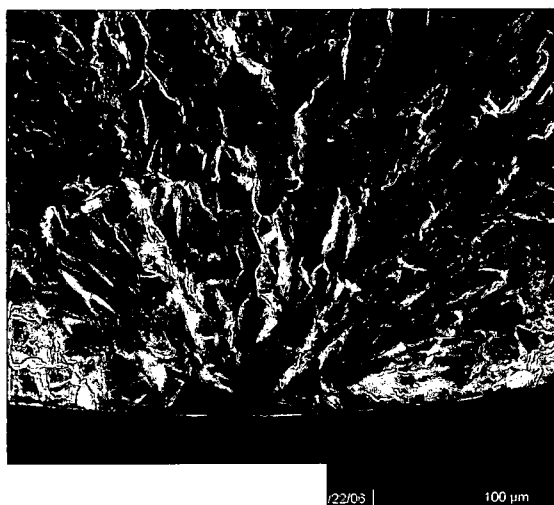


Figure 38. 06-014 at 200X

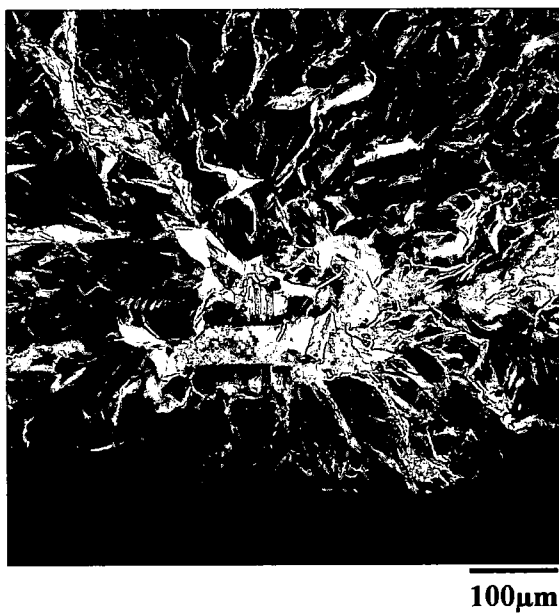
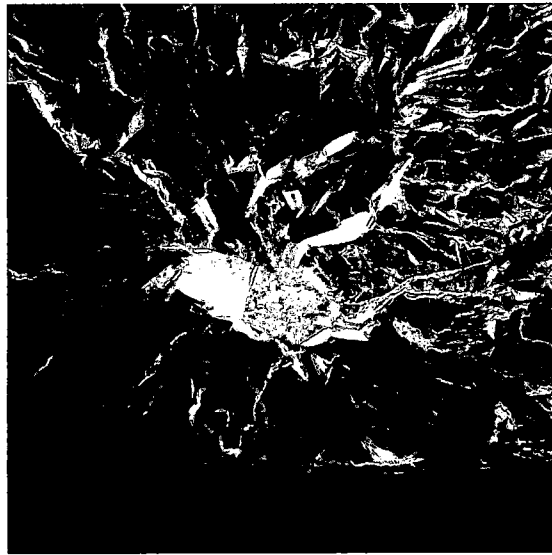
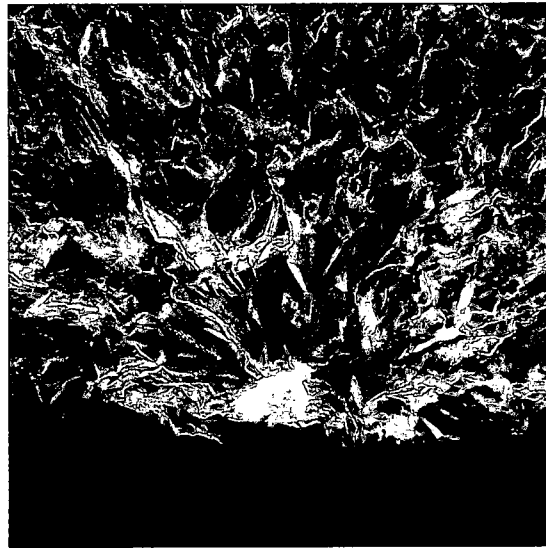


Figure 39. 06-015 at 200X



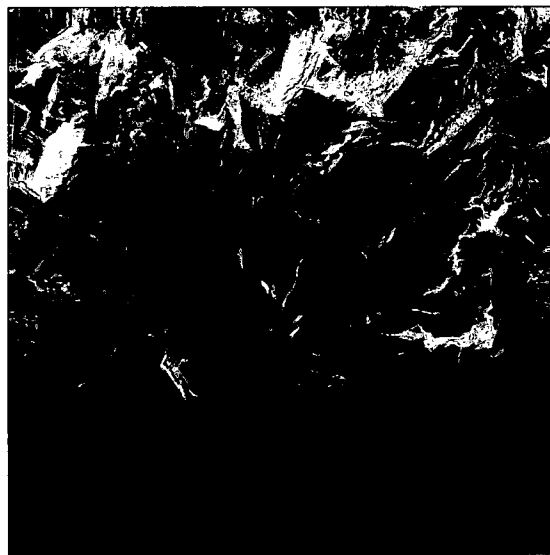
100μm

Figure 40. 06-016 at 200X



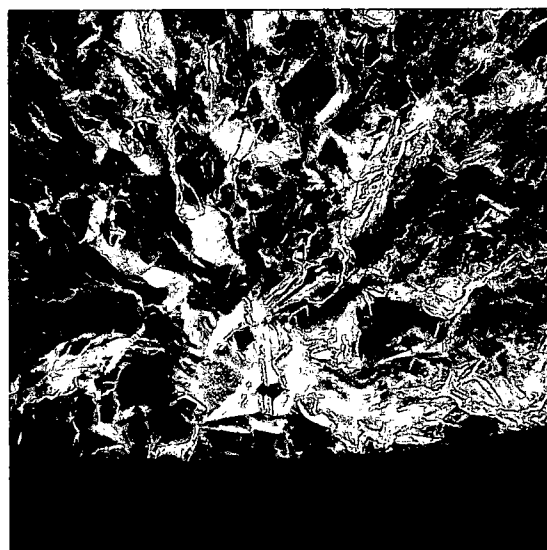
100μm

Figure 41. 06-017 at 200X



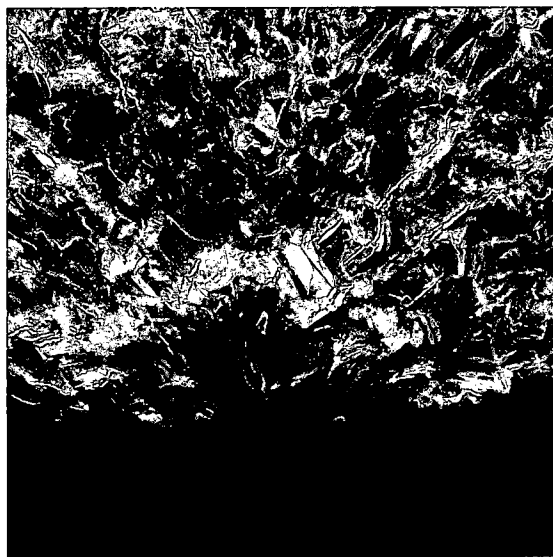
100μm

Figure 42. 06-018 at 200X



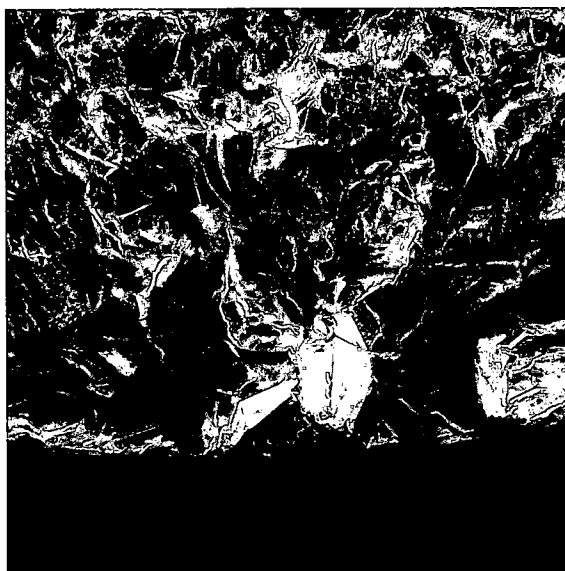
100μm

Figure 43. 06-019 at 200X



100μm

Figure 44. 06-020 at 200X



100μm

Figure 45. 06-021 at 200X

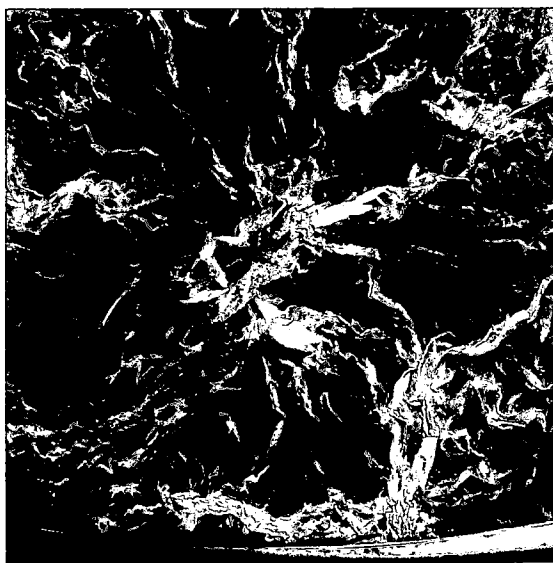


Figure 46. 06-023 at 150X

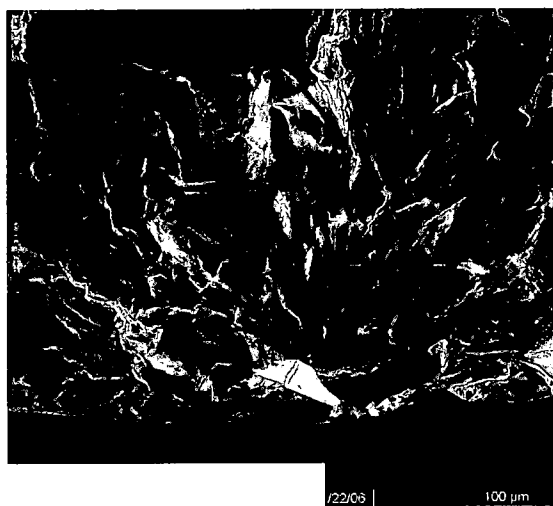


Figure 47. 06-024 at 200X

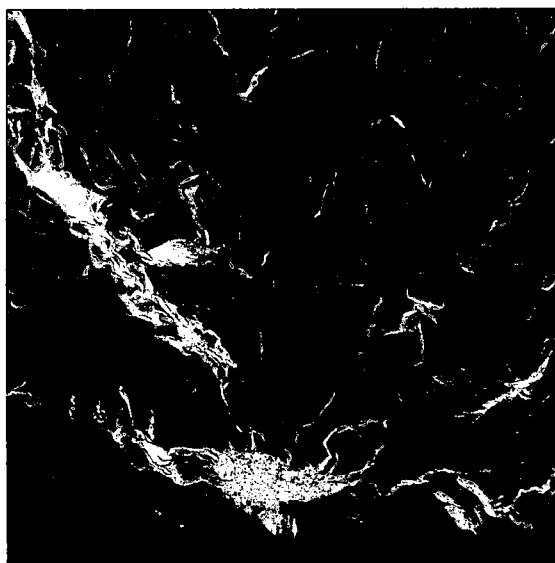


Figure 48. 06-025 at 200X

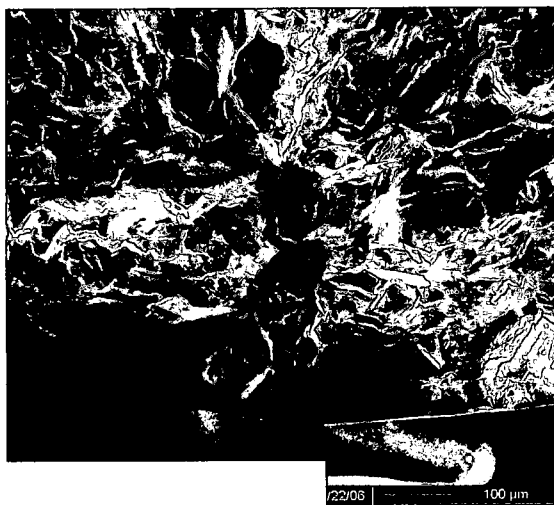


Figure 49. 06-026 at 200X

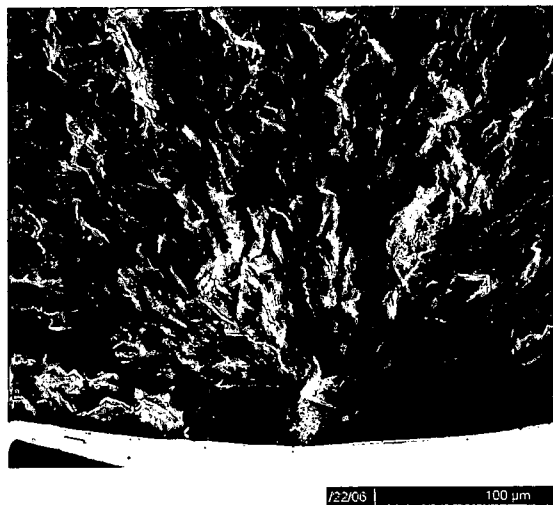


Figure 50. 06-027 at 200X

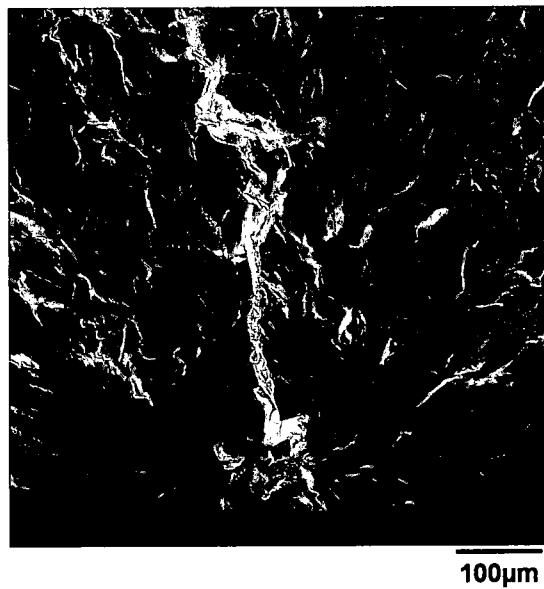
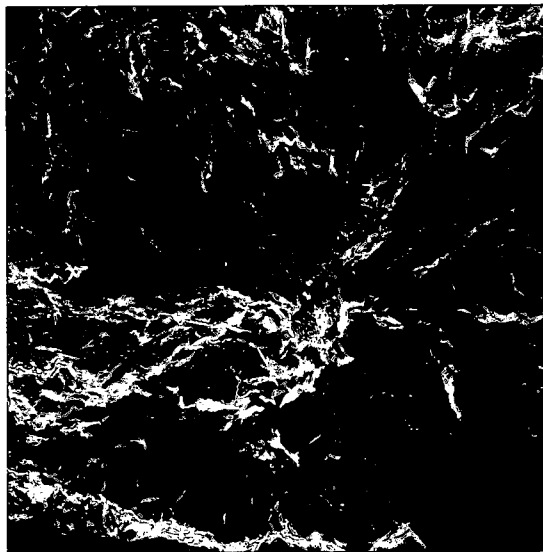


Figure 51. 06-029 at 200X



100µm

Figure 52. 06-112 at 200X



200µm

Figure 53. 06-113 at 150X

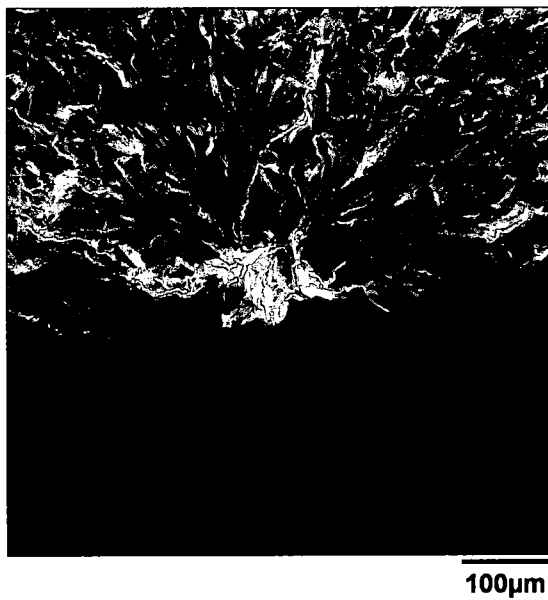


Figure 54. 06-114 at 200X

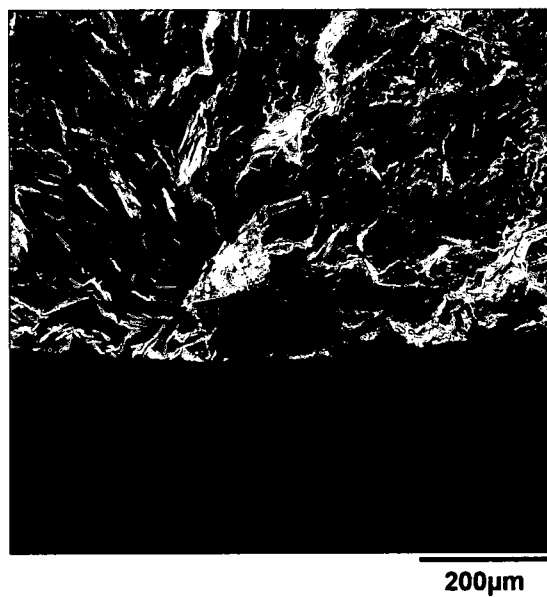
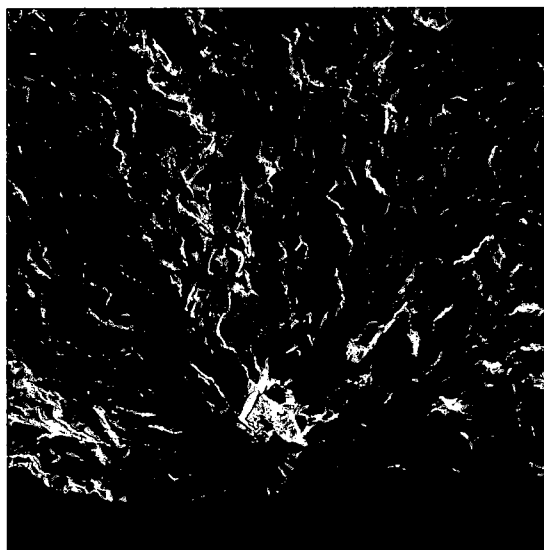
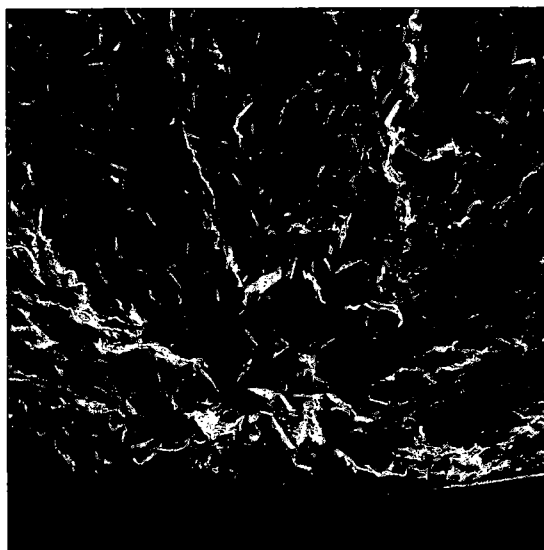


Figure 55. 06-115 at 150X



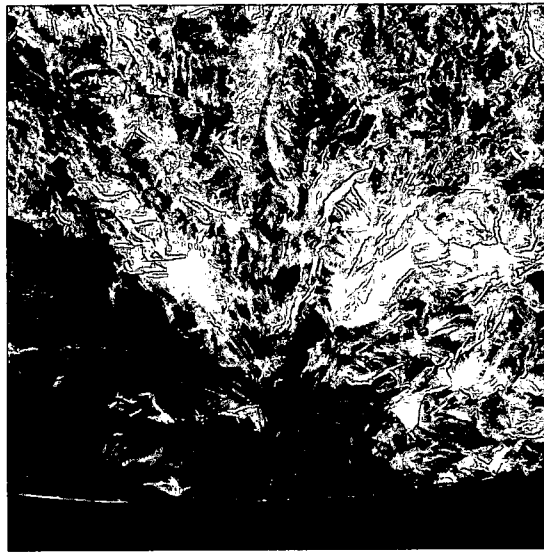
100µm

Figure 56. 06-116 at 200X



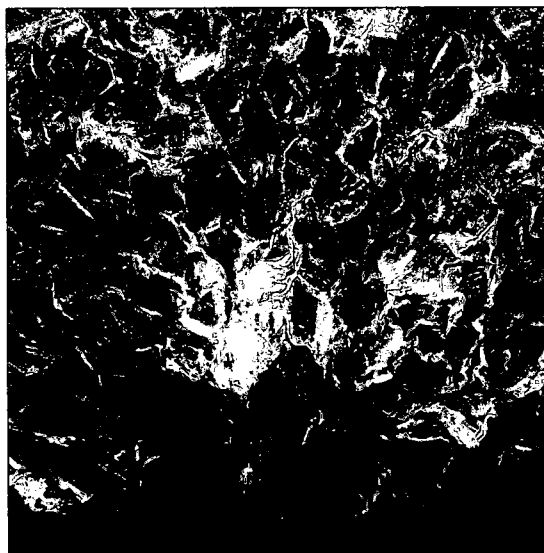
100µm

Figure 57. 06-117 at 200X



100µm

Figure 58. 06-118 at 200X



200µm

Figure 59. 06-119 at 150X

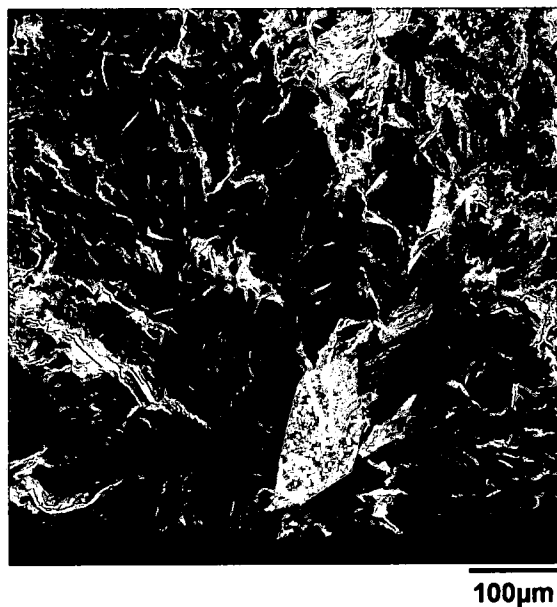


Figure 60. 06-120 at 200X

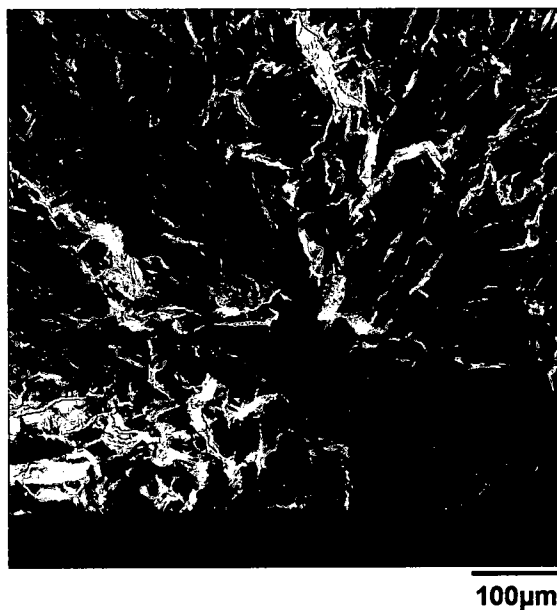
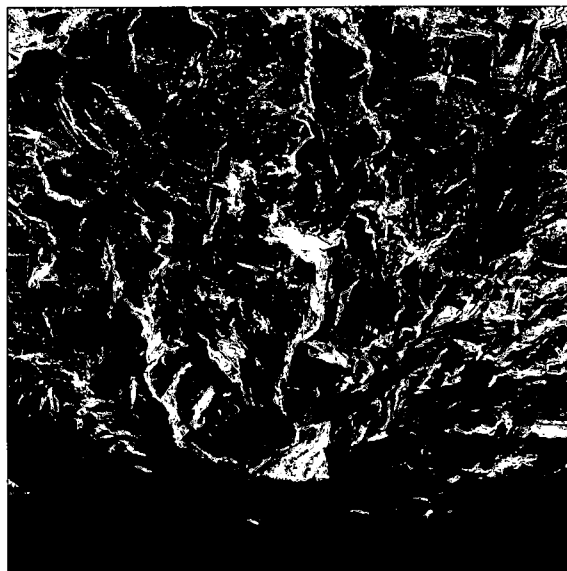
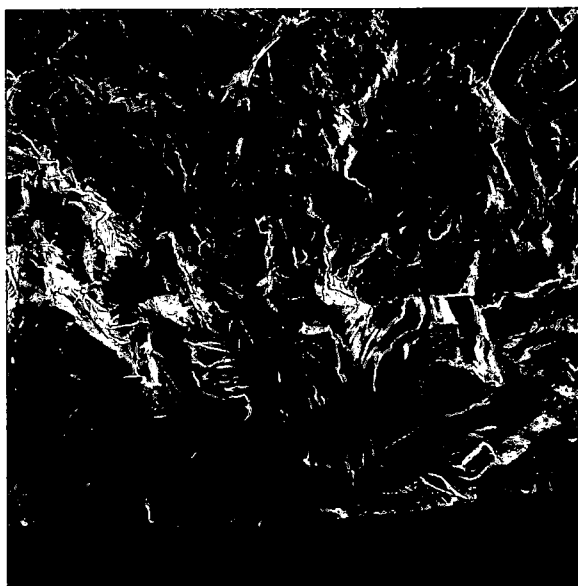


Figure 61. 06-121 at 200X



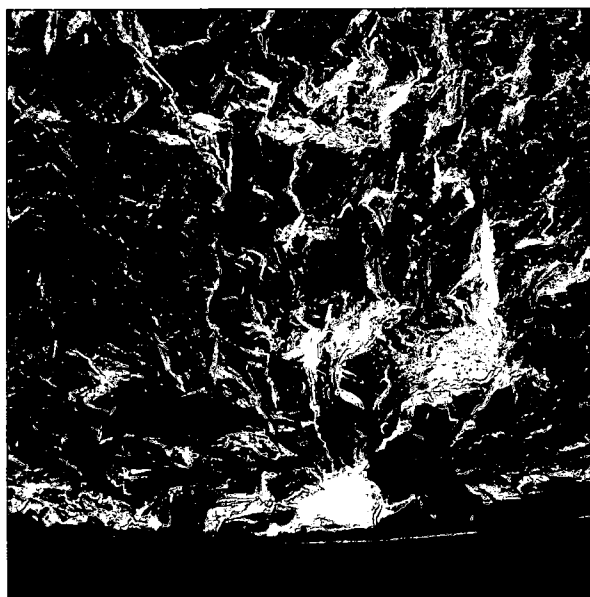
100μm

Figure 62. 06-122 at 200X



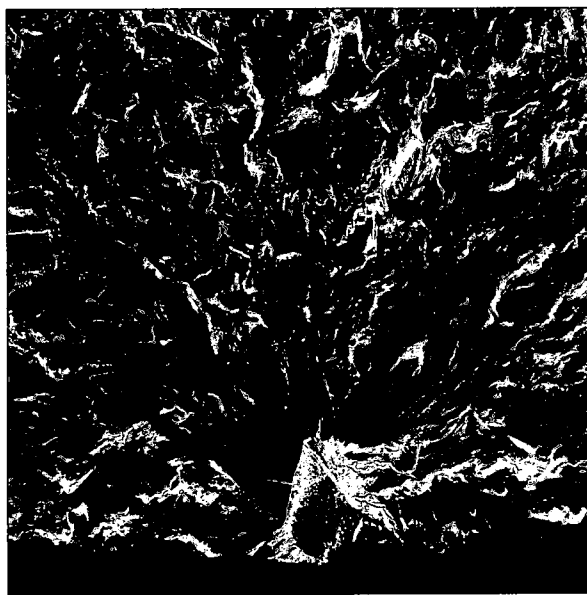
100μm

Figure 63. 06-123 at 200X



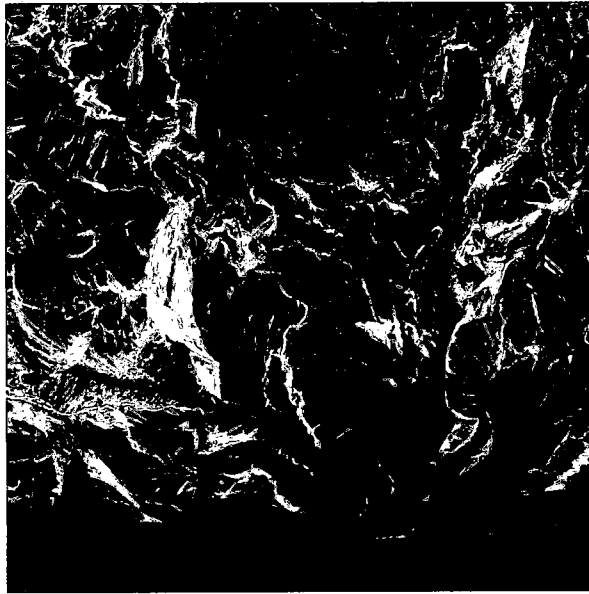
200μm

Figure 64. 06-125 at 150X



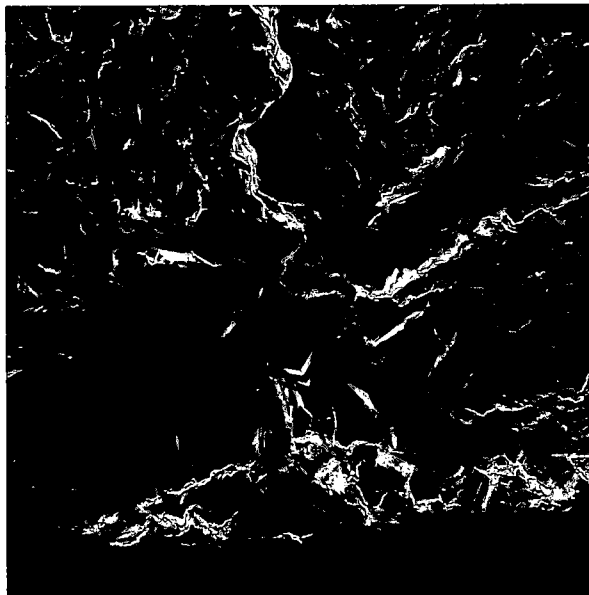
200μm

Figure 65. 06-126 at 150X



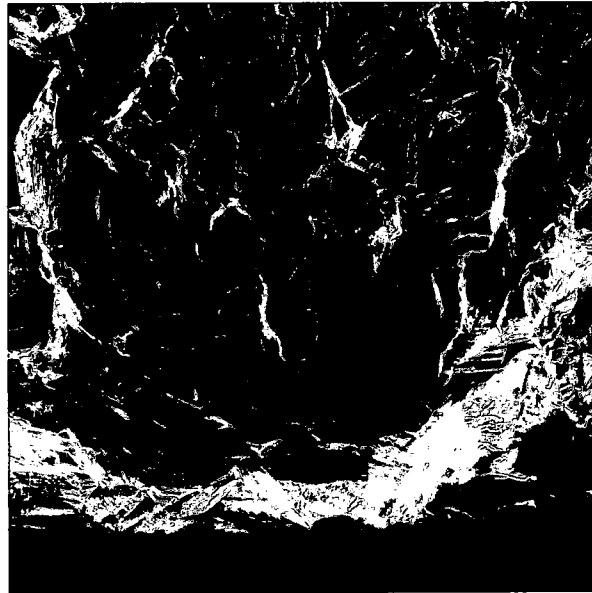
100μm

Figure 66. 06-127 at 200X



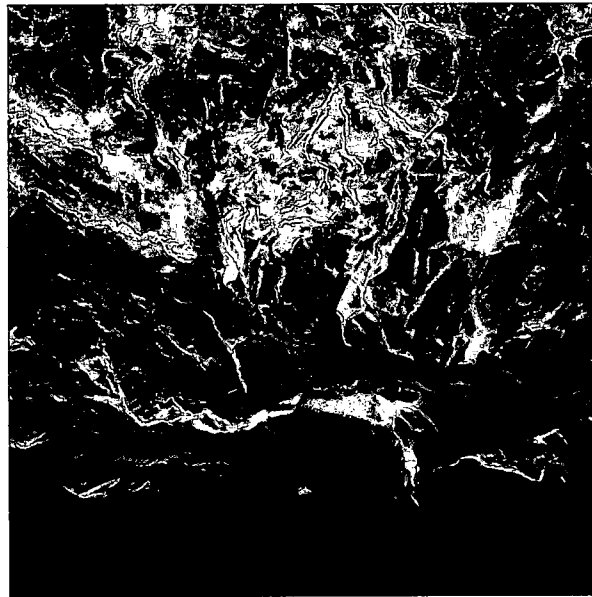
100μm

Figure 67. 06-128 at 200X



100μm

Figure 68. 06-130 at 200X



200μm

Figure 69. 06-131 at 150X

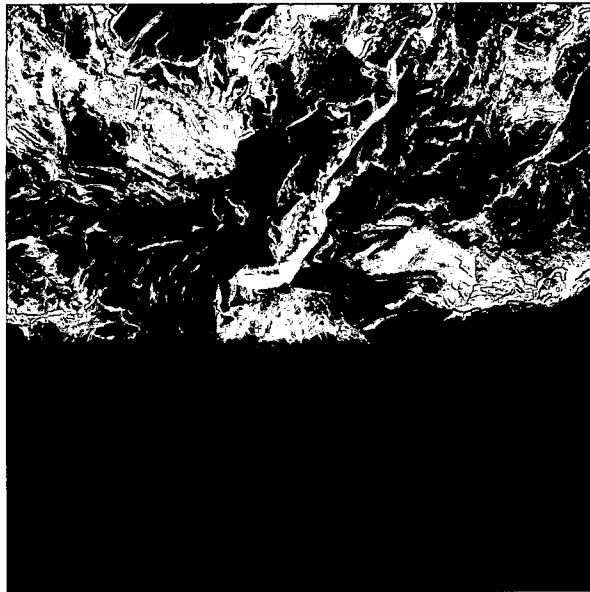


Figure 70. 06-132 at 200X

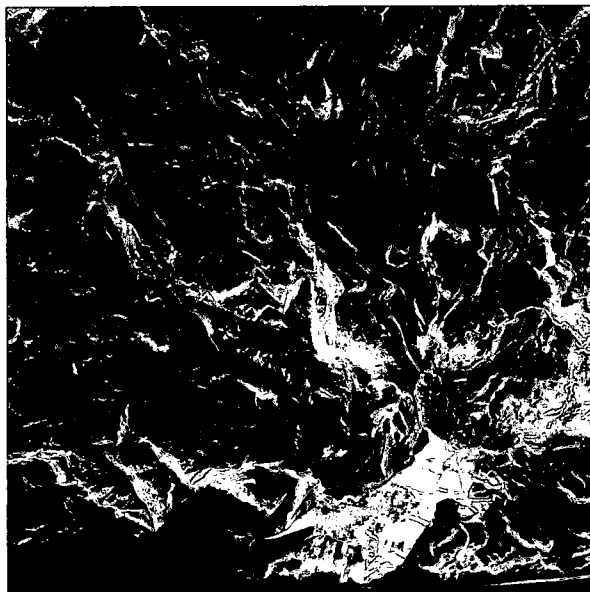


Figure 71. 06-133 at 200X

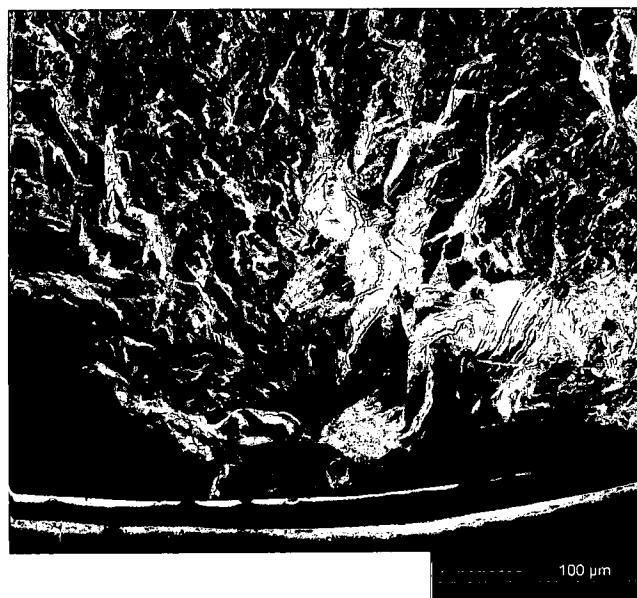


Figure 72. 06-134 at 200X

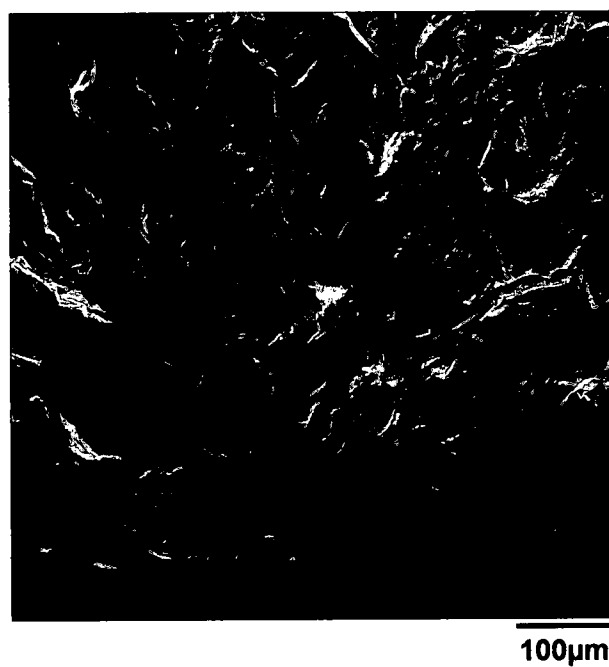


Figure 73. 06-135 at 200X

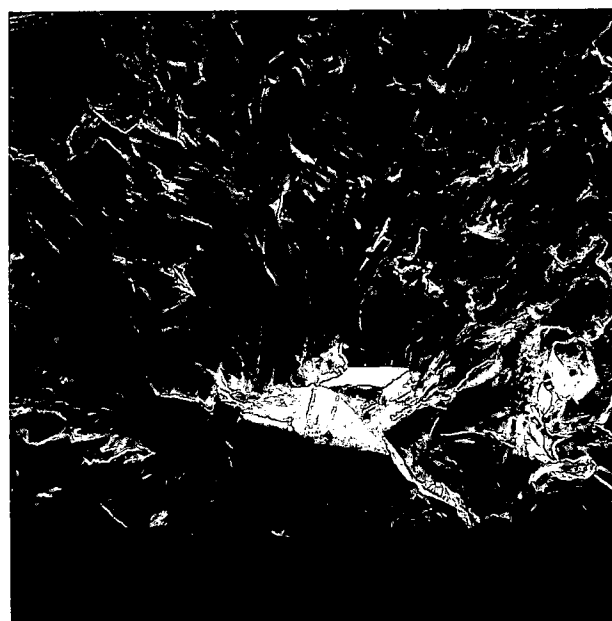


Figure 74. 06-136 at 200X

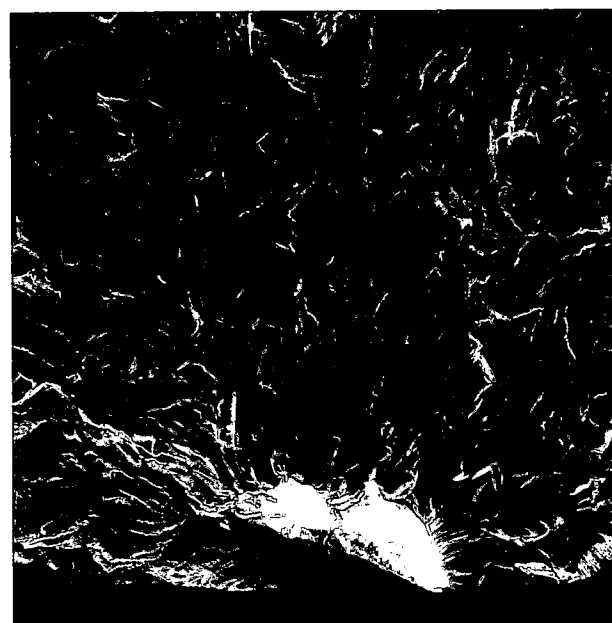


Figure 75. 06-137 at 200X

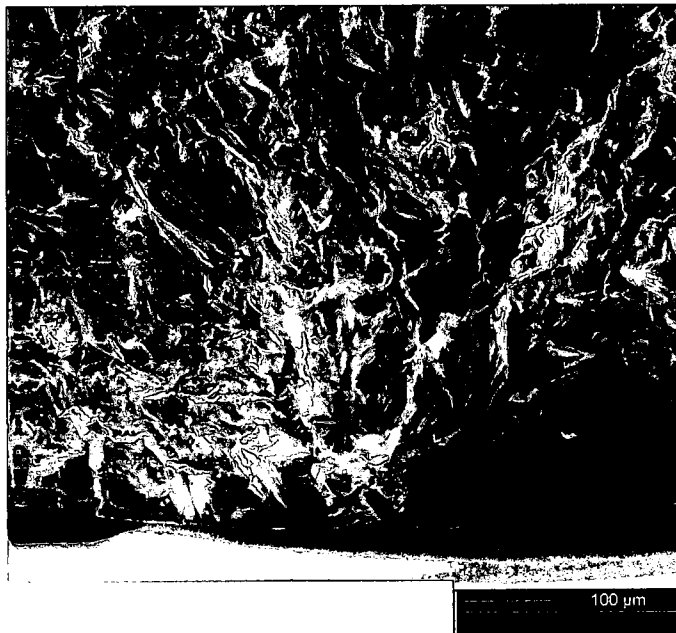


Figure 76. 06-139 at 200X

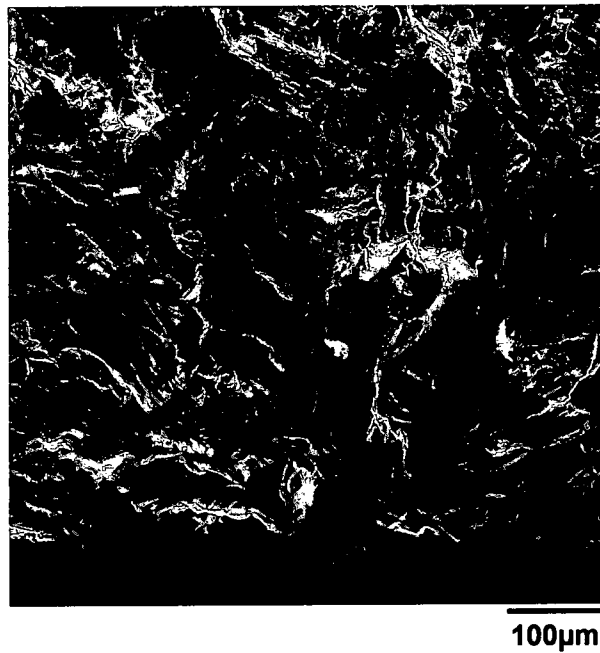
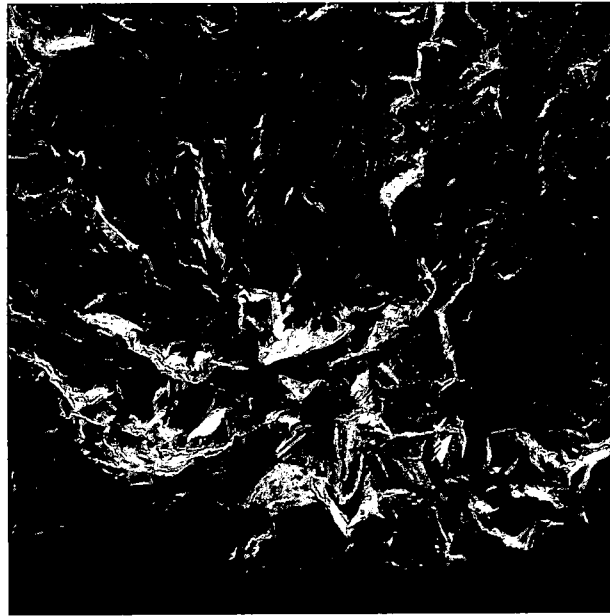


Figure 77. 06-140 at 200X



200µm

Figure 78.06-141 at 150X

Appendix B

MeX Images of Specimens.

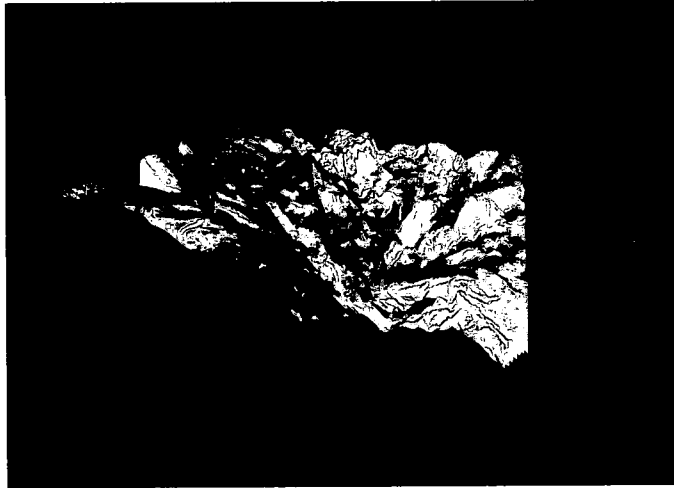


Figure 79. 06-000 at 200X



Figure 80. 06-002 at 200X

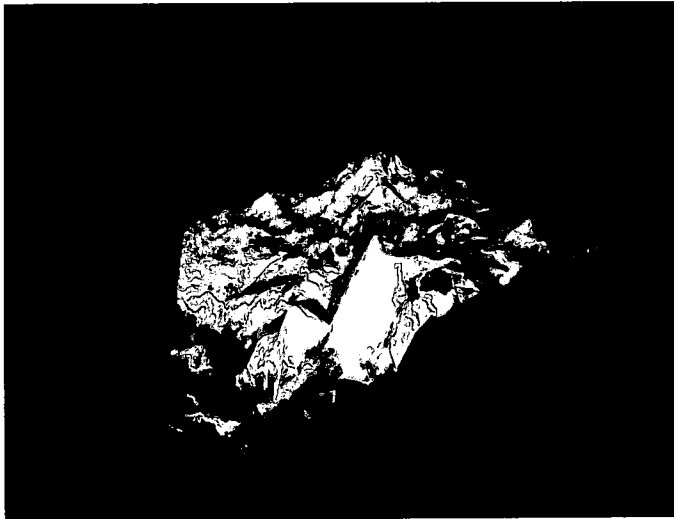


Figure 81. 06-003 at 200X

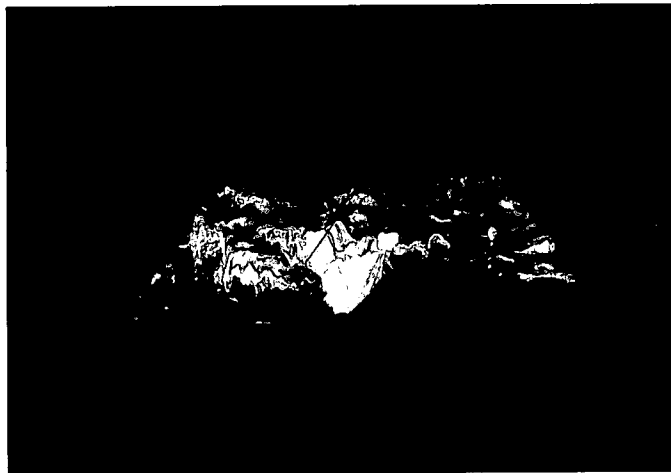


Figure 82. 06-004 at 200X

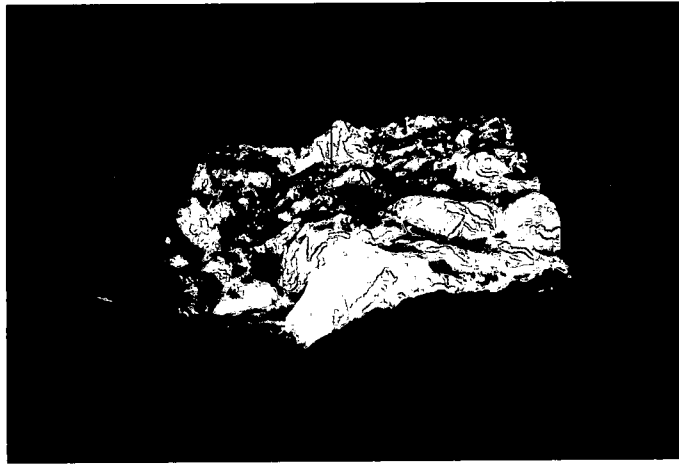


Figure 83. 06-005 at 200X

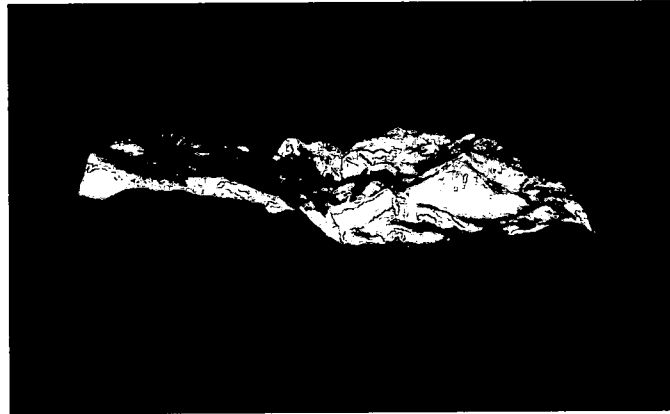


Figure 84. 06-006 at 200X

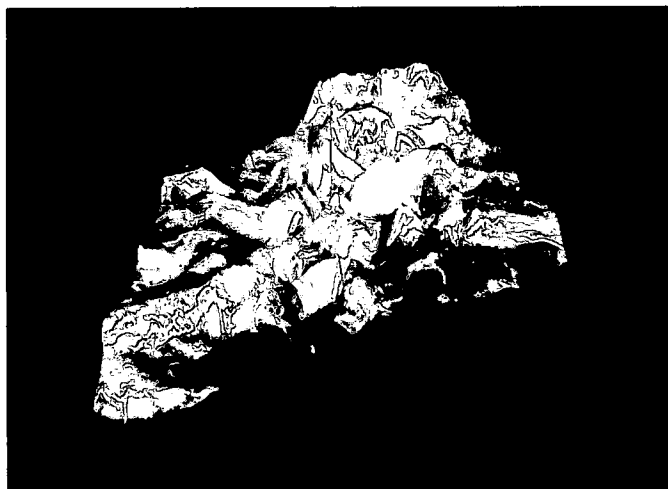


Figure 85. 06-008 at 200X



Figure 86. 06-009 at 200X

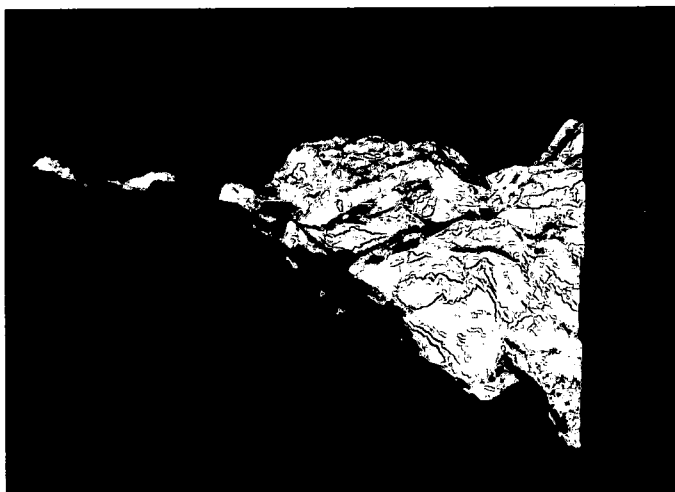


Figure 87. 06-010 at 200X

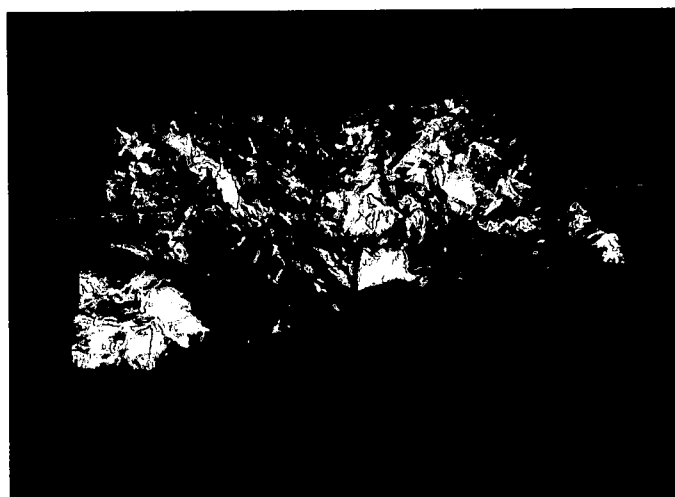


Figure 88. 06-011 at 200X



Figure 89. 06-012 at 200X

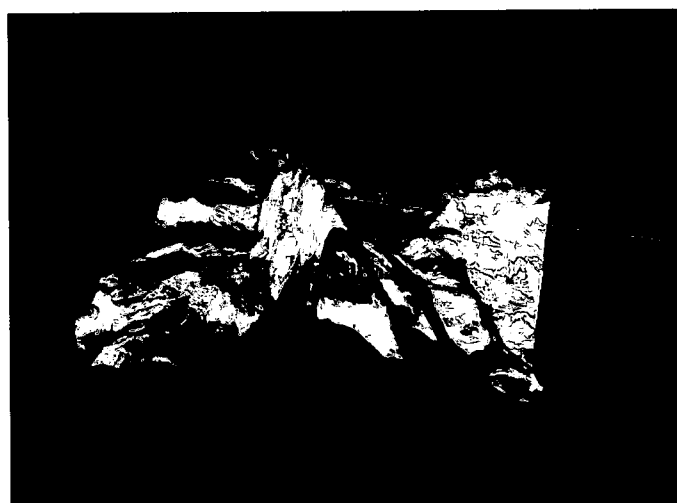


Figure 90. 06-013 at 200X

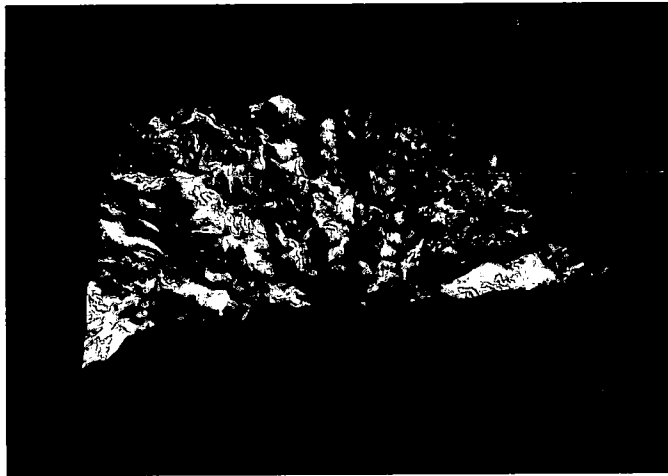


Figure 91. 06-014 at 200X

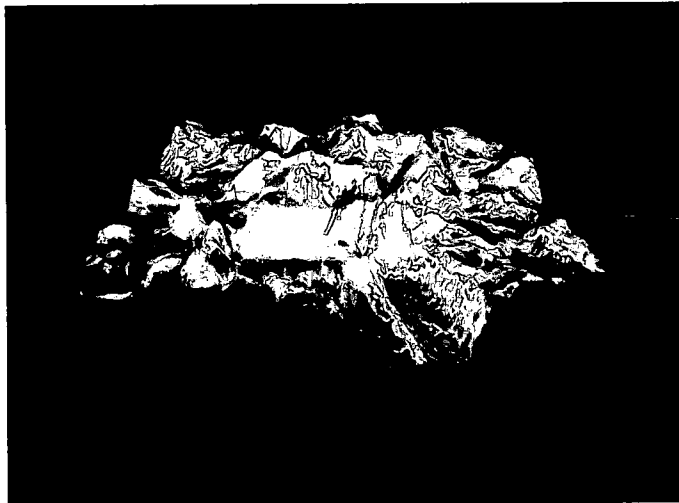


Figure 92. 06-015 at 200X

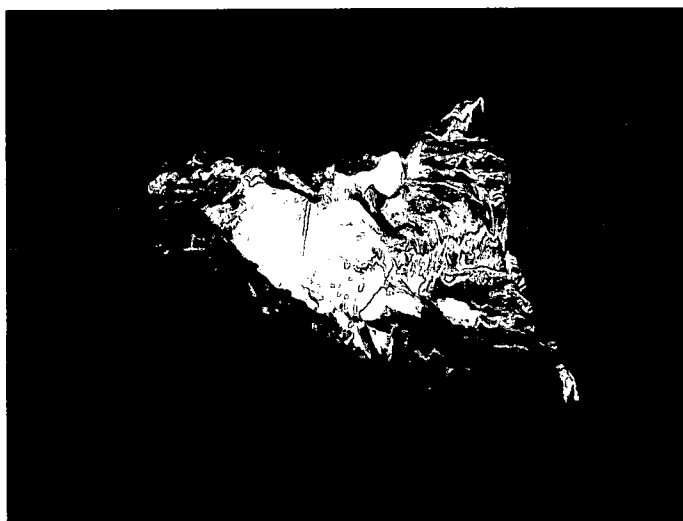


Figure 93. 06-016 at 200X

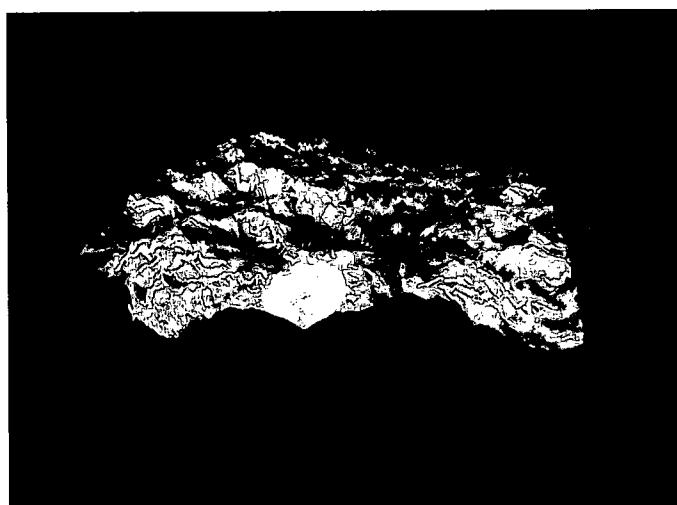


Figure 94. 06-017 at 200X



Figure 95. 06-018 at 200X



Figure 96. 06-019 at 200X

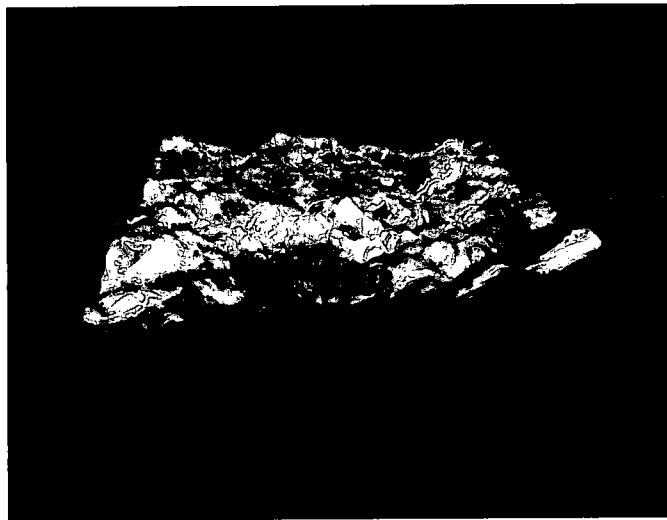


Figure 97. 06-020 at 200X

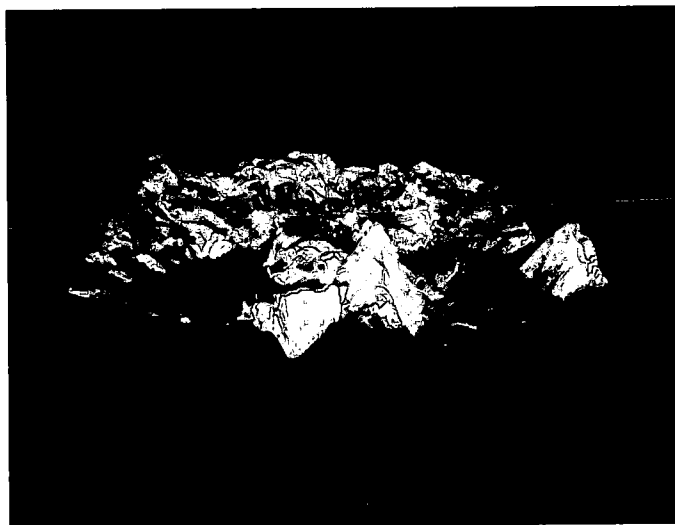


Figure 98. 06-021 at 200X

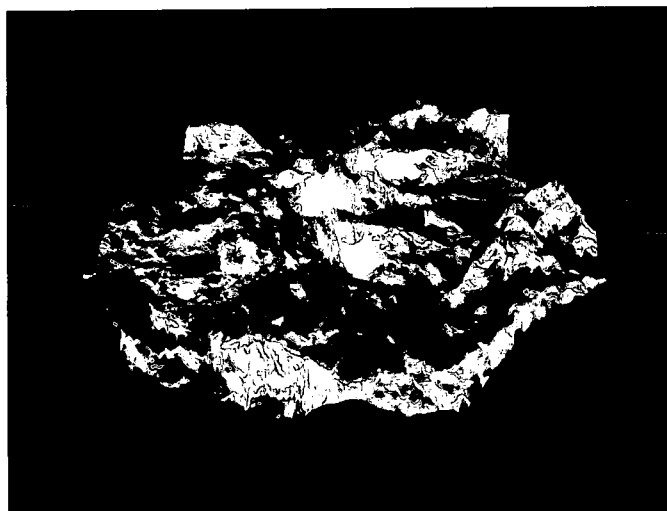


Figure 99. 06-023 at 150X

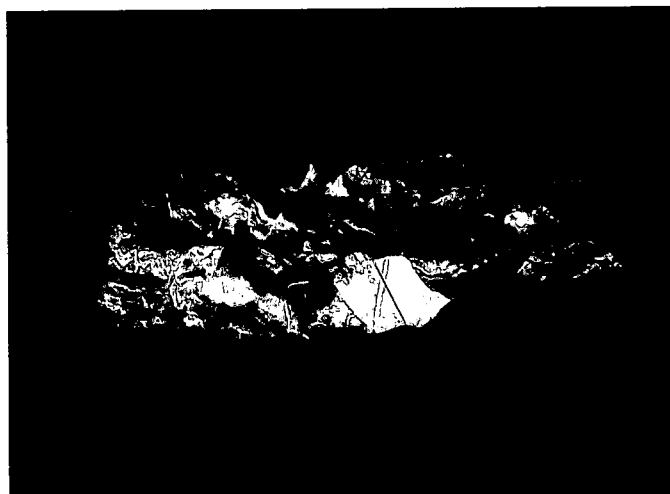


Figure 100. 06-024 at 200X

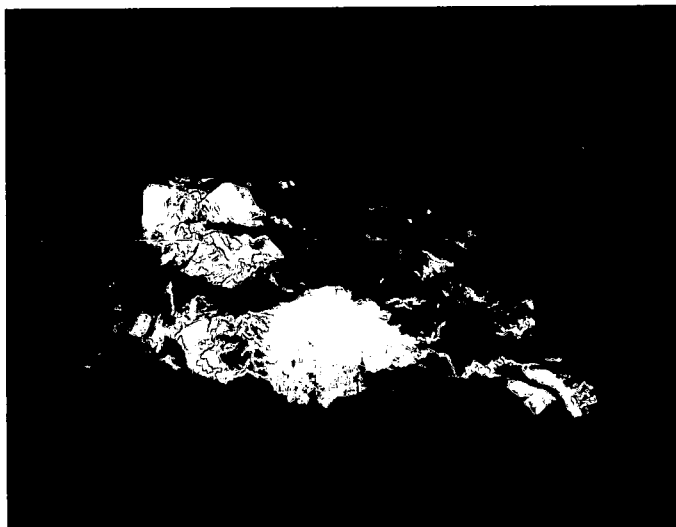


Figure 101. 06-025 at 200X

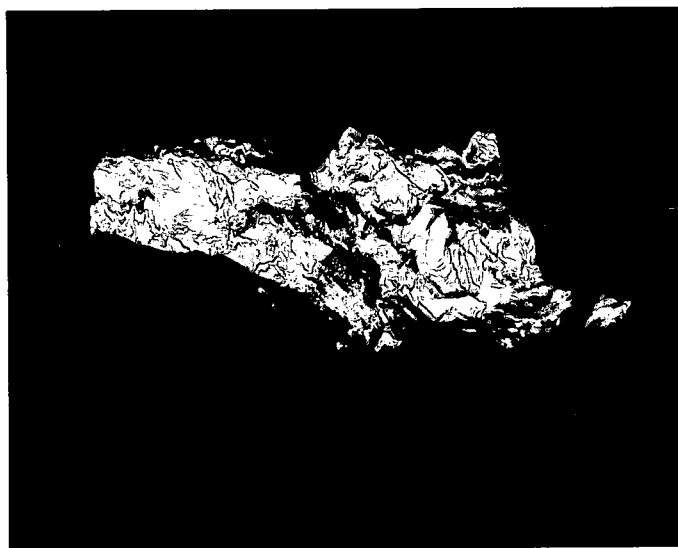


Figure 102. 06-026 at 200X

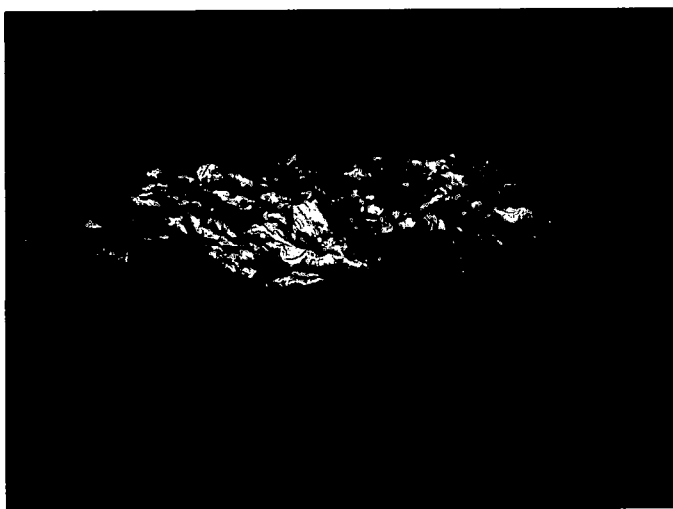


Figure 103. 06-027 at 200X

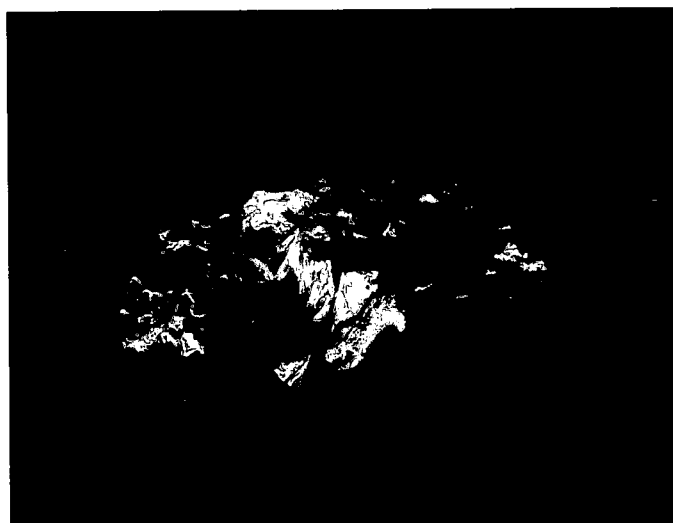


Figure 104. 06-029 at 200X

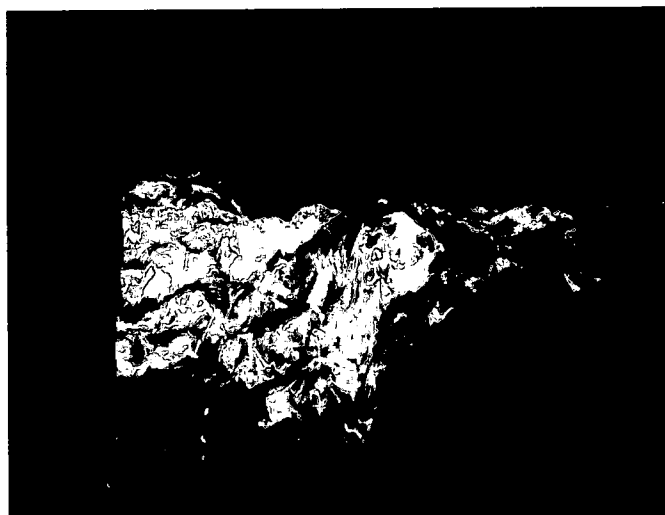


Figure 105. 06-112 at 200X

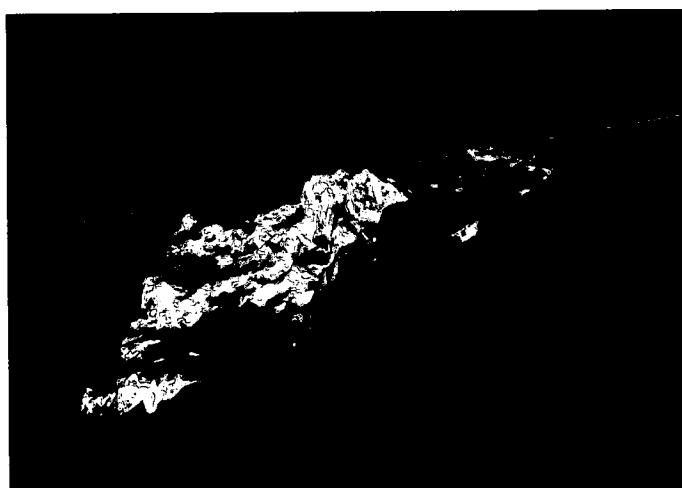


Figure 106. 06-113 at 150X



Figure 107. 06-114 at 200X

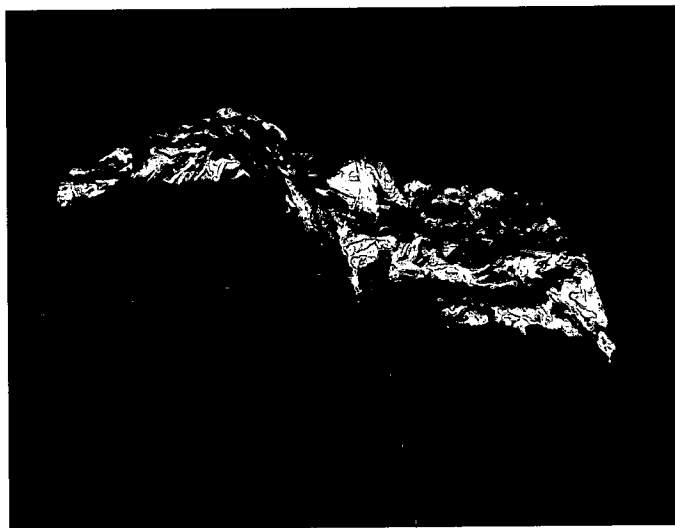


Figure 108. 06-115 at 150X

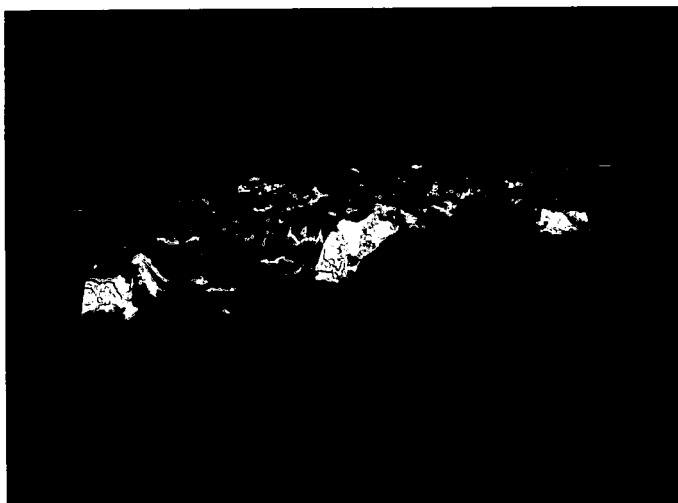


Figure 109. 06-116 at 200X



Figure 110. 06-117 at 200X

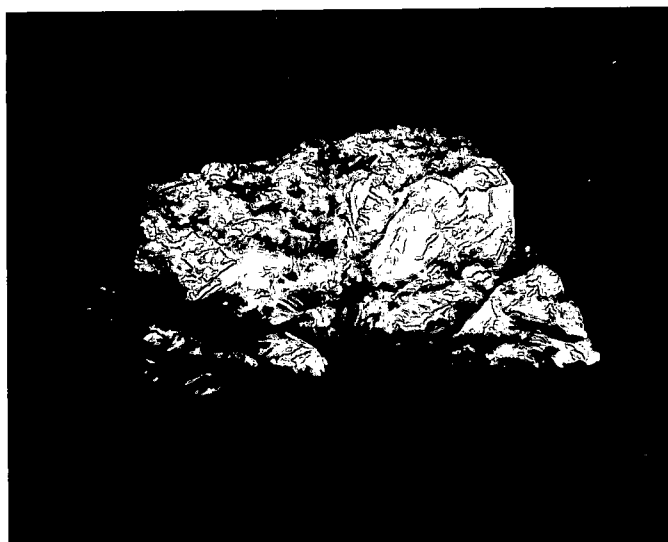


Figure 111. 06-118 at 200X

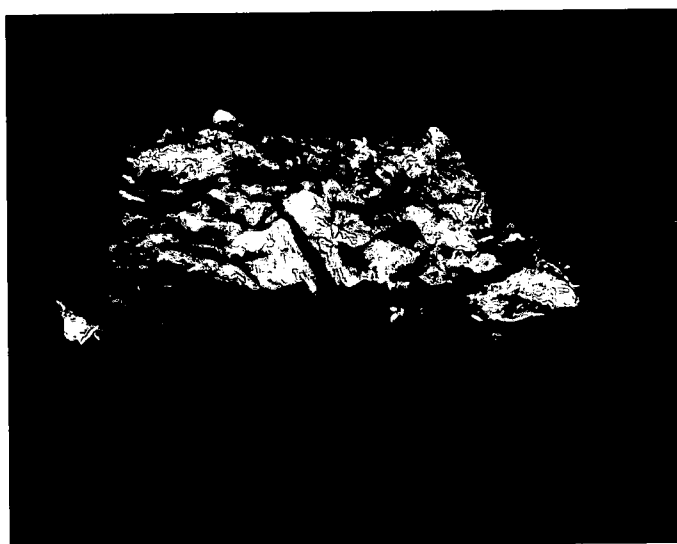


Figure 112. 06-119 at 150X

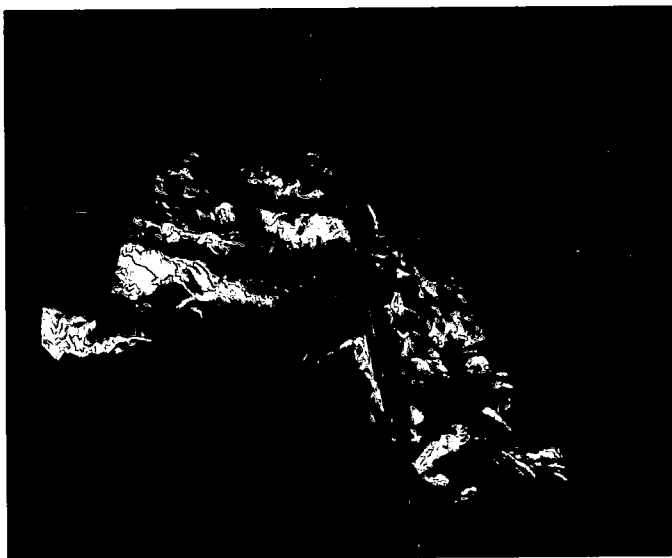


Figure 113. 06-120 at 200X

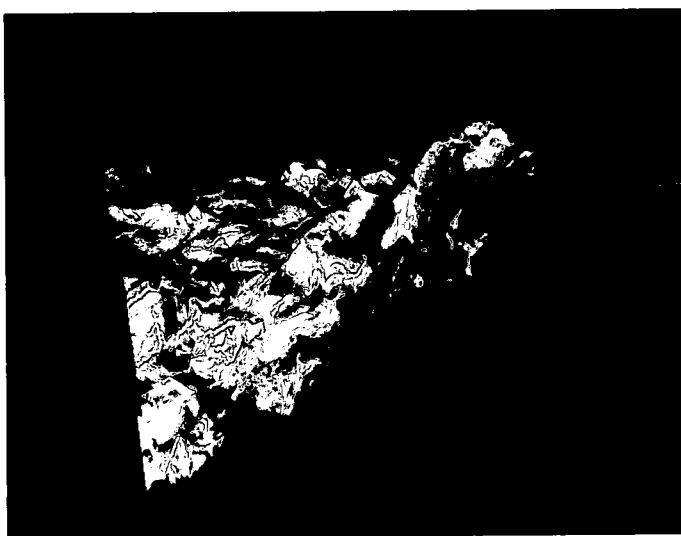


Figure 114. 06-121 at 200X

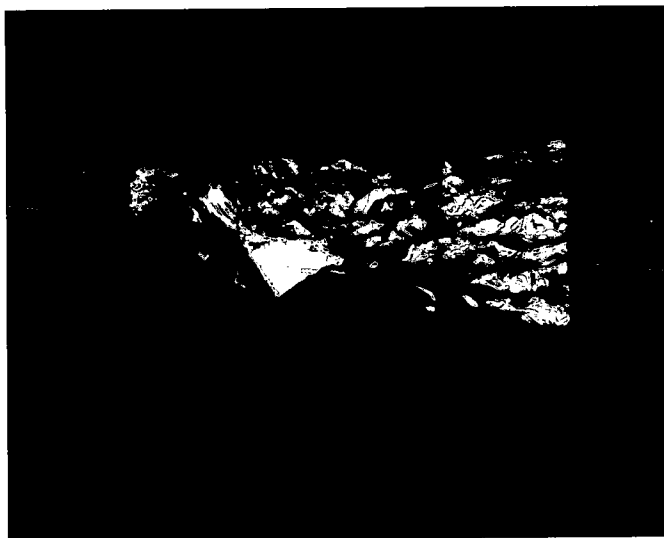


Figure 115. 06-122 at 200X

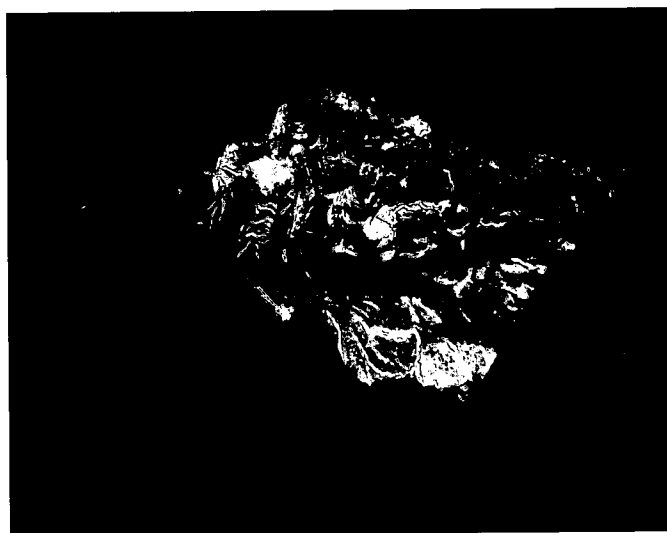


Figure 116. 06-123 at 200X

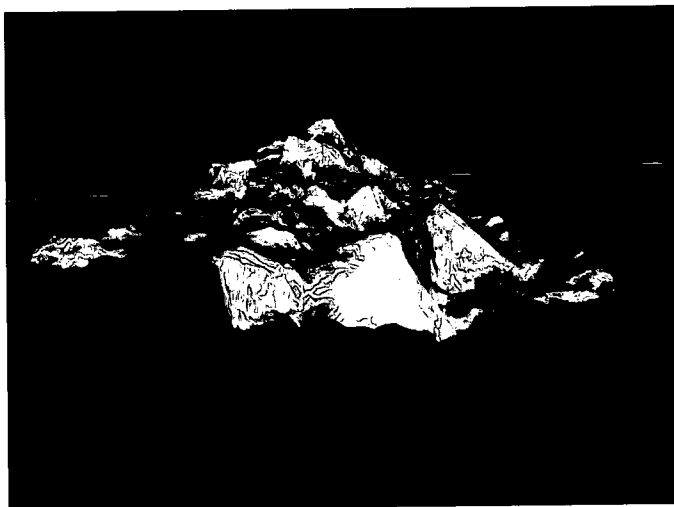


Figure 117. 06-125 at 150X

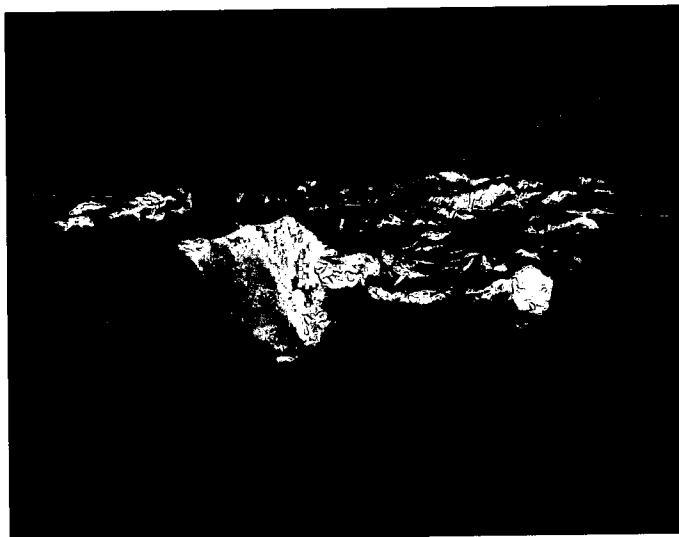


Figure 118. 06-126 at 150X

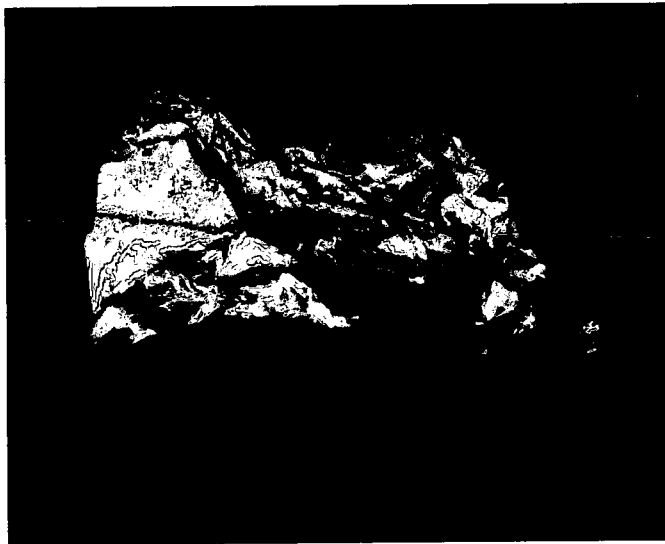


Figure 119. 06-127 at 200X



Figure 120. 06-128 at 200X

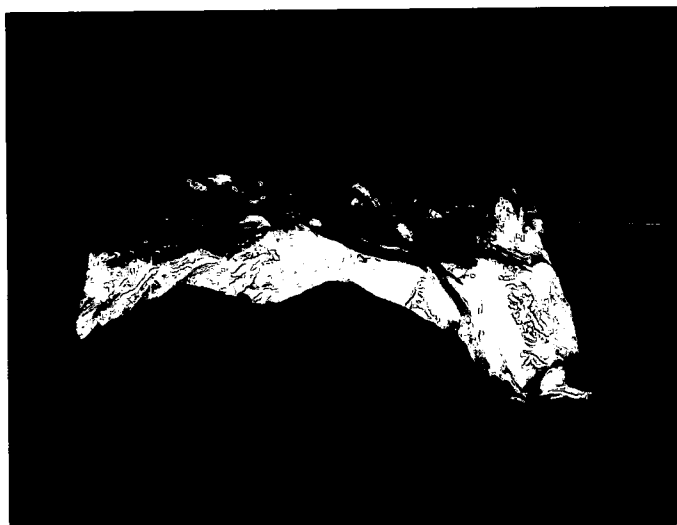


Figure 121. 06-130 at 200X

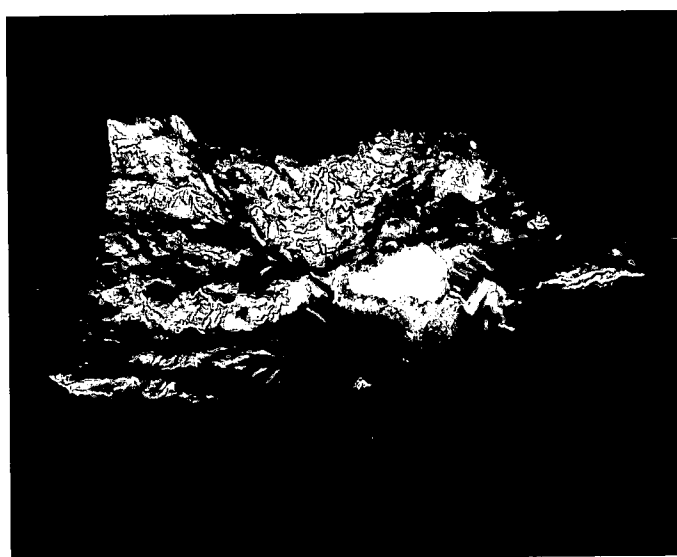


Figure 122. 06-131 at 150X

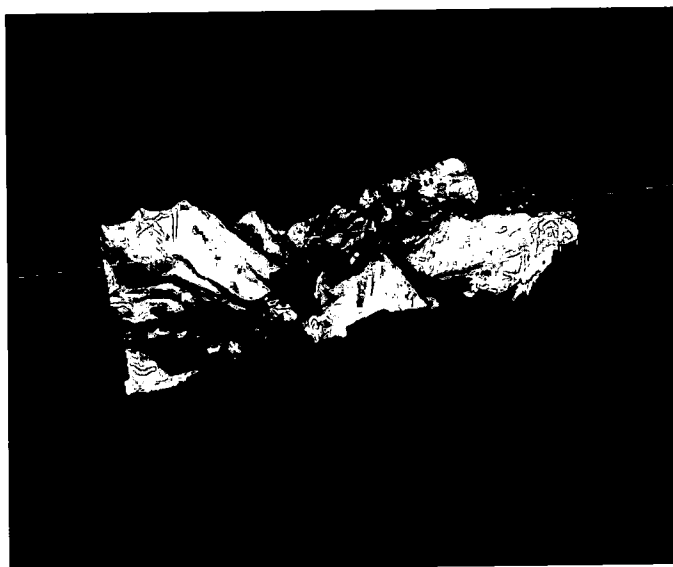


Figure 123. 06-132 at 200X

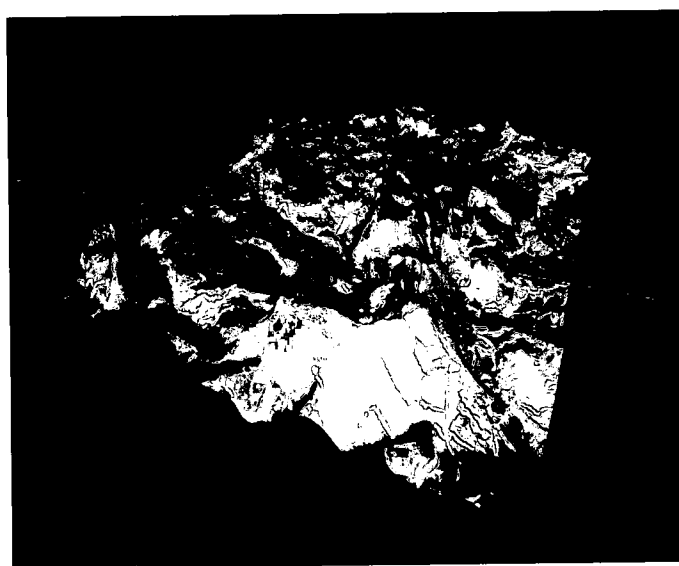


Figure 124. 06-133 at 200X

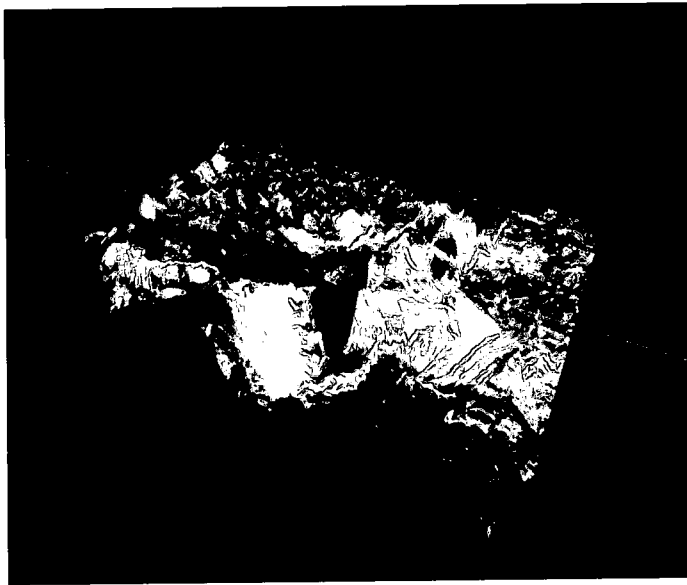


Figure 125. 06-134 at 200X



Figure 126. 06-135 at 200X

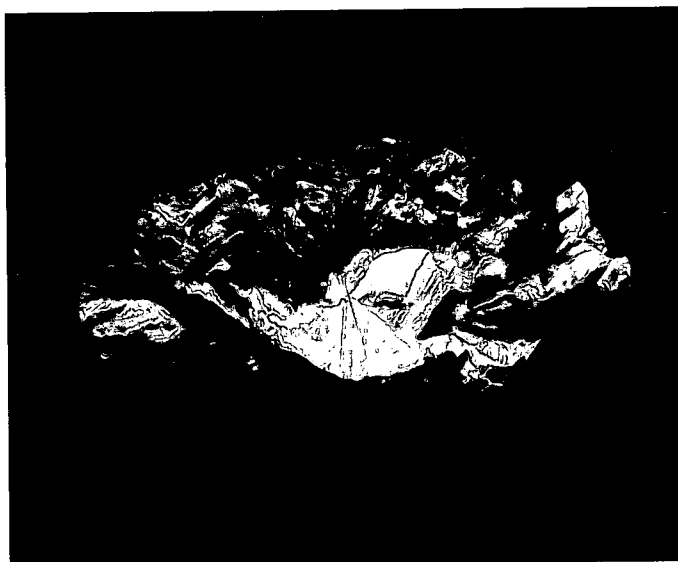


Figure 127. 06-136 at 200X

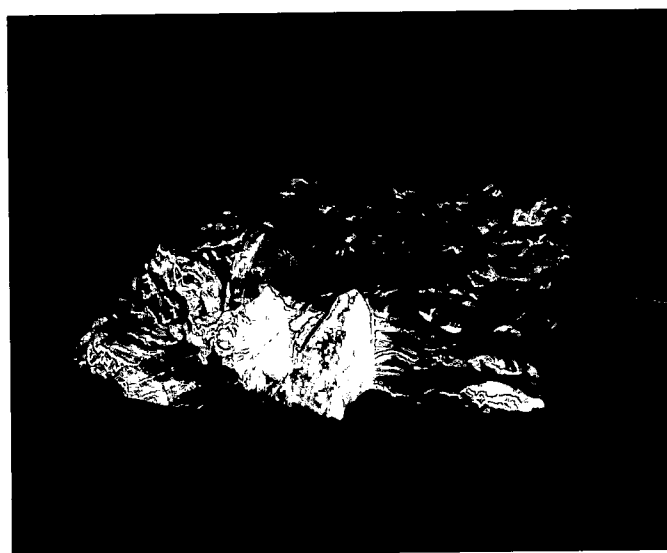


Figure 128. 06-137 at 200X

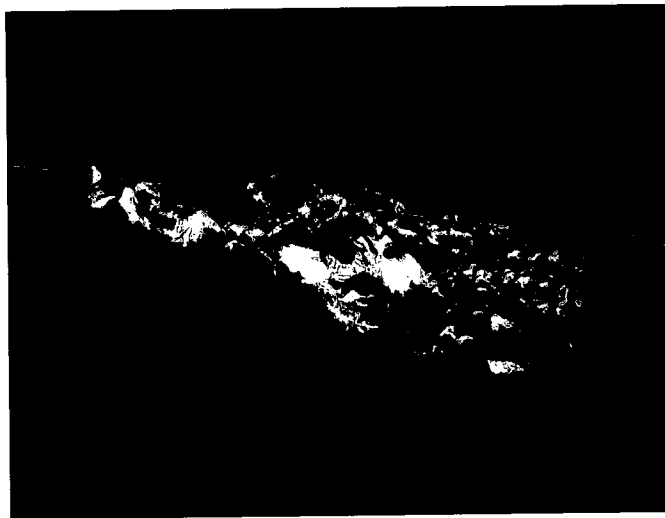


Figure 129. 06-139 at 200X

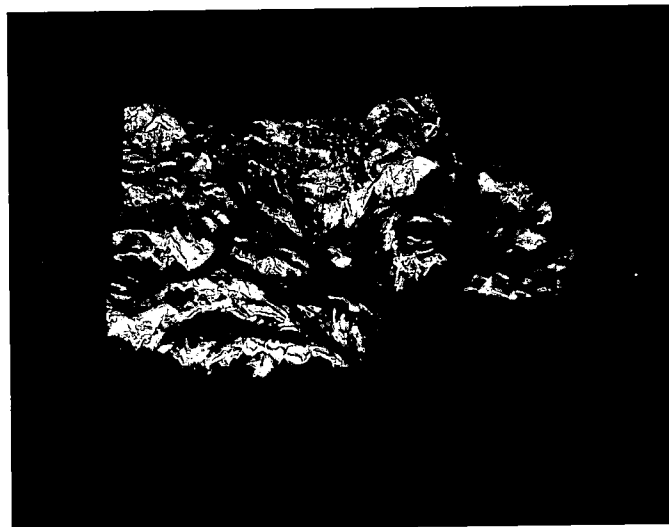


Figure 130. 06-140 at 200X



Figure 131.06-141 at 150X

Appendix C

Table 5. Pertinent Test Information

| Sample Number | Stress (MPa) | Life (cycles) | Test Frame | Initiation Location | Dist. From Surface (μm) | Billet Location |
|---------------|--------------|---------------|------------|---------------------|--------------------------------------|-----------------|
| 06-000 | 910 | 211477 | SH #42 | surface | | A1 |
| 06-002 | 955 | 186055 | SH #16 | near surface | 70 | A3 |
| 06-003 | 910 | 235679 | SH #42 | near surface | 130 | B1 |
| 06-004 | 955 | 124713 | SH #42 | near surface | 100 | B2 |
| 06-005 | 955 | 102377 | SH #16 | surface | | B3 |
| 06-006 | 910 | 282761 | SH #42 | surface | | C1 |
| 06-008 | 910 | 453310 | SH #42 | internal | 210 | C3 |
| 06-009 | 910 | 202821 | SH #42 | surface | | D1 |
| 06-010 | 955 | 109234 | SH #1A | near surface | 80 | D2 |
| 06-011 | 955 | 122719 | SH #42 | surface | | D3 |
| 06-012 | 910 | 298841 | SH #42 | internal | 1,000 | E1 |
| 06-013 | 910 | 306669 | SH #42 | internal | 165 | E2 |
| 06-014 | 955 | 110006 | SH #42 | near surface | 105 | E3 |
| 06-015 | 910 | 262580 | SH #42 | near surface | 130 | F1 |
| 06-016 | 910 | 349548 | SH #42 | near surface | 150 | F2 |
| 06-017 | 955 | 133870 | SH #1A | surface | | F3 |
| 06-018 | 910 | 256093 | SH #42 | near surface | 90 | G1 |
| 06-019 | 955 | 135647 | SH #16 | near surface | 75 | G2 |

| Sample Number | Stress (MPa) | Life (cycles) | Test Frame | Initiation Location | Dist. From Surface (μm) | Billet Location |
|---------------|--------------|---------------|------------|---------------------|--------------------------------------|-----------------|
| 06-020 | 955 | 24852 | SH #1A | surface | | G3 |
| 06-021 | 910 | 263742 | SH #42 | near surface | 120 | H1 |
| 06-023 | 955 | 213340 | SH #1A | internal | 405 | H3 |
| 06-024 | 955 | 152658 | SH #42 | surface | | I1 |
| 06-025 | 955 | 112443 | SH #16 | surface | | I2 |
| 06-026 | 955 | 207859 | SH #42 | surface | | I3 |
| 06-027 | 955 | 68699 | SH #16 | surface | | J1 |
| 06-029 | 910 | 410250 | SH #42 | near surface | 105 | J3 |
| 06-112 | 955 | 531310 | SH #42 | internal | 750 | K4 |
| 06-113 | 955 | 568882 | SH #16 | internal | 370 | K5 |
| 06-114 | 955 | 517296 | SH #1A | surface | | K6 |
| 06-115 | 955 | 27570 | SH #1A | surface | | M4 |
| 06-116 | 955 | 437451 | SH #22 | surface | | M5 |
| 06-117 | 955 | 163314 | SH #1A | near surface | 110 | M6 |
| 06-118 | 955 | 112667 | SH #42 | surface | | N4 |
| 06-119 | 955 | 108053 | SH #42 | near surface | 300 | N5 |
| 06-120 | 955 | 84207 | SH #1A | surface | | N6 |
| 06-121 | 955 | 137819 | SH #42 | near surface | 110 | P4 |
| 06-122 | 955 | 119902 | SH #42 | surface | | P5 |
| 06-123 | 955 | 83868 | SH #1A | surface | | P6 |
| 06-125 | 955 | 91043 | SH #42 | surface | | R5 |
| 06-126 | 955 | 65491 | SH #42 | surface | | R6 |
| 06-127 | 955 | 104224 | SH #42 | surface | | S4 |
| 06-128 | 955 | 491309 | SH #1A | internal | 220 | S5 |
| 06-130 | 955 | 68009 | SH #42 | surface | | T4 |
| 06-131 | 955 | 179404 | SH #42 | surface | | T5 |
| 06-132 | 955 | 78358 | SH #1A | surface | | T6 |
| 06-133 | 955 | 91287 | SH #42 | near surface | 75 | U4 |
| 06-134 | 955 | 109509 | SH #42 | surface | | U5 |

| Sample Number | Stress (MPa) | Life (cycles) | Test Frame | Initiation Location | Dist. From Surface (μm) | Billet Location |
|---------------|--------------|---------------|------------|---------------------|--------------------------------------|-----------------|
| 06-135 | 955 | 44513 | SH #16 | surface | | U6 |
| 06-136 | 955 | 118706 | SH #1A | near surface | 100 | V4 |
| 06-137 | 955 | 122127 | SH #42 | surface | | V5 |
| 06-139 | 955 | 138755 | SH #16 | surface | | W4 |
| 06-140 | 955 | 171804 | SH #1A | surface | | W5 |
| 06-141 | 955 | 161855 | SH #1A | near surface | 160 | W6 |

Appendix D

Specimen Life Vs. Billet Location

ALA Bars-Different Locations

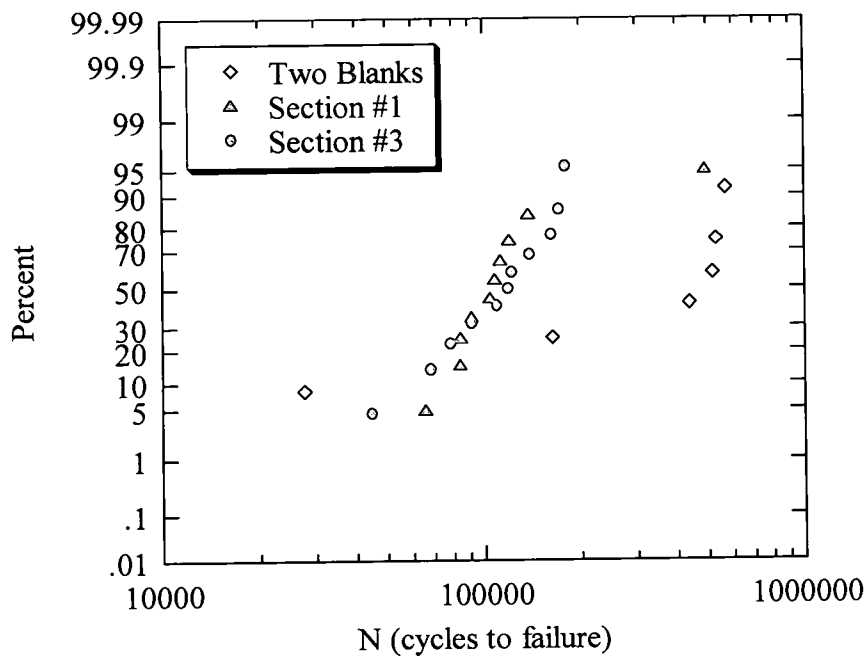


Figure 132. Cumulative distribution function showing life based on location from billet.

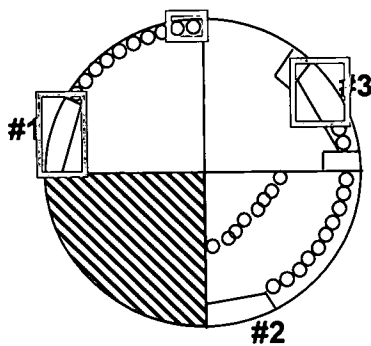


Figure 133. Representative locations of specimens (color coded with Figure 132).

BIBLIOGRAPHY

1. H. Sizek, unpublished research, University of Dayton Research Institute, Dayton, OH, 2003.
2. Technical Bulletin, Waspaloy Alloy, (n.d) Retrieved November 29, 2006, from <http://www.specialmetalswiggins.co.uk/documents/Waspaloy.pdf>
3. *ASTM Standards 2006: Section 3-Metals Test Methods and Analytical Procedures*, Vol. 03.01, pp. 760-765; 2006.
4. R. M. Forbes Jones, L. A. Jackman: *The Structural Evolution of Superalloy Ingots during Hot Working*: JOM, 1999, Vol 51, p 27.
5. R. E. Bailey: *Some Effects for Hot Working Practice on Waspaloy's Structure and Tensile Properties: Superalloys 1972*, TMS, Warrendale, PA, 1972, pp. J1-J21.
6. H. H. Ruble, S. L. Semiatin: *Forging of Nickel-Base Superalloys: ASM Handbook*, Vol. 14A, Forming and Forging.
7. S.L. Semiatin, P.N. Fagin, M.G. Glavicic, D. Raabe: *Deformation Behavior of Waspaloy at Hot-Working Temperatures: Scripta Materialia*, November 18, 2003.
8. . *Life Prediction Methodologies for Aerospace Materials*: edited by N.E. Ashbaugh, et al., AFRL-ML-WP-TR-2004-4026, Wright Patterson Air Force Base, OH 2004.
9. *Turn your SEM into a 3-D Measurement Device* (n.d.) Retrieved November 27, 2006, from http://www.alicon.com/upload/pdf/MeX_E_brochure_highresolution.pdf
10. G. P. Romanoski, R. M., Pelloux: *The Fatigue Behavior of Small Cracks in an Aircraft Turbine Disk Alloy: Elevated Temperature Crack Growth: Proceedings of Symposium*, ASME Winter Annual Meeting. 1990. Dallas, TX.

11. E. S. Huron: *Serrated Yielding in a Nickel-base Superalloy*: in *Superalloys 1992*, edited by S.D. Antolovich, et al., TMS Warrendale, PA 1992, pp. 675-684.
12. S. K. Jha, J. M. Larsen and A. H. Rosenberger: *The role of competing mechanisms in the fatigue life variability of a nearly fully-lamellar γ -TiAl based alloy*: *Acta Materialia*, v 53, n 5, pp. 1293-1304; 2004
13. M. J. Caton, S. K. Jha, A. H. Rosenberger, and J.M. Larsen: *Divergence of Mechanisms and the Effect on the Fatigue Life Variability of Rene 88DT*: in *Superalloys 2004*. 2004. p. 305-312.
14. S. K. Jha, J. M. Larsen, A. H. Rosenberger, and G. A. Hartman: *Dual Fatigue Failure Modes in Ti-6Al-2Sn-4Zr-6Mo and Consequences on Probabilistic Life Prediction*: *Scripta Materialia*, Vol. 48, pp. 1637-1642, 2003.
15. L.F. Coffin, Jr.: *Fatigue at High Temperatures: Fatigue at Elevated Temperatures*, ASTM STP 520, American Society for Testing and Materials, 1973, pp. 5-34.
16. R. G. Tryon, A. Dey, L. Nasser, Y. Zhao, G. Krishnan, A. Iyer: *Prognostic Microstructurally-Based Reliability Tool for Mechanical Systems*: DOD Contract No. DAAH01-02-C-R196, January 27, 2005.

R002592939